# ISOTOPIC GEOCHEMISTRY OF MERCURY IN ACTIVE AND FOSSIL HYDROTHERMAL SYSTEMS

by

Christopher Nelson Smith

A dissertation submitted in partial fulfillment
of the requirements for the degree of
Doctor of Philosophy
(Geology)
in The University of Michigan
2010

Doctoral Committee:

Professor Stephen E. Kesler, Co-Chair
Professor Joel D. Blum, Co-Chair
Professor Eric J. Essene
Professor Gerald J. Keeler

Table of Contents

List of Figures

Figure

List of Tables

Table

List of Appendices

ABSTRACT

ISOTOPIC GEOCHEMISTRY OF MERCURY IN ACTIVE AND FOSSIL HYDROTHERMAL SYSTEMS

by

Christopher Nelson Smith

Co-Chairs: Stephen E. Kesler and Joel D. Blum

Presented here are the first studies of stable Hg isotope geochemistry in hydrothermal systems. A new analytical method for the determination of high precision Hg isotope ratios by cold-vapor multiple-collector inductively-coupled-plasma mass-spectrometry (CV-MC-ICP-MS) was developed and the total range of Hg isotopic compositions measured in natural samples was found to be 5.8 ‰ $\delta^{202}$Hg ($\delta^{202}$Hg/$^{198}$Hg; relative to NIST 3133) or greater than 72 times the analytical precision (± 0.08 ‰, 2 SD) of the method.

The Hg isotopic compositions of samples throughout the vertical extent of two fossil hydrothermal systems in Nevada can be grouped by mineralogy and position; $\delta^{202}$Hg values at the tops of the systems are lowest in cinnabar-rich sinter and distinct from the higher $\delta^{202}$Hg values of metacinnabar-rich sinter, deeper seated veins have $\delta^{202}$Hg values that are higher than cinnabar-rich sinter. Low $\delta^{202}$Hg values in cinnabar-rich sinter are most likely due to mass-dependent fractionation that occurred

during boiling of the hydrothermal fluid, while the differences between cinnabar and metacinnabar are potentially due to kinetic effects associated with mineral precipitation.

The Hg isotopic compositions of rocks, ore deposits, and active spring deposits from the California Coast Ranges were measured. Ore deposits have similar average Hg isotopic compositions that are indistinguishable from averages for the source rocks. This observation suggests that there is little or no isotopic fractionation ($<\pm 0.5‰$) during release of Hg from source rocks into hydrothermal solutions. Isotopic fractionation does appear to take place during transport and concentration of Hg in deposits, however, especially in their uppermost parts, expressed on the surface as hot springs. Boiling of hydrothermal fluids, separation of a Hg-bearing $CO_2$ vapor or reduction and volatilization of $Hg^0$ in the near-surface environment are likely the most important processes causing the observed mass-dependent Hg isotope fractionation. This should result in the release of Hg with low $\delta^{202}Hg$ values into the atmosphere from the top of these hydrothermal systems. Estimates of mass balance suggest that residual Hg reservoirs are not measurably enriched in heavy Hg isotopes as a result of this process because only a small amount of Hg (<4%) leaves actively ore-forming systems.

# CHAPTER I.

# INTRODUCTION

This thesis presents the first systematic attempt to utilize Hg isotopes to trace the source and fate of Hg in active and fossil hydrothermal systems. This study is important to a wide spectrum of geoscience disciplines because of the toxicity and mobility of Hg in the Earth. Direct isotopic analysis of Hg-bearing materials is the first step in developing studies that will examine the migration and accumulation of this volatile element.

Stable isotopes have been essential tools in the exploration of geochemical cycles and processes. Our understanding of the subsurface processes occurring in hydrothermal systems, including active geothermal systems and their fossil analogues, preserved as ore deposits, have been advanced through the analysis of O, H, S, C, and N isotope ratios (Criss, 1999; Hoefs, 2004). These light stable isotopes provide information on the source of hydrothermal fluids and the dissolved and gaseous components in the fluid. Processes of isotopic exchange, boiling and mineral precipitation are recorded in the stable isotope compositions of the gas, solid and liquid phases of the fluid. However, the source of metals in these systems has remained elusive, and inferences as to their source have come from extrapolation based on associated light stable isotope signatures (e.g. the magmatic water box on a $\delta D$ vs. $\delta^{18}O$ plot).

Measurement of heavy stable isotope ratios would allow the source and cycling of heavy elements, such as metals, in the Earth to be assessed directly. Recent advances in instrumentation technology have enabled new investigation into heavy stable isotope ratios using multiple-collector inductively-coupled-plasma mass-spectrometry (MC-ICP-MS) (see review by Halliday et al., 1995). This instrument combines the ionizing efficiency of a plasma source with the ability to measure multiple signals simultaneously, which is essential for obtaining high precision measurements.

Recent investigations have found isotope ratios of Fe (Anbar et al., 2000; Bullen et al., 2001), Cr (Ellis et al., 2002), Cu (Marechal et al., 1999; Zhu et al., 2000), Zn (Marechal et al., 1999), Mo (Barling et al., 2001; Seibert et al., 2001) and Tl (Rehkamper and Halliday, 1999; Rehkamper et al., 2002) range over several per mil (‰) (reviewed by Johnson et al., 2004). Both biotic and abiotic processes have been shown to cause isotopic fractionation (Beard et al., 1999; Anbar et al., 2000). These new isotope systems have thus far been used to determine the extent of $Cr^{6+}$ reduction in a contaminated aquifer (Ellis et al., 2002) and to provide constraints on the redox state of the Archean and Proterozoic oceans using Mo and Fe isotopes (Arnold et al., 2004; Rouxel et al., 2005). Metal fluxes through seafloor hydrothermal vents have been investigated using Tl (Nielsen et al., 2006) and Zn isotopes (John et al., 2008). Graham et al. (2004) have used Fe and Cu isotope ratios to trace the source of metals in the Grasberg porphyry complex. Asael et al. (2007) used Cu isotopes to trace the source and redox state of the ore fluid in a sedimentary-hosted Cu deposit. Initial studies of Hg isotopes have proven to be similarly useful in the study of metal geochemistry.

Recent experimental studies of Hg isotope fractionation have shown that volatilization causes measurable changes in isotopic compositions by the preferential reduction and vaporization of lighter Hg isotopes (Zheng et al., 2007). This is significant in the study of ancient hydrothermal systems because it supports boiling and vapor separation in a near surface environment as a mechanism that causes the mass-dependent fractionation of Hg isotopes (Smith et al., 2005, 2008). Laboratory studies have also confirmed that biological reduction and abiotic photoreduction cause significant mass dependent fractionation of Hg isotopes in surficial environments (Bergquist and Blum, 2007; Kritee et al., 2007; Biswas et al., 2008). In both biotic and abiotic reduction, lighter isotopes of Hg were preferentially reduced to the volatile $Hg^0$ species, leaving isotopically heavier Hg in the remaining residue. These studies indicate that Hg isotopes might be useful in studies of ore deposits by: 1) providing insight on the physical conditions of the hydrothermal system during ore formation; 2) assessing the role of biological interactions in ore deposition; and 3) quantifying the role of ore deposits and active hydrothermal systems in the global cycling of Hg.

In Chapter II a new and robust method for obtaining high precision measurements of Hg isotope ratios by cold vapor (CV) generation MC-ICP-MS from a variety of sample matrices is presented. A new method for extracting Hg from samples by sequential pyrolysis, combustion and liquid trapping is described. A significant range of Hg isotope ratios were found in several types of hydrothermal ore deposits and among organic and inorganic and organic standard reference materials.

Variations in Hg isotopic compositions throughout the vertical extent of two fossil geothermal systems are explored in Chapter III (Smith et al., 2005). Boiling of the

hydrothermal fluids and gas phase separation appears to be a major mechanism of mass-dependent Hg isotopic fractionation in these systems. Cinnabar deposited from gaseous Hg at the surface has a lighter isotopic composition than Hg hosted in sulfides in deeper-seated veins. Metacinnabar deposited in sinter at the surface has distinctly heavier Hg isotopic compositions than cinnabar-rich sinter, and is trace metal-rich, suggesting deposition from deeper vein fluids.

In Chapter IV (Smith et al., 2008), the first study of the isotopic composition of mercury in rocks, ore deposits, and active spring deposits from the California Coast Ranges, a part of Earth's crust with unusually extensive evidence of mercury mobility and enrichment, is presented. The region hosts abundant Hg mineralization that began to form 2.3 Ma, coinciding with the inception of volcanic activity in the area (Rytuba, 1995). There are two types of mercury deposits present in the area, hot-spring deposits that form at shallow depths (<300 m) and silica-carbonate deposits that extend to depths of 1000 m. Active springs and geothermal areas continue to precipitate Hg and Au and are analogues to the fossil hydrothermal systems preserved as ore deposits.

Hot spring and silica carbonate ore deposits have similar mean Hg isotopic compositions to the potential source rocks, but there is more variability in the isotopic compositions of the ore deposits. Active hot springs in the region are fed by mixtures of meteoric and connate fluids, considered to be analogous to the ore-forming fluids in the district and can precipitate sulfidic mud that contains up to 4890 ppm Hg and 14 ppm Au (Peters, 1991; 1993). The Hg isotopic compositions of these precipitates are in, general, lighter than ore deposits and host rocks in the region.

Hg isotopic compositions from the California Coast Ranges suggest that processes that leach and transport Hg from source rocks cause very little isotopic fractionation (< ± 0.5‰). Significant mass-dependent isotopic fractionation occurs in the near-surface zones of hydrothermal systems. Boiling of hydrothermal fluids or separation of a mercury-bearing $CO_2$ vapor is likely the most important process causing of the observed Hg isotope fractionation. This should result in the release of mercury with low $\delta^{202}Hg$ values into the atmosphere from the top of these hydrothermal systems. Estimates of mass balance indicate that only a small amount of Hg (< 3.5%) leaves active ore-forming systems and residual Hg reservoirs are not measurably enriched in heavy Hg isotopes as a result.

The results of the studies presented in this thesis show that Hg isotope ratios can: 1) provide information on Hg fluxes to the atmosphere and sedimentary record; 2) be used to calculate mass transfer between source, ore deposit and the surface; and 3) constrain the mineralizing environment of sulfides in active and fossil geothermal systems. These are important first steps in integrating Hg isotopes into studies of global Hg cycling and identifying anthropogenic and geogenic inputs to the Hg cycle. Given the relative abundance of lighter Hg isotopes in the upper levels of ore deposits and the contrasting Hg isotope ratios between bedrock and ore deposits, Hg isotopic compositions could be used to calculate the relative inputs from anthropogenic sources and from weathering of bedrock in a watershed where mining was extensive. Hg isotopes will also be useful in the study of ore deposits.

Hg isotopic compositions might be used to explore for extremophile influences on mineralization in hydrothermal systems. Hg isotopic biosignatures might also identify

source rocks in sedimentary basin-hosted deposits, such as Mississippi Valley-type Pb-Zn deposits. Redox changes recorded in Hg isotopic compositions may prove similarly useful as Mo and Fe isotopes have been in the study of the evolution of the Earth's early atmosphere and oceans. The distinctive isotopic composition of vaporized Hg could be used to identify zones of paleo-boiling in ore deposits and provide insight on the tectonic and thermal evolution of a mineralized district, such as the enigmatic Carlin Trend in northern Nevada. All of these avenues of study have significant impact on the geological sciences and the way in which we understand hydrothermal systems.

**REFERENCES CITED**


Anbar, A.D., 2004, Iron stable isotopes: beyond biosignatures. Earth and Planetary Science Letters, v. 217, p. 223-236.

Anbar, A.D., Roe, J.E., Barling, J., and Nealson, K.H., 2000, Nonbiological fractionation of iron isotopes. Science, v. 288, p. 126-128.

Arnold, G.L., Anbar, A.D., Barling, J., and Lyons, T.W., 2004, Molybdenum isotope evidence for widespread anoxia in mid-Proterozoic oceans. Science, v. 304, p. 87-90.

Asael, D., Matthews, A., Bar-Matthews, M., and Halicz, L., 2007. Copper isotope fractionation in sedimentary copper mineralization (Timna Valley, Israel). Chemical Geology, v. 243, p. 238-254.

Barling, J., Arnold, G.L., and Anbar, A.D., 2001, Natural mass-dependent variations in the isotopic composition of molybdenum. Earth and Planetary Science Letters, v. 193, p. 447-457.

Beard, B.L., Johnson, C.M., Cox, L., Sun, H., Nealson, K.H., and Aguilar, C., 1999, Iron isotope biosignatures. Science, v. 285, p. 1889-1892.

Bergquist, B.A. and Blum, J.D., 2007, Mass-dependent and -independent fractionation of Hg isotopes by photoreduction in aquatic systems. Science, v. 318, p. 417-420.

Biswas, A., Blum, J.D., Lammers, A. and Douglas, T., 2008. Isotopic evidence for changing sources of mercury to the Arctic. Goldschmidt Conference Abstracts, p. A86.

Bullen, T.D., White, A.F., Childs, C.W., Vivit, D.V., and Schulz, M.S., 2001, Demonstration of significant abiotic iron isotope fractionation in nature. Geology, v. 29, p. 699-702.

Criss, R.E., 1999, Principles of stable isotope distribution. New York, Oxford University Press, 254 p.

Ellis, A.S., Johnson, T.M., and Bullen, T.D., 2002, Chromium isotopes and the fate of hexavalent chromium in the environment. Science, v. 295, p. 2060-2062.

Graham, S., Pearson, N., Jackson, S., Griffin, W., and O'Reilly, S.Y., 2004, Tracing Cu and Fe from source to porphyry: in situ determination of Cu and Fe isotope ratios in sulfides from the Grasberg Cu-Au deposit. Chemical Geology, v. 207, p. 147-169.

Halliday, A.N., Lee, D.C., Christensen, J.N., Walder, A.J., Freedman, P.A., Jones, C.E., Hall, C.M., Yi, W., and Teagle, D., 1995, Recent developments in inductively-

coupled plasma magnetic-sector multiple collector mass-spectrometry. International Journal of Mass Spectrometry and Ion Processes, v. 146, p. 21-33.

Hoefs, J., 2004, Stable Isotope Geochemistry. Berlin, Springer-Verlag, 201 p.

John, S.G., Rouxel, O.J., Craddock, P.R., Engwall, A.M., and Boyle, E.A., 2008. Zinc stable isotopes in seafloor hydrothermal vent fluids and chimneys. Earth and Planetary Science Letters, v. 269, p. 17-28.

Johnson, C.M., Beard, B.L., and Albarede, F., 2004, Overview and general concepts, *in* Johnson, C.M., Beard, B.L., and Albarede, F., eds., Geochemistry of Non-Traditional Stable Isotopes, Volume 55, Reviews in Mineralogy and Geochemistry, p. 1-24.

Kritee, K., Blum, J.D., Johnson, M.W., Bergquist, B., Barkay, T., 2007. Mercury stable isotope fractionation during reduction of Hg(II) to Hg(0) by mercury resistant bacteria. Env. Sci Tech, v. 41, p.1889-1995.

Marechal, C.N., Telouk, P., and Albarede, F., 1999, Precise analysis of copper and zinc isotopic compositions by plasma-source mass spectrometry. Chemical Geology, v. 156, p. 251-273.

Nielsen, S.G., Rehkamper, M., Teagle, D.A.H., Butterfield, D.A., Alt, J.C., and Halliday, A.N., 2006. Hydrothermal fluid fluxes calculated from the isotopic mass balance of thallium in the ocean crust. Earth and Planetary Science Letters, v. 251, p. 120-133.

Peters, E.K., 1991, Gold-Bearing hot-spring systems of the northern Coast Ranges, California. Economic Geology and the Bulletin of the Society of Economic Geologists, v. 86, p. 1519-1528.

Peters, E.K., 1993, $\delta^{18}O$ enriched waters of the Coast Range Mountains, Northern California; connate and ore-forming fluids. Geochimica et Cosmochimica Acta, v. 57, p. 1093-1104.

Rehkamper, M., Frank, M., Hein, J.R., Porcelli, D., Halliday, A., Ingri, J., and Liebetrau, V., 2002, Thallium isotope variations in seawater and hydrogenetic, diagenetic, and hydrothermal ferromanganese deposits. Earth and Planetary Science Letters, v. 197, p. 65-81.

Rehkamper, M., and Halliday, A.N., 1999, The precise measurement of Tl isotopic compositions by MC-ICPMS: application to the analysis of geological materials and meteorites. Geochimica et Cosmochimica Acta, v. 63, p. 935-944.

Rouxel, O.J., Bekker, A., and Edwards, K.J., 2005, Iron isotope constraints on the Archean and Paleoproterozoic ocean redox state. Science, v. 307, p. 1088-1091.

Rytuba, J.J., 1995, Cenozoic metallogeny of California, *in* Coyner, A.R.F., Patrick L, ed., Geology and ore deposits of the American Cordillera: Reno, NV, Geological Society of Nevada, p. 803-822.

Siebert, C., Nagler, T.F., and Kramers, J.D., 2001, Determination of molybdenum isotope fractionation by double-spike multicollector inductively coupled plasma mass spectrometry. Geochemistry Geophysics Geosystems, v. 2, paper number 2000GC000124.

Smith, C.N., Kesler, S.E., Klaue, B. and Blum, J.D., 2005. Mercury isotope fractionation in fossil hydrothermal systems. Geology, v. 33, p. 825-828.

Smith, C.N., Kesler, S.E., Blum, J.D., and Rytuba, J.J., 2008. Isotope Geochemistry of Mercury in Source Rocks, Mineral Deposits and Spring Deposits of the California Coast Ranges, USA. Earth and Planetary Science Letters, v. 269, p. 399-407.

Zheng, W., Foucher, D. and Hintelman, H., 2007. Mercury isotope fractionation during volatilization of Hg(0) from solution into the gas phase. Journal of Analytical Atomic Spectrometry, 22, 1097-1104.

Zhu, X.K., O'Nions, R.K., Guo, Y., Belshaw, N.S., and Rickard, D., 2000, Determination of natural Cu-isotope variation by plasma-source mass spectrometry: implications for use as geochemical tracers. Chemical Geology, v. 163, p. 139-149.

## CHAPTER II.

## HIGH PRECISION ANALYSIS OF NATURAL MERCURY ISOTOPE VARIATIONS BY COLD VAPOR MULTIPLE-COLLECTOR INDUCTIVELY COUPLED PLASMA MASS SPECTROMETRY


### Abstract

This paper presents our analytical method for the determination of high precision Hg isotope ratios by cold-vapor multiple-collector inductively-coupled-plasma mass-spectrometry (CV-MC-ICP-MS). Cold-vapor, or gaseous $Hg^0$, generation with $Sn^{2+}$ as the reducing reagent allows the fast and selective chemical separation of mercury from the sample matrix with an efficiency of >99.9%. Instrumental mass-bias is corrected using an internal thallium (Tl) spike (NIST 997) introduced as an aerosol to the sample gas flow as well as by sample-standard bracketing using a NIST 3133 solution matched in concentration and matrix to each sample. Data is presented in standard delta notation in permil relative to the NIST 3133 Hg standard. $\delta^{202}Hg$ values are calculated as:

$$\delta^{202}Hg = 1000*\{[(^{202}Hg/^{198}Hg)_{sample}]/[(^{202}Hg/^{198}Hg)_{NIST3133}]-1\}.$$

A method for removing Hg from complex geological matrices has been developed incorporating a two-stage furnace that employs sequential pyrolysis, combustion and liquid trapping of Hg in an oxidizing solution of $KMnO_4$. The oven method is >99% efficient in removing Hg from sample powders and the total procedural blank for the method is <20 pg Hg. Elements that produce significant chemical interferences with cold

vapor generation, such as Se, I, Au, Ag, Pt, and Ni are completely separated from Hg, allowing many different sample types to be analyzed. Typical internal precision of ±0.03‰ (2SE) was achieved for $^{202}Hg/^{198}Hg$ ratios on a daily basis. The results of repeated analysis of NIST 3133 and Almadèn elemental Hg show a long-term external precision for $\delta^{202}Hg$ of better than ±0.08 ‰ (2SD, n=43). The external reproducibility of natural samples in a variety of geologic matrices is better than ±0.09 ‰ (2SD, n=60). High precision analyses were obtained with as little as 50 ng of Hg. Samples of a variety of ore deposit types analyzed show a range of fractionation greater than 5‰ in $\delta^{202}Hg$, or 1.25‰ $amu^{-1}$, which is similar to the variations observed in the Fe, Se, Zn, Sb and Tl isotopic systems. Such variation in Hg isotopic compositions may be exploited as a useful geological and biogeochemical tracer.

## 1. Introduction

The study of Hg has wide ranging implications because of its bioaccumulation, toxicity and role as a global pollutant, as well as its extreme mobility during natural geologic processes, especially those involving hydrothermal systems. Of particular interest is the potential application of Hg isotopic variations to provide new insights into the processes that account for Hg mobility and the sources from which it is derived. Recent studies employing multiple-collector inductively-coupled-plasma mass-spectrometry (MC-ICP-MS) have revealed important information on the isotopic composition of Hg in terrestrial systems (Klaue et al., 2000; Evans et al., 2001; Hintlemann and Lu, 2003; Jackson et al., 2004; Smith et al., 2005; Foucher and

Hintelmann, 2006; Kritee et al., 2007; Bergquist and Blum, 2007; Jackson et al., 2008), particularly in hydrothermal ore deposits.

High precision measurements of transition metal stable isotope ratios have been made over the last 10 years following the development of MC-ICP-MS technology (see reviews by Halliday et al., 1998; Johnson et al., 2004). Thermal ionization is extremely inefficient for elements with high first ionization potentials (e.g. Zn, Se, Hg) making isotope ratio measurements by TIMS difficult or impossible. This obstacle is overcome by the ionizing efficiency of the plasma source in MC-ICP-MS instruments.

Recent investigations using this new generation of mass spectrometers have found variations that range over several per mil for the isotope ratios of Fe (Anbar et al., 2000; Bullen et al., 2001), Cr (Ellis et al., 2002), Cu (Marechal et al., 1999; Zhu et al., 2000), Mo (Barling et al., 2001; Seibert et al., 2001) and Tl (Rehkamper and Halliday, 1999; Rehkamper et al., 2002). Both biotic and abiotic processes have been shown to cause fractionation (Beard et al., 1999; Anbar et al., 2000; Bullen et al., 2001). These new isotope systems have thus far been used to determine the extent of $Cr^{6+}$ reduction in a contaminated aquifer (Ellis et al., 2002) and to provide constraints on the redox state of the Archean and Proterozoic oceans using Mo and Fe isotopes (Arnold et al., 2004; Rouxel et al., 2005). Graham et al. (2004) used Fe and Cu isotope ratios to infer the source of metals in the Grasberg porphyry Cu-Au complex. Recent studies of Hg isotopes have proven the system to be a similarly useful tool in the geosciences (Bergquist and Blum, 2007; Jackson et al., 2008; Kritee et al., 2007; Smith et al., 2005, 2008; Xie et al., 2005).

Hg has seven naturally occurring stable isotopes, $^{196}Hg$, $^{198}Hg$, $^{199}Hg$, $^{200}Hg$, $^{201}Hg$, $^{202}Hg$, and $^{204}Hg$ with relative abundances of 0.15%, 10.04%, 16.94%, 23.14%, 13.18%, 29.74% and 6.82% respectively (Blum and Bergquist, 2007). This large span of masses among its stable isotopes ($\Delta m/m_{avg} = 4\%$), along with its high volatility, multiple redox states and ability to form bonds of a covalent nature, suggest that it may undergo isotopic fractionation in nature (Nier, 1950; O'Neil, 1986). In particular, the high volatility and multiple redox states of Hg should cause variations in Hg isotopic compositions in low temperature hydrothermal systems and in the environment (Smith et al., 2005, 2008).

The dominant forms of Hg in nature are as $Hg^0$, ionic $Hg^{2+}$ and methyl ($CH_3Hg^+$) and dimethyl Hg ($(CH3)_2Hg^{2+}$). In geothermal systems most Hg occurs as $Hg^0_{aq}$ or as $Hg^0_g$ where hydrothermal fluids have boiled and separated a gas phase (Varekamp and Buseck, 1984; Christenson and Mroczek, 2003). In S-rich fluids associated with ore-forming hydrothermal systems, Hg is predominantly complexed with bisulfide ligands (Barnes and Seward, 1997), and in sedimentary basins Hg can be found complexed with organic species and dissolved in petroleum (Krupp, 1988; Fein and Williams-Jones, 1997). In the environment, Hg is mobilized as $Hg^0$ and deposited from the atmosphere as ionic $Hg^{2+}$ or as particulate Hg (Fitzgerald, 1993). In biological systems, methyl Hg ($CH_3Hg^+$), a toxic form of Hg, is bioaccumulated in aquatic food webs (Barkay, 2000).

Low temperature geochemical and biological processes have been shown to cause mass dependent fractionation of metal stable isotopes (see review by Johnson et al., 2004). Redox reactions resulting from biotic and abiotic processes are important mechanisms in the fractionation of Fe (Anbar et al., 2000; Bullen et al., 2001; Wiesli et

al., 2003), Cr (Ellis et al., 2002), and Cu (Marechal et al., 1999). The geochemistry of Hg is unique in that the reduction process also induces a phase change:

$$Hg^{2+}_{aq} \rightarrow Hg^{0}_{aq} \rightarrow Hg^{0}_{g}. \quad (1)$$

In the near surface environment, the $Hg^0$ species is strongly partitioned to the gas phase and significant mass-dependent fractionation is expected to occur with this phase change (Smith et al., 2005; Chapter III, IV). Photoreduction of $Hg^{2+} \rightarrow Hg^0$ has been shown to cause both mass-dependent and mass-independent fractionation of Hg isotopes in biogeochemical systems (Kritee et al., 2007; Bergquist and Blum, 2007).

Few studies of Hg isotope ratios have been published thus far. Recent analyses of Hg isotopic compositions in a fossil hydrothermal system show mass dependent variations of up to 5 ‰ in $\delta^{202}Hg/^{198}Hg$ values that can be correlated with zones of boiling and Hg host mineralogy (Smith et al., 2005; Chapter III; Chapter IV). Similar Hg isotopic variations have been measured in other ore deposits (Klaue and Blum, 2000; Hintelmann and Lu, 2003; Smith et al., 2004, 2008), coal and coal flyash (Evans et al., 2001), fish and sediment cores (Bergquist and Blum, 2007; Foucher and Hintelmann, 2006; Jackson et al., 2008) and biological reference materials (Xie et al., 2005). Carbonaceous chondrites were found to have Hg isotopic compositions similar to terrestrial values (Lauretta et al., 2001).

One of the challenges to high precision Hg isotope analysis is the very low (sub-ng) concentrations of Hg in many types of environmental samples such as natural waters and atmospheric aerosols. Recent studies have tried to obtain reproducible analyses for low Hg samples using transient signals derived from the thermal release of small amounts (~1 ng) of Hg (Evans et al., 2001; Xie et al., 2005). While this approach may potentially

produce high quality data as the pre-concentration step in the process is further refined, thus far no reproducible Hg isotope ratios from natural samples have been obtained by this method.

The method described here focuses on deriving a steady state signal by cold vapor generation of natural samples in an analysis routine that typically consumes 50 to 100 ng of Hg. In this study, we report high precision analyses of Hg isotopic compositions from analyses of standard reference materials and ore deposits using CV-MC-ICP-MS. The ±0.09 ‰ (2SD) external precision of natural samples using our method is an order of magnitude lower than previously published studies of Hg isotope analysis (Evans et al., 2001; Xie et al., 2005; Foucher and Hintelmann, 2006). Isotopic compositions that we have measured so far have a range that is more than 50 times the external reproducibility (2SD) of the measurements.

The advantage of this technique over the transient signal approach is the robustness of the analysis in both the internal and external precision of the measurement. Using cold vapor generation, high precision analyses of solutions containing as little as 10 ng Hg are possible. This then presents the possibility of analyzing even low level environmental samples with modest sample preparation techniques involving pre-concentration of samples by transfer of Hg from gold traps into solution.

A method for quantitative extraction of Hg from the matrix of ore and other complex samples rich in elements known to interfere with cold vapor generation is also presented. This method employs sequential pyrolysis, combustion and liquid trapping of Hg in an oxidizing solution of $KMnO_4$. Isotopic data from standard reference materials are presented and the potential for the use of Hg isotopes as geologic tracers is discussed.

## 2. Analytical Methods

### 2.1 Reagents

All standard, reagent and sample solutions were prepared with 18 MΩ double deionized water (DDI) (Millipore®). Glassware and Savillex® PFA vessels were cleaned with trace metal grade nitric acid, bromine monochloride and deionized water before use. High purity HCl and $HNO_3$ (Seastar®) acids were used in sample digestions. Bromine monochloride 1% (w/v) was prepared with reagent grade potassium bromide (Baker®), potassium bromate (Baker®), and high purity HCl and used for sample dilution. Potassium permanganate 1% (w/v) was prepared daily from reagent grade potassium permanganate (Alfa Aesar®) and high purity $H_2SO_4$ (Seastar®). Hydroxylamine hydrochloride (Baker®) 1% (w/v) was prepared with DDI water. A reducing solution of stannous (II) chloride 2% (w/v) used in cold vapor generation was prepared as needed from reagent grade stannous chloride (Baker®) in 1M HCl (Fisher® trace metal grade) and purged with Ar for one hour before use.

### 2.2 Sample Preparation

#### 2.2.1 Acid Dissolution

Samples were decomposed for analysis using either acid dissolution or combustion, depending on the concentration of Hg in the sample and the composition of the sample matrix. Cinnabar and most sulfide minerals containing high concentrations of Hg and low concentrations of Au, Ag, Cu, Se and I were digested in acids. Sample powders (~0.05 - 0.10 g) were weighed into 15 mL Teflon® (PFA) vessels and a 3:1 mixture of concentrated HCl/$HNO_3$ was added. The vessels were tightly capped and

placed on a hot plate at 90 °C overnight. The acidic solution was centrifuged and the supernatent was removed from the undissolved residues, which typically consisted of silicate and oxide minerals that contain negligible amounts of Hg. The digested samples were stored in borosilicate glass vials with PFA lined caps to retain Hg in solution.

2.2.2 Thermal Release

Samples that contain Se and I at concentrations as low as 50 ppm can generate chemical interferences with cold vapor generation by $Sn(II)Cl_2$ (Welz, 1985) and Hg must therefore be separated from these elements for efficient cold vapor generation. This separation was accomplished by sequential pyrolysis and combustion in a linear tube furnace apparatus (Fig. 2-1) using a step heating procedure.

Powdered samples were weighed into glazed ceramic boats that were first baked in a muffle furnace at 800 °C to remove any Hg blank and loaded into the first segment of the linear furnace. The furnace consists of a 28 mm I.D. quartz glass tube of 1 mm thickness with two chambers connected by a 1.5 mm orifice. The two chambers were wrapped with approximately 10 cm and 15 cm of insulated 18 gauge Nichrome resistance wire and surrounded with Ni foil acting as a shield. A type K thermocouple was inserted into the interior of the shield of the first chamber and heating was controlled by a Barnant® temperature controller (London, Canada).

The first segment was heated in an argon stream of 80 mL $min^{-1}$ with a two-stage program, ramping to 500 °C in 5 min and holding for 5 min and then ramping to 800 °C in 5 min and holding for 5 min. Thermal release profiles show that most Hg is released during the heating to 500 °C. Heating to 800 °C further ensures complete release of Hg

from the sample as well as removing any potential Hg blank from the pyrolysis chamber prior to subsequent analyses.

The Ar stream carrying the pyrolysis products was passed through a 1.5 mm heated orifice into the second segment of the furnace, which was kept at a constant 1000 °C. At the entrance to the second chamber a stream of oxygen was introduced at 100 mL $min^{-1}$ to provide complete oxidation of the pyrolysis products. The furnace gas was introduced to a 1% potassium permanganate trapping solution using a glass impinger in a tall, narrow flask that allowed gas bubbles to react thoroughly with the solution. $Hg^0$ from the gas stream was efficiently trapped in the solution as non-volatile $Hg^{2+}$. The trapping solution was then treated with hydroxylamine hydrochloride until manganese oxides are dissolved leaving a clear solution ready for dilution and analysis.

Liquid trapping is a common method for sampling flue gases with relatively high concentrations of Hg in industrial settings (EPA 7470). The advantages of liquid trapping of Hg over other approaches were established by experimenting with the pyrolysis and combustion of a variety of geological and biological materials including coal, coal fly ash, dogfish muscle and ore deposit samples. The release of abundant gases and water vapor during the decomposition of samples, especially coal and biological samples, was found to foul cold trapping devices. Acidic trapping solutions alone are not effective when employed as a single trap. Other types of solutions capable of oxidizing gaseous Hg, such as bromine monochloride (BrCl), react quickly with the $O_2$ in the combustion gases, degrading their oxidizing efficiency. Liquid trapping using a 1% potassium permanganate ($KMnO_4$) solution acidified with 10% ultra pure $H_2SO_4$ was found to have

the lowest Hg blank (~ 20 pg) and highest trapping efficiency. Initial tests that employed multiple $KMnO_4$ traps found that a single trap was > 99% effective.

One of the drawbacks of the $KMnO_4$ trapping solution is a suppression of the Hg signal relative to BrCl when analyzing Hg by cold-vapor MC-ICP-MS. While the trapping and release of Hg is still quantitative from the $KMnO_4$, there is a ~30% reduction in sensitivity when analyzing Hg in a $KMnO_4$ matrix. This reduction in signal intensity may be due to matrix effects associated with the hydroxylamine solution used to reduce the $KMnO_4$ solutions prior to analysis. To avoid the possibility of matrix effects standards and samples were matched in either BrCl or $KMnO_4$ matrices. The concentrations of Hg in standards and samples were also matched to within ± 5% because of the effects of analyte concentration on the precision of measured $\delta^{202}$Hg values.

2.3 Standards and Spikes

A Hg standard solution (NIST 3133) from the National Institute of Standards and Technology was selected for use as a reference standard for reporting Hg isotopic values. Additionally, a laboratory standard was prepared from elemental Hg produced at the Almadèn mine (Castilla La Mancha, Spain), to monitor long-term external precision of the isotopic composition relative to the NIST 3133 standard. Of the few geologic materials available that have certified Hg chemical abundances, we chose NIST SRM 1633b trace elements in coal fly ash (141 ppb Hg) to calibrate the efficiency of our sample preparation procedures.

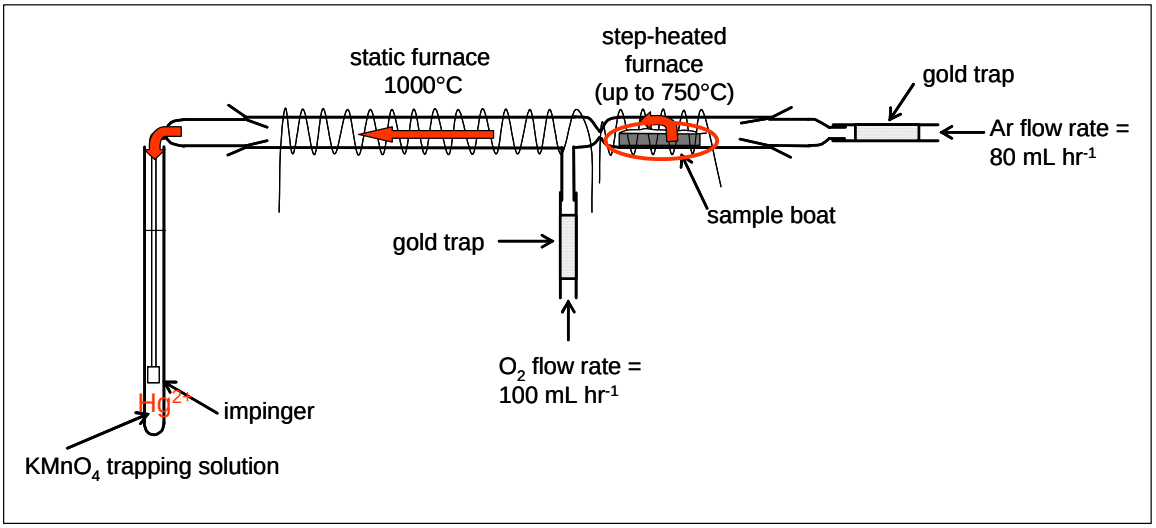


Figure 2-1. Furnace apparatus used in the pyrolysis and combustion of samples. Sample material is loaded into glazed ceramic boats and placed in the pyrolysis chamber. Step heating releases $Hg^0$ into a flow of inert Ar that carries sample gases into the combustion chamber where gases are oxidized at 1000˚C. Combustion gases then flow into an oxidizing $KMnO_4$-$H_2SO_4$ solution where $Hg^{2+}$ is trapped and other gases are released to the atmosphere.

## 2.4 Mass Spectrometry

### 2.4.1 Instrumentation

Hg isotopic ratios were measured on a Nu Instruments (Wrexham, UK) Nu-Plasma double focusing magnetic sector inductively-coupled-plasma mass-spectrometer equipped with 12 fixed faraday collectors (Belshaw, 1998). The instrument has a variable zoom ion optics system that optimizes peak shapes and coincidence on a fixed detector array allowing optimal mass dispersion. Normal operating conditions for the mass spectrometer are summarized in Table 2-1. The signals of Hg (196, 198, 200, 201, 202, and 204), Tl (203, 205) and Pb (206) were simultaneously monitored in static mode (Table 2-2).

### 2.4.2 Cold-vapor introduction

The continuous-flow, cold-vapor (CV) generation apparatus consists of a frosted-tip liquid-gas separator modified from the design of Klaue and Blum (1999; Fig. 2-2). A solution of 2% Sn(II)$Cl_2$ in 1 M HCl is used to reduce $Hg^{2+}$ in the sample solution to $Hg^0$. The sample solution and the reducing $Sn^{2+}$ solution are mixed online and pumped into the gas-liquid separator. The $Hg^0$ vapor separated from the liquid is then swept into the plasma source of the MC-ICP-MS by a continuous flow of argon. As this process is > 99% quantitative, the Hg that is swept into the plasma is not measurably fractionated given the analytical uncertainty of the method (± 0.09 ‰).

Table 2-1 Instrument operating conditions and signal measurement parameters.

| | |
|---|---|
| RF power | 1400 W |
| Plasma gas flow rate | 32 L/min |
| Interface cones | nickel |
| Accelerating voltage | 4 kV |
| Ion lens setting | Optimized for max. intensity |
| Instrument resolution | ~300 |
| Mass analyzer pressure | $2 \times 10^{-9}$ mbar |
| Detector | 12 Faraday collectors |
| Nebulizer | microconcentric |
| Spray chamber temp. | 110 ºC |
| Desolvator temp. | 160 ºC |
| Sweep gas (argon) | 3.7 L/min. optimized daily |
| Sample uptake rate | 0.7 mL/min. |
| Typical sensitivity | 200 V/ppm Hg |
| Sampling time | two repetitions of 200 s |
| Background time | 20 s |

Table 2-2 Faraday collector assignment.

| H4 | H3 | H2 | H1 | Ax | L1 | L2 | L3 | L4 |
|---|---|---|---|---|---|---|---|---|
| $^{206}Pb$ | $^{205}Tl$ | $^{204}Hg$ | $^{203}Tl$ | $^{202}Hg$ | $^{201}Hg$ | $^{200}Hg$ | $^{198}Hg$ | $^{196}Hg$ |

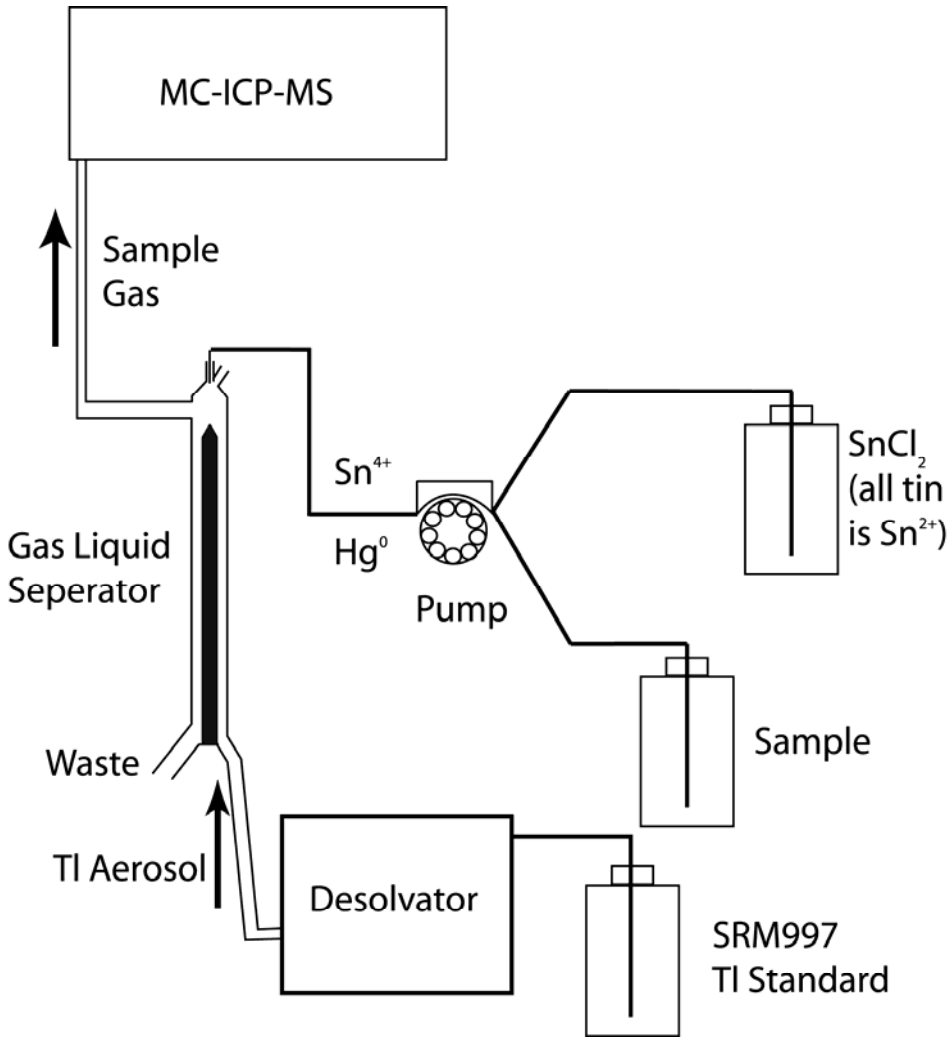


Figure 2-2. Schematic illustration of the gas-liquid separator. Modified from the design of Klaue and Blum (1999).

One advantage of CV generation using $Sn(II)Cl_2$ is that it does not cause the reduction of other metals typically present in geologic samples. However, Se and I have strong effects on the reduction reaction and as little as 50 ppm Se can result in inefficient generation of $Hg^0$ vapor (Welz, 1985). An alternative reductant, sodium tetrahydridoborate, has the disadvantage that it can reduce metals such as Au, Ag, Cu and Ni, creating fine precipitates in the sample introduction tubing that may retain Hg (Anderson, 2000). These metals are also common in many ore deposits in quantities great enough to pose a significant analytical interference and therefore sodium tetrahydridoborate should be avoided as a reductant. Due to the common presence of Se, Au and Ag in epithermal precious metal vein deposits there is the possibility for inefficient $Hg^0$ vapor generation using either type of reductant. In this study, samples that contain both Se and metals were processed by thermal release to separate the Hg from the complex sample matrix as described in section 2.2.2.

2.4.3 Mass Interferences

Mass spectral interferences with $^{196}Hg$, $^{198}Hg$ and $^{204}Hg$ are possible from the isobars $^{196}Pt$, $^{198}Pt$, and $^{204}Pb$. Molecular interferences are possible for $^{198}Hg$, $^{199}Hg$, $^{200}Hg$, $^{202}Hg$, and $^{204}Hg$ from the oxides $^{182}WO$, $^{183}WO$, $^{184}WO$, $^{186}WO$ and the hydride $^{203}TlH$. The cold vapor generation process avoids these potential interferences, by separating Hg vapor from the sample solution in the gas-liquid separator (Fig. 2-2), leaving other metals and oxides in solution. The potential TlH interference from the Tl external standard is minimized by the use of a desolvation unit (Fig. 2-2). The level of any of the potential spectral interferences are very low relative to the Hg signal and in all cases, were below detection in the mass scan after CV sample introduction.

2.4.4 Mass Bias Correction

Instrumental mass fractionation was corrected using the NIST SRM 997 Isotopic Standard for Thallium as an internal standard. This technique has been employed routinely in the analysis of Pb isotopes by ICP-MS (Walder and Furuta, 1993; Hirata, 1996; Rehkamper and Halliday, 1998). The SRM 997 standard was diluted to 75 ppb in a 5% $HNO_3$ solution and introduced by free aspiration to a CETAC Airdus desolvation unit by a MCN-2 micro-concentric nebulizer (Omaha, Nebraska). The dry Tl aerosol was mixed with the sample stream in the gas-liquid separator (Fig. 2-2) and swept into the plasma.

The measured Hg isotope ratios were corrected based on the measured Tl isotope ratios using a power law fractionation function (Hirata, 1996; Habfast, 1998; Rehkamper and Halliday, 1998; Marechal et al., 1999; White et al., 2000; Lauretta et al., 2001). The certified $^{205}Tl/^{203}Tl$ value for NIST 997 is 2.38714 and the fractionation factor used for correction based on this certified value is:

$$f = \ln(^{205}Tl/^{203}Tl_{true}/^{205}Tl/^{203}Tl_{obs})/\ln(M_{205}/M_{203}),$$

and Hg isotope ratios are corrected from this certified value according to:

$$^{202}Hg/^{198}Hg_{true} = (^{202}Hg/^{198}Hg)_{obs}\,(M_{202}/M_{198})^{f},$$

where $M_i$ is the atomic mass of the isotope of interest. Standard-sample bracketing alone compensates for mass bias by comparing the signal intensities of standard and sample under identical instrument operating conditions.

The inter-element fractionation correction is mainly intended to improve the accuracy of MC-ICP-MS measurements. Deltas calculated from standard bracketed samples ensure that instrumental fraction effects are negligible under stable instrument

operating conditions. The Tl external correction is a well-established method for lead isotopic measurements, but even for the chemically and electronically similar elements Tl and Pb, the external correction yields absolute ratios that are slightly different from the certified values (Rehkaemper and Halliday, 1998). Addition of an isotopically enriched double-spike by the method of isotope dilution is necessary if the highest levels of accuracy for isotope ratios are required (Dodson, 1963).

2.4.5 Data Acquisition and Presentation

The sample introduction system was operated by computer control of a Gilson autosampler (GL-222) (Middleton, Wisconsin) with standards, samples, blanks and washes automatically selected during batch runs. Blanks due to memory effects of the gas-liquid separator were typically below 1-10 mV on $^{202}Hg$ after a 5 minute DDI water wash cycle between sample runs, depending on the previous sample concentration. Blanks were typically <0.1% of the total signal intensity. Data was acquired in 2 blocks of 20 measurements with 10 second integration times, and 30 second background measurements were made prior to each block. Internal precision of the measurement was typically better than ± 0.01 ‰ for 40 ratios measured.

All samples were analyzed with standard runs bracketing two runs of the sample and a blank measurement was made after each bracketing run. The reported δ for each ratio is the mean of the two sample analyses, relative to the mean of the bracketing standards. Hg isotope ratios are reported in δ per mil notation relative to the NIST 3133 standard :

$$\delta^{202}Hg = 1000*\{[(^{202}Hg/^{198}Hg)_{sample}]/[(^{202}Hg/^{198}Hg)_{3133}]-1\}.$$

The $^{202}Hg/^{198}Hg$ ratio was selected to report Hg isotopic data because this ratio offers the best balance between precision, which decreases with increasing mass difference, and a 4 amu mass difference, which accentuates the variation in isotopic composition. Other Hg isotope ratios would also be suitable for data reporting (e.g. $^{202}Hg/^{200}Hg$), although $^{196}Hg$ is of low abundance (0.15%) and $^{204}$-Hg suffers from a potential isobaric interference by $^{204}Pb$, and should not be referenced in the reporting of Hg isotope ratios. The odd isotopes, $^{199}Hg$ and $^{201}Hg$, are affected by mass-independent fractionation and are not suitable for reporting mass-dependent fractionation (Bergquist and Blum, 2007).

## 3. Results

### 3.1 Isotopic composition of Terrestrial Hg

This study demonstrates that the isotopic abundance of terrestrial Hg varies by as much as 5 ‰ (Table 2-3; Chapter III). Thus, there is no single terrestrial Hg isotopic composition. Results from this author's recent studies of Hg isotopes indicate that isotopic fractionation occurs among natural reservoirs of Hg and the results listed in Table 2-3 should be viewed in light of this. The $^{202}Hg/^{198}Hg$ reported by Neir (1950) and Zadnik (1989) differ by 7.1 ‰, which is greater than observed magnitude of fractionation in natural samples as yet reported (Smith et al., 2005; Chapter III) and is likely due to a combination of analytical uncertainty and variations in the isotopic composition of terrestrial Hg measured by each study. Our isotopic abundances are closer to those of Neir (1950) than Zadnik (1989) and this may reflect the similarity of Almaden Hg with the Hg analyzed by Neir. The isotopic composition of Almaden Hg determined by this study is 0.9‰ heavier than previously determined by Lauretta et al. (2001) when both

results are considered relative to the NIST 3133 Hg standard ($\delta^{202}Hg_{NIST3133} = \delta^{202}Hg_{Alm}$ - 0.55 ‰). This difference is attributed to the more robust analytical method presented here as well as the demonstrated high external precision of the method compared to the much greater 0.2 to 0.5 ‰ external reproducibility of the results of Lauretta et al. (2001).

3.2 Analysis of Standard Solutions

To investigate the long-term reproducibility of our Hg isotope ratio measurements by MC-ICP-MS, we analyzed the NIST 3133 Hg standard and Almadèn purified Hg product throughout our analytical sessions. The long-term reproducibility of isotopic ratio measurements by MC-ICP-MS are strongly affected by long and short-term variations in instrumental mass bias. Data reported as δ values is preferred as the relative difference between the two values shows much less variation than the individual ratios over time. The reproducibility of the $\delta\ ^{202}Hg$ between the Almadèn and NIST 3133 standard solutions was –0.55 ±0.08‰ (2σ) based on 43 measurements over 5 months (Fig. 2-3). The internal precision of data blocks of 20 measurements is better than 0.05‰ (2SE) on all ratios except for $^{204}Hg/^{196}Hg$, the ratio with the largest mass difference and lowest isotope abundances. Typical in-run precision of better than ±0.05‰ (2SD), based on the deviation between bracketing standard runs, can be achieved on a daily basis. In-run precision is an important measure of the quality of an individual measurement as poor in-run precision can indicate problems with the cold vapor generation process.

Table 2-3 Terrestrial Hg Isotopic Abundances

| | IUPAC 1983[a] | IUPAC 1989[b] | Lauretta et al., 2001[c] | This study[d] | This study[e] |
|---|---|---|---|---|---|
| $^{202}Hg/^{196}Hg$ | 203.660 | 194.5525 | 192.9385 | 193.5615 | 193.6432 |
| $^{202}Hg/^{198}Hg$ | 2.9744 | 2.9958 | 2.965071 | 2.967906 | 2.968982 |
| $^{202}Hg/^{199}Hg$ | 1.7699 | 1.7699 | 1.756512 | n.a.[†] | n.a.[†] |
| $^{202}Hg/^{200}Hg$ | 1.2885 | 1.2930 | 1.285892 | 1.286367 | 1.286612 |
| $^{202}Hg/^{201}Hg$ | 2.2538 | 2.2655 | 2.258815 | 2.258296 | 2.258815 |
| $^{204}Hg/^{202}Hg$ | 0.2299 | 0.2299 | 0.229467 | 0.229422 | 0.22917 |

[a]based on Neir (1950)
[b]based on Zadnik (1989)
[c]Almaden Hg product measured on a Fisons P54 MC-ICP-MS
[d]Almaden Hg product measured on a Nu Plasma MC-ICP-MS
[e]NIST 3133 Hg standard measured on a Nu Plasma MC-ICP-MS
[†] $^{199}Hg$ is not routinely measured in our method due to the fixed collector configuration of the Nu Plasma (see Table 2-2)

### 3.3 Reproducibility of Natural Samples

Repeated Hg isotope analyses of several cinnabar and native Hg ore samples were used as internal standards to characterize the external reproducibility of the analytical technique for natural samples. Each value reported is from a separate aliquot of dissolved sample analyzed over the period of this study. Sample SC-2 is Hg ore from the Silver Cloud Hg mine, Elko County, Nevada and is composed of microcrystalline silica sinter with cinnabar (HgS) mineralization. Sample NMNH 15107-2 is Hg ore from the New Almaden mine, Santa Clara County, California and contains cinnabar replacing sandstone. Sample NMNH 98616-3 is also from the New Almaden mine, and contains cinnabar associated with silica-carbonate alteration of serpentinite. The 2SD reproducibility of these three natural samples was ±0.06‰ (n = 8), ±0.09‰ (n = 26), and ±0.09‰ (n = 26) respectively (Fig. 2-4)(Table 2-4). Therefore a conservative estimate of external precision for our method based on these replicate analyses is ±0.1‰ (2SD). When the $^{202}Hg/^{198}Hg$ and $^{202}Hg/^{200}Hg$ ratios for these data are plotted in a 3-isotope diagram, the analyses lie along a single mass fractionation line ($r^2$ = 0.9994), demonstrating the mass dependency of Hg isotope fractionation in these hydrothermal ore deposit samples (Fig. 2-5). Instrumental mass bias in the mass range of Hg is on the order of 3%, favoring the extraction of heavier Hg and Tl ions from the plasma, and Tl-corrected ratios are correspondingly lighter than the raw data (Fig. 2-6). The tighter cluster of values of the corrected ratios also shows that Tl-correction provides more accurate reported ratios.

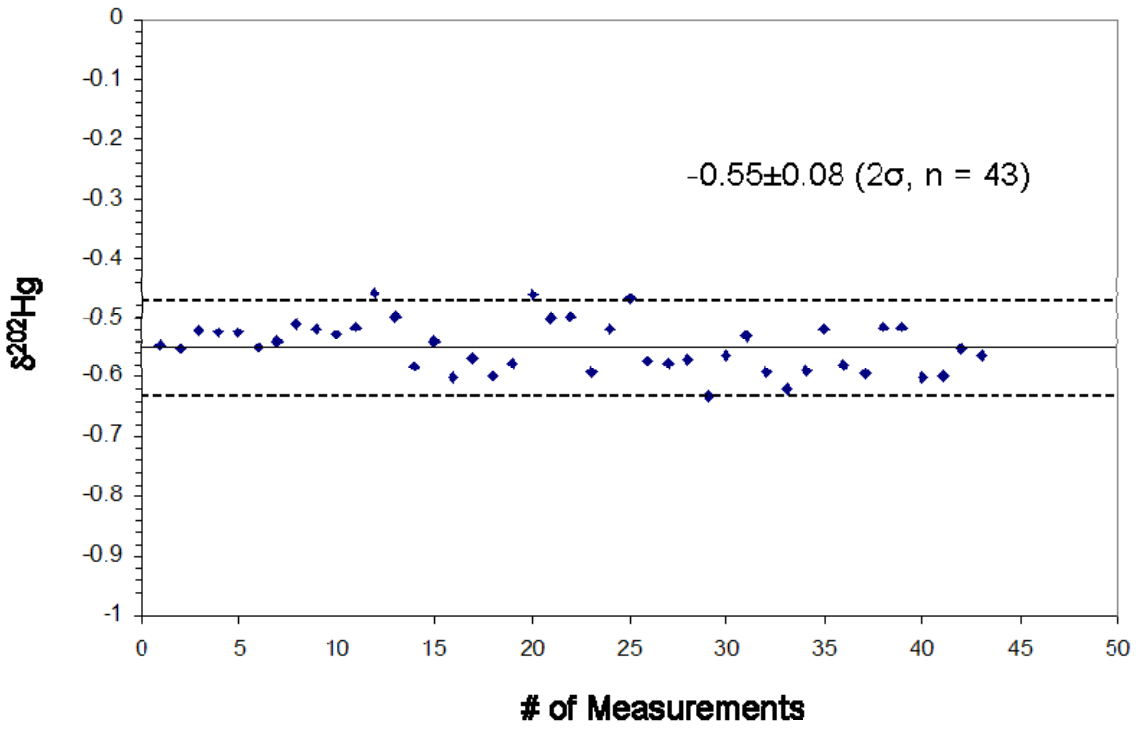


Figure 2-3. External precision of the method. Demonstrated by the long-term reproducibility of the NIST 3133 Hg standard relative to the Michigan Almadèn standard (-0.55±0.08 ‰ (2SD) $\delta^{202}$Hg).

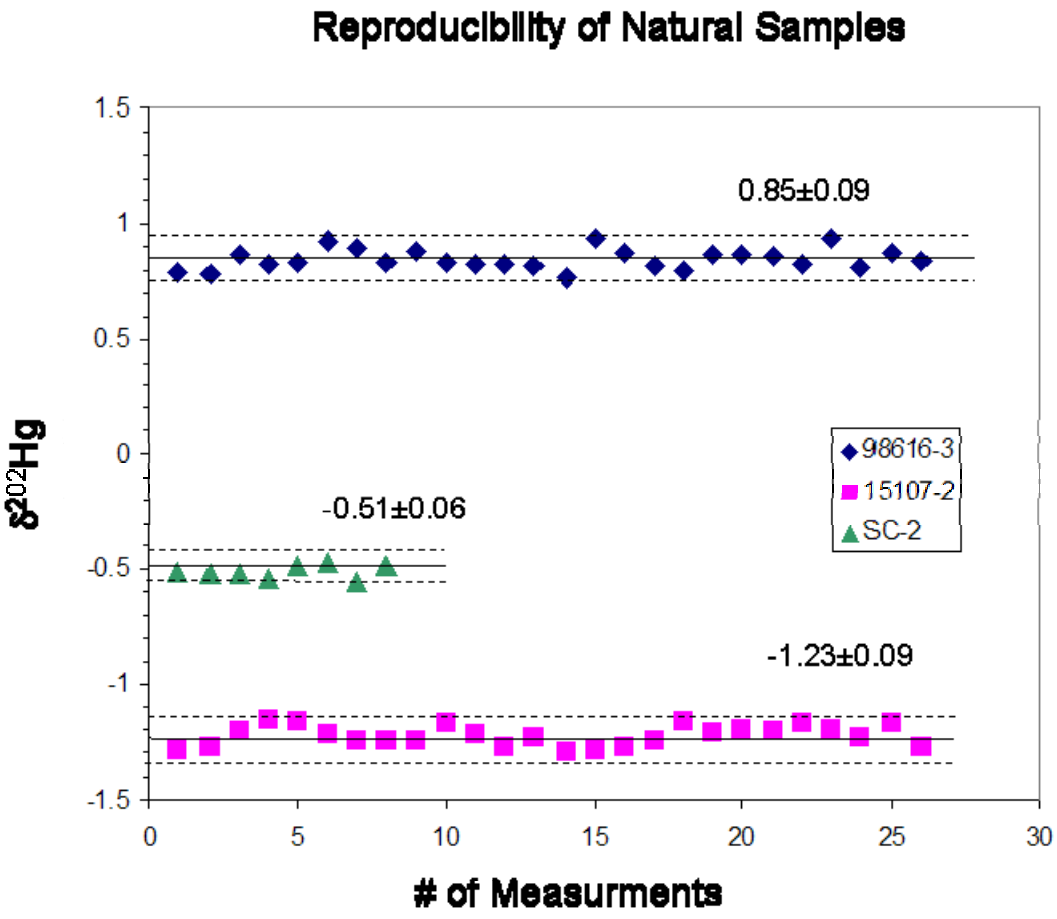


Figure 2-4. Long-term external reproducibility of natural ore deposit samples. Average $\delta^{202}$Hg and uncertainty expressed as 2 SD of the mean shown for each sample.

Recent studies report mass independent fractionation (MIF) processes can affect the natural distribution of odd mass Hg isotopes ($^{199}Hg$, $^{201}Hg$) (Bergquist and Blum, 2007; Jackson et al., 2008). Photoreduction of aqueous Hg species has been shown to cause significant MIF excursions from the expected mass dependent fractionation (MDF) behavior. Physical and chemical processes known to be active in the formation of ore deposits are almost exclusively mass dependent in nature, and do not include photochemical reactions that can produce MIF, as a result, little MIF is expected in ore samples. The expected $\delta^{201}Hg$ values for the three ore samples presented here show very little variation from the MDF line (Fig. 2-7). A quantification of MIF as $\Delta^{201}Hg$ is calculated by the approximation:

$$\Delta^{201}Hg = \delta^{201}Hg - (\delta^{202}Hg - 0.752)$$

and shows virtually no significant excursions from the expected MDF values (Fig. 2-7).

3.4 Analysis of Standard Reference Materials

Several standard reference materials that are widely available were analyzed to investigate Hg isotopic variations among organic and inorganic commercial products and to promote inter-laboratory correlation of Hg isotopic compositions (Table 2-5). Hg in coal (NIST 1630) is contained in sulfides as $Hg^{2+}$ and coal fly ash (NIST 1633b) as $Hg^{2+}$ in silicate mineral residues and amorphous glass. Dogfish muscle (NRCC DORM-2) contains 95% methyl-Hg. Values reported here for DORM-2 agree closely with those measured by Bergquist and Blum (2007).

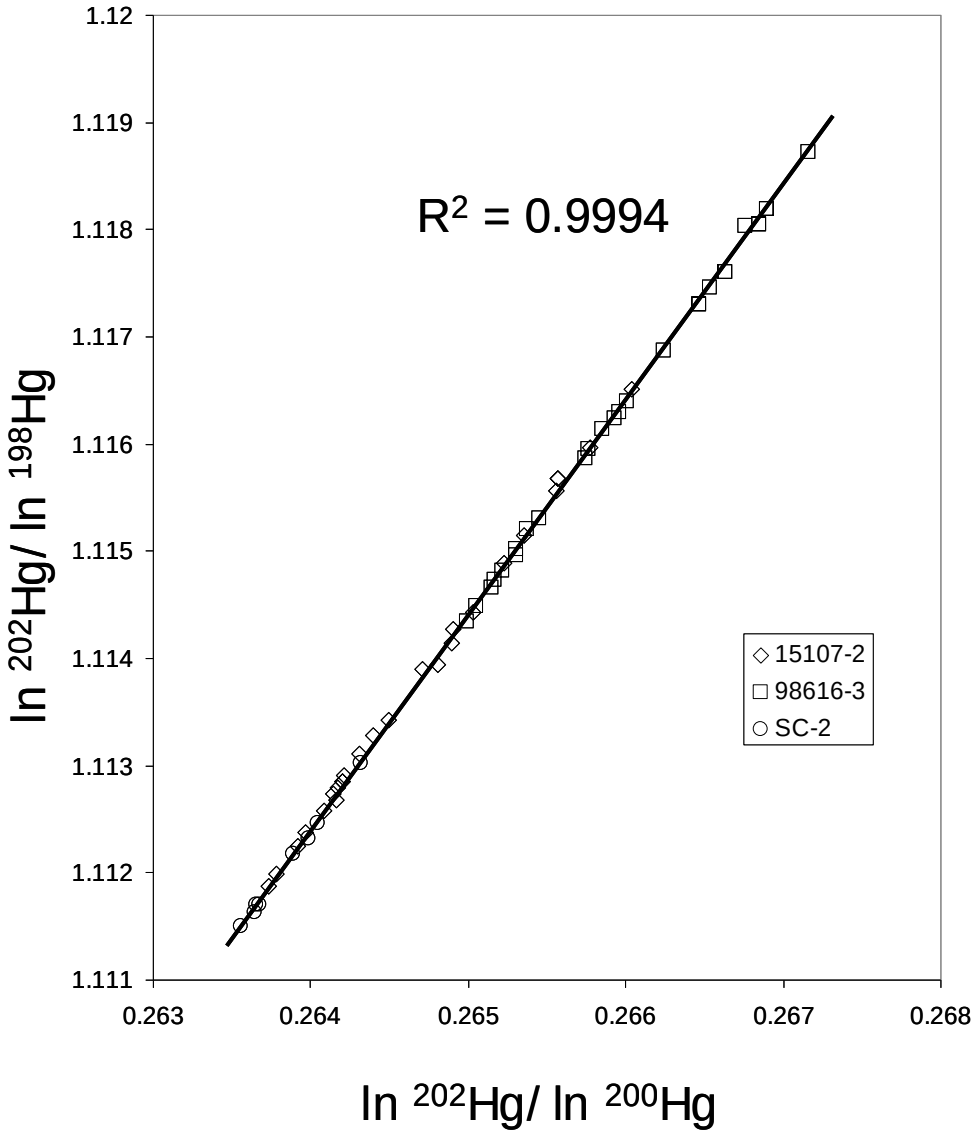


Figure 2-5. Three isotope diagram with raw data from Figure 2-4 plotted. All samples fall along a single mass-dependent fractionation line.

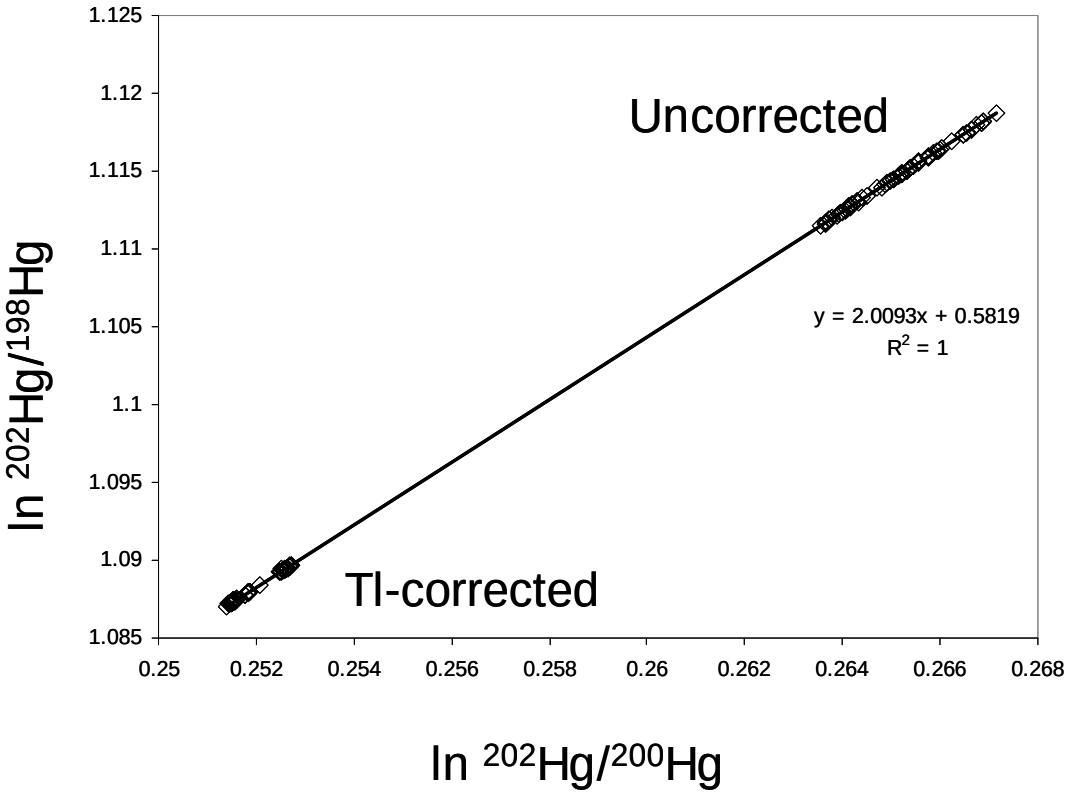


Figure 2-6. Tl-corrected ratios from Figure 2-5 plotted on a 3 isotope diagram. Corrected values are lighter because of the preferential extraction of heavy ions into the mass spectrometer.

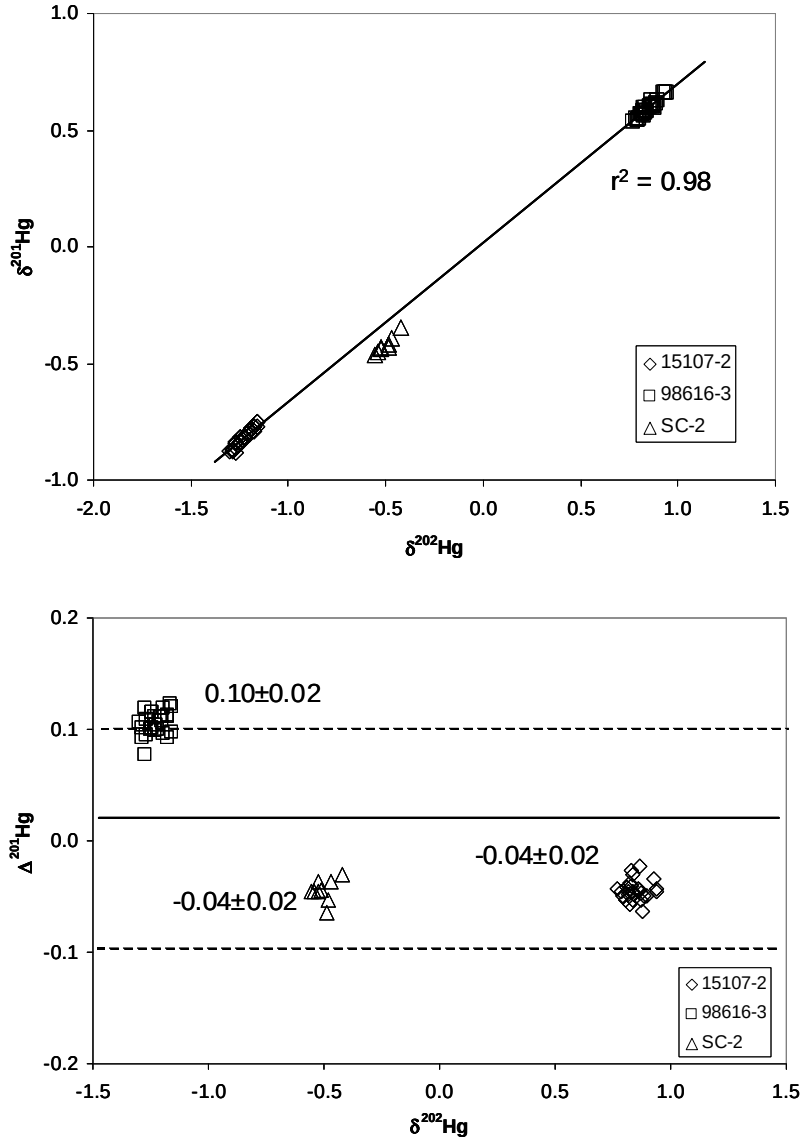


Figure 2-7. Ore deposit samples fall along a mass dependent fraction line showing no significant mass independent fraction (MIF) related to the odd isotope $^{201}$Hg. Average $\Delta^{201}$Hg values are reported with 2SD of the mean values. External reproducibility (2SD) of natural samples is indicated with the dashed lines. Small $\Delta^{201}$Hg values are consistent with other inorganic samples (Bergquist and Blum, 2007).

Table 2-4. Ore sample δ-values.

| | δ202/196 | δ202/198 | δ202/200 | δ202/201 | δ204/202 | δ201/198 | Δ201 |
|---|---|---|---|---|---|---|---|
| 15107-2 | 0.64 | 0.79 | 0.41 | 0.25 | 0.38 | 0.54 | -0.05 |
| 15107-2 | 1.47 | 0.79 | 0.40 | 0.24 | 0.40 | 0.55 | -0.05 |
| 15107-2 | 0.85 | 0.87 | 0.42 | 0.24 | 0.44 | 0.63 | -0.02 |
| 15107-2 | 1.77 | 0.83 | 0.41 | 0.23 | 0.43 | 0.59 | -0.03 |
| 15107-2 | 1.72 | 0.83 | 0.43 | 0.26 | 0.45 | 0.57 | -0.05 |
| 15107-2 | 0.99 | 0.92 | 0.46 | 0.26 | 0.48 | 0.66 | -0.03 |
| 15107-2 | 1.02 | 0.90 | 0.46 | 0.27 | 0.45 | 0.62 | -0.05 |
| 15107-2 | 0.63 | 0.84 | 0.44 | 0.25 | 0.42 | 0.58 | -0.05 |
| 15107-2 | 1.17 | 0.88 | 0.46 | 0.27 | 0.44 | 0.62 | -0.05 |
| 15107-2 | 0.91 | 0.83 | 0.42 | 0.24 | 0.42 | 0.60 | -0.03 |
| 15107-2 | 1.09 | 0.82 | 0.41 | 0.24 | 0.41 | 0.58 | -0.04 |
| 15107-2 | 0.88 | 0.83 | 0.43 | 0.25 | 0.43 | 0.58 | -0.04 |
| 15107-2 | 0.64 | 0.82 | 0.42 | 0.25 | 0.41 | 0.57 | -0.05 |
| 15107-2 | 0.82 | 0.77 | 0.40 | 0.23 | 0.37 | 0.53 | -0.04 |
| 15107-2 | 0.80 | 0.94 | 0.48 | 0.28 | 0.43 | 0.66 | -0.05 |
| 15107-2 | 1.54 | 0.88 | 0.45 | 0.28 | 0.44 | 0.60 | -0.06 |
| 15107-2 | 1.14 | 0.81 | 0.43 | 0.25 | 0.40 | 0.57 | -0.05 |
| 15107-2 | 0.88 | 0.80 | 0.44 | 0.25 | 0.41 | 0.55 | -0.05 |
| 15107-2 | 0.31 | 0.87 | 0.45 | 0.27 | 0.42 | 0.60 | -0.05 |
| 15107-2 | 1.52 | 0.87 | 0.43 | 0.26 | 0.40 | 0.61 | -0.04 |
| 15107-2 | 1.57 | 0.86 | 0.44 | 0.26 | 0.44 | 0.60 | -0.04 |
| 15107-2 | 1.38 | 0.83 | 0.41 | 0.26 | 0.41 | 0.56 | -0.06 |
| 15107-2 | 1.12 | 0.94 | 0.46 | 0.28 | 0.45 | 0.66 | -0.04 |
| 15107-2 | 1.46 | 0.81 | 0.43 | 0.24 | 0.40 | 0.57 | -0.04 |
| 15107-2 | 1.12 | 0.87 | 0.45 | 0.26 | 0.43 | 0.61 | -0.05 |
| 15107-2 | 1.54 | 0.84 | 0.44 | 0.26 | 0.43 | 0.58 | -0.05 |
| 98616-3 | -2.60 | -1.29 | -0.66 | -0.42 | -0.63 | -0.87 | 0.10 |
| 98616-3 | -2.06 | -1.27 | -0.66 | -0.41 | -0.65 | -0.86 | 0.09 |
| 98616-3 | -1.76 | -1.20 | -0.63 | -0.41 | -0.61 | -0.79 | 0.11 |
| 98616-3 | -1.68 | -1.16 | -0.61 | -0.41 | -0.60 | -0.75 | 0.12 |
| 98616-3 | -1.83 | -1.16 | -0.61 | -0.39 | -0.60 | -0.77 | 0.10 |
| 98616-3 | -1.64 | -1.22 | -0.62 | -0.40 | -0.60 | -0.82 | 0.10 |
| 98616-3 | -1.59 | -1.24 | -0.64 | -0.42 | -0.63 | -0.82 | 0.12 |
| 98616-3 | -2.36 | -1.24 | -0.63 | -0.42 | -0.63 | -0.82 | 0.11 |
| 98616-3 | -2.07 | -1.25 | -0.63 | -0.41 | -0.64 | -0.84 | 0.10 |
| 98616-3 | -1.18 | -1.18 | -0.60 | -0.40 | -0.58 | -0.77 | 0.11 |
| 98616-3 | -2.43 | -1.22 | -0.63 | -0.41 | -0.61 | -0.82 | 0.10 |
| 98616-3 | -1.90 | -1.27 | -0.67 | -0.44 | -0.65 | -0.84 | 0.12 |
| 98616-3 | -1.59 | -1.23 | -0.62 | -0.40 | -0.64 | -0.83 | 0.10 |
| 98616-3 | -1.61 | -1.30 | -0.66 | -0.43 | -0.66 | -0.87 | 0.11 |
| 98616-3 | -2.07 | -1.29 | -0.66 | -0.41 | -0.67 | -0.88 | 0.09 |
| 98616-3 | -1.98 | -1.27 | -0.65 | -0.39 | -0.64 | -0.88 | 0.08 |
| 98616-3 | -2.12 | -1.24 | -0.64 | -0.41 | -0.62 | -0.83 | 0.10 |
| 98616-3 | -2.12 | -1.16 | -0.60 | -0.41 | -0.61 | -0.75 | 0.12 |
| 98616-3 | -2.00 | -1.21 | -0.63 | -0.41 | -0.65 | -0.80 | 0.11 |
| 98616-3 | -2.14 | -1.19 | -0.62 | -0.42 | -0.62 | -0.78 | 0.12 |
| 98616-3 | -2.14 | -1.20 | -0.63 | -0.41 | -0.62 | -0.80 | 0.11 |
| 98616-3 | -1.91 | -1.18 | -0.61 | -0.40 | -0.56 | -0.77 | 0.11 |
| 98616-3 | -2.14 | -1.20 | -0.63 | -0.39 | -0.64 | -0.80 | 0.10 |
| 98616-3 | -1.35 | -1.23 | -0.63 | -0.42 | -0.64 | -0.81 | 0.11 |
| 98616-3 | -0.93 | -1.18 | -0.61 | -0.38 | -0.59 | -0.79 | 0.09 |
| 98616-3 | -1.50 | -1.27 | -0.64 | -0.42 | -0.64 | -0.85 | 0.11 |
| SC-2 | -0.08 | -0.42 | -0.20 | -0.07 | -0.19 | -0.35 | -0.03 |
| SC-2 | -0.83 | -0.51 | -0.24 | -0.08 | -0.23 | -0.43 | -0.04 |
| SC-2 | -0.63 | -0.52 | -0.26 | -0.09 | -0.27 | -0.43 | -0.04 |
| SC-2 | -1.12 | -0.52 | -0.25 | -0.08 | -0.26 | -0.44 | -0.05 |
| SC-2 | -1.38 | -0.54 | -0.25 | -0.09 | -0.27 | -0.45 | -0.05 |
| SC-2 | -1.24 | -0.49 | -0.23 | -0.06 | -0.23 | -0.43 | -0.06 |
| SC-2 | -0.77 | -0.47 | -0.24 | -0.08 | -0.23 | -0.39 | -0.04 |
| SC-2 | -0.62 | -0.55 | -0.29 | -0.09 | -0.30 | -0.46 | -0.05 |
| SC-2 | -1.05 | -0.48 | -0.25 | -0.07 | -0.25 | -0.42 | -0.05 |

Table 2-5. Analytical results for laboratory and Standard Reference Materials

| Sample | Description | Method | $\delta^{202}$Hg | Mean ± 2σ $\delta^{202}$Hg |
|---|---|---|---|---|
| NIST 1630 | Trace Hg in Coal | Acid digest | -0.68 | – |
| NIST 1633 | Hg in Coal Fly Ash | Acid digest | -0.32 | – |
| NIST 1641 | Hg in Water | Acid digest | -0.03, -0.04 0.02 | -0.02 ± 0.05 |
| NIST 3133 | Hg Standard Solution | Acid digest | 0.00 | 0.00 |
| Alm | Michigan Almadèn $Hg^0$ standard | Acid digest | – | -0.55[a] ± 0.08 |
| J-M HgO | Alfa Aesar Puratronic HgO | Oven | -0.48 | -0.48 |
| DORM-2 | Dogfish Muscle | Acid digest | 0.16, 0.19 | 0.18 |

[a]Average of 43 analyses.

## 4. Discussion

### 4.1 Hg Isotope Variations in Ore Deposits

A wide range of Hg isotopic compositions is expected in ore deposits that formed under varying conditions of redox, fluid chemistry, temperatures and host rock type. The 2.08 ‰ $\delta^{202}$Hg range in two samples from the massive New Almden mine indicates that ore-forming processes can significantly fractionate Hg isotopic compositions within the same hydrothermal system. Mass dependent processes appear to be the most important in the formation of ore deposits.

Isotopic variations related to mineralogy and spatial position in hydrothermal systems have been documented in Nevada epithermal deposits (Smith et al., 2005; Chapter III) and active and fossil hot springs in the California Coast Ranges (Smith et al., 2008; Chapter IV). Hg isotopic compositions were found to be heavier in deep veins and lighter in surface sinter deposits due to boiling and gas transport of Hg during ore formation . Spring precipitates from active hot springs in California were found to be on average >1 ‰ lower in $\delta^{202}$Hg than adjacent ore deposits due to similar conditions of boiling in the near surface. It is anticipated that further understanding of Hg fractionation factors will enhance future interpretations of Hg isotope variations in natural systems.

## 5. Conclusions

Techniques for the high-precision determination of Hg isotope ratios by MC-ICP-MS have been developed. A novel method for the quantitative extraction of Hg by a combination of pyrolysis, combustion and liquid trapping was presented, allowing Hg to

be separated from sample matrices that prevent CV generation. The external precision of this method is better than ±0.10‰ (2SD) for a range of natural samples. High precision analyses are fundamental to further studies where expected fractionations could be on the order of 0.1-1.0 ‰. Routine measurement of Hg isotope ratios are now possible with the use of innovative sample preparation techniques, such as those presented here, and MC-ICP-MS instrumentation.

**Acknowledgments**

This study was funded by NIEHS SBR Grant ES07373-06 to JDB and NSF Grant EAR-01-06730 to Stephen E. Kesler, Joel D. Blum and Björn Klaue. Additional funding for field work came from a Hugh E. McKinstry grant from the Society of Economic Geologists and a University of Michigan Scott Turner Award to the author. We thank the Division of Petrology and Volcanology, Department of Mineral Sciences of the Smithsonian Institution for providing us with samples from the New Idria and New Almadèn mines. Björn Klaue, Marcus Johnson and Andrea Klaue are thanked for their assistance in the laboratory and for maintaining the Nu Plasma instrument.

**References Cited**


Anbar, A.D., Roe, J.E., Barling, J. and Nealson, K.H., 2000. Nonbiological fractionation of iron isotopes. Science, v. 285, p. 126-128.

Anderson, K.A., 2000. Mercury Analysis in Environmental Samples by Cold Vapor Techniques. In: R.A. Myers (Editor), Encyclopedia of Analytical Chemistry: Instrumentation and Applications. John Wiley & Sons, Chichester, p. 2890-2903.

Arnold, G.L., Anbar, A.D., Barling, J., and Lyons, T.W., 2004. Molybdenum isotope evidence for widespread anoxia in mid-Proterozoic oceans. Science, v. 304, p. 87-90.

Barkay, T.K., 2000. Mercury Cycle Encyclopedia of Microbiology, p. 171-181.

Barling, J., Arnold, G.L., and Anbar, A.D., 2001, Natural mass-dependent variations in the isotopic composition of molybdenum. Earth and Planetary Science Letters, v. 193, p. 447-457.

Barnes, H.L. and Seward, T.M., 1997. Geothermal systems and mercury deposits. In: H.L. Barnes (Editor), Geochemistry of Hydrothermal Ore Deposits. John Wiley & Sons, New York, p. 699-736.

Beard, B.L., Johnson, C.M., Cox, L., Sun, H., Nealson, K.H., and Aguilar, C., 1999, Iron isotope biosignatures. Science, v. 285, p. 1889-1892.

Belshaw, N.S., Freedman, P.A., O'Nions, R.K., Frank, M. and Guo, Y., 1998. A new variable dispersion double-focusing plasma mass spectrometer with performance illustrated for Pb isotopes. International Journal of Mass Spectrometry, v. 181, p. 51-58.

Bergquist, B.A. and Blum, J.D., 2007, Mass-dependent and  -independent fractionation of Hg isotopes by photoreduction in aquatic systems. Science, v. 318, p. 417-420.

Blum, J.D and Berquist, B.A., 2007. Reporting of variations in the natural isotopic composition of mercury. Analytical and Bioanalytical Chemistry, v. 233, p. 353-359.

Bullen, T.D., White, A.F., Childs, C.W., Vivit, D.V., and Schulz, M.S., 2001, Demonstration of significant abiotic iron isotope fractionation in nature. Geology, v. 29, p. 699-702.

Christenson, B.W. and Mroczek, E.K., 2003. Potential reaction pathways of Hg in some New Zealand hydrothermal environments. In: S.F. Simmons and I. Graham (Editors), Volcanic, geothermal and ore-forming processes; rulers and witnesses of processes within the Earth: Society of Economic Geologists Special Publication, p. 111-132.

Cline, J.S., 2001. Timing of gold and arsenic sulfide mineral deposition at the Getchell Carlin-type gold deposit, north-central Nevada. Economic Geology v. 96, p.75-89.

Dodson, M.H., 1963. A theoretical study of the use of internal standards for precise isotopic analysis by the surface ionization technique: Part I - General first-order algebraic solutions. Journal of Scientific Instruments, v. 40, p. 289-295.

Ellis, A.S., Johnson, T.M. and Bullen, T.D., 2002. Chromium isotopes and the fate of hexavalent chromium in the environment. Science, v. 295, p. 2060-2062.

Evans, R.D., Hintelmann, H. and Dillon, P.J., 2001. Measurement of high precision isotope ratios for mercury from coals using transient signals. Journal of Analytical Atomic Spectrometry, v. 16, p. 1064-1069.

Fein, J.B. and Williams-Jones, A.E., 1997. The role of mercury-organic interactions in the hydrothermal transport of mercury. Economic Geology, v. 92, p. 20-28.

Fitzgerald, W.F., 1993. Mercury as a global polutant. The World and I, p. 192-199.

Foucher, D. and Hintelmann, H., 2006. High-precision measurement of mercury isotope ratios in sediments using cold-vapor generation multi-collector inductively coupled plasma mass spectrometry. Analytical and Bioanalytical Chemistry, v. 384, p. 1470-1478.

Graham, S., Pearson, N., Jackson, S., Griffin, W., and O'Reilly, S.Y., 2004, Tracing Cu and Fe from source to porphyry: in situ determination of Cu and Fe isotope ratios in sulfides from the Grasberg Cu-Au deposit. Chemical Geology, v. 207, p. 147-169.

Habfast, K., 1998. Fractionation correction and multiple collectors in thermal ionization isotope ratio mass spectrometry. International Journal of Mass Spectrometry, v. 176, p. 133-148.

Halliday, A.N. et al., 1998. Applications of multiple collector-ICPMS to cosmochemistry, geochemistry, and paleoceanography. Geochimica Et Cosmochimica Acta, v. 62, p. 919-940.

Hintelmann, H. and Lu, S.Y., 2003. High precision isotope ratio measurements of mercury isotopes in cinnabar ores using multi-collector inductively coupled plasma mass spectrometry. Analyst, v. 128, p. 635-639.

Hirata, T., 1996. Lead isotopic analyses of NIST standard reference materials using multiple collector inductively coupled plasma mass spectrometry coupled with a modified external correction method for mass discrimination effect. Analyst, v. 121, p. 1407-1411.

Jackson, T.A., 2001. Variations in the isotope composition of mercury in a freshwater sediment sequence and food web. Canadian Journal of Fisheries and Aquatic Science, v. 58, p. 185-196.

Jackson, T.A., Muir, D.C.G. and Vincent, W.F., 2004. Historical variations in the stable isotope composition of mercury in arctic lake sediments. Environmental Science and Technology, v. 38, p. 2813-2821.

Jackson, T.A., Whittle, M.D., Evans, M.S. and Muir, D.C.G., 2008. Evidence for mass-independent and mass-dependent fractionation of the stable isotopes of mercury by natural processes in aquatic ecosystems. Applied Geochemistry, v. 23, p. 547-571.

Johnson, T.M., 2004. A review of mass-dependent fractionation of selenium isotopes and implications for other heavy stable isotopes. Chemical Geology, v. 204, p. 201-214.

Klaue, B. and Blum, J.D., 1999. Trace analyses of arsenic in drinking water by inductively coupled plasma mass spectrometry: High resolution versus hydride generation. Analytical Chemistry, v. 71, p. 1408-1414.

Klaue, B. and Blum, J.D., 2000. Mercury isotopic analyses by single and multi-collector magnetic sector inductively coupled mass spectrometry. Journal of Conference Abstracts: Goldschmidt 2000, v. 5, 591 p.

Klaue, B., Kesler, S.E. and Blum, J.D., 2000. Investigation of natural fractionation of stable mercury isotopes by inductively coupled plasma mass spectrometry. Proceedings of the International Conference on Heavy Metals in the Environment. contribution 1101, Ann Arbor.

Kritee, K., Blum, J.D., Johnson, M.W., Bergquist, B., Barkay, T., 2007. Mercury stable isotope fractionation during reduction of Hg(II) to Hg(0) by mercury resistant bacteria. Environmental Science & Technology, v. 41, p.1889-1995.

Krupp, R., 1988, Physicochemical Aspects of Mercury Metallogenesis. Chemical Geology, v. 69, p. 345-356.

Lauretta, D.S., Klaue, B., Blum, J.D. and Buseck, P.R., 2001. Mercury abundances and isotopic compositions in the Murchison (CM) and Allende (CV) carbonaceous chondrites. Geochimica et Cosmochimica Acta, v. 65, p. 2807-2818.

Marechal, C.N., Telouk, P. and Albarede, F., 1999. Precise analysis of copper and zinc isotopic compositions by plasma-source mass spectrometry. Chemical Geology, v. 156, p. 251-273.

Nier, A.O., 1950. A redetermination of the relative abundances of the isotopes of neon, krypton, rubidium, xenon, and mercury. Physical Review, v. 79, p. 450-454.

O'Neil, J.R. (Editor), 1986. Theoretical and experimental aspects of isotopic fractionation. Stable isotopes in high temperature geological processes, Reviews in Mineralogy, v. 16, 1-40 p.

Rehkamper, M. and Halliday, A.N., 1998. Accuracy and long-term reproducibility of lead isotopic measurements by multiple-collector inductively coupled plasma mass spectrometry using an external method for correction of mass discrimination. International Journal of Mass Spectrometry, v. 181, p. 123-133.

Rehkamper, M., and Halliday, A.N., 1999, The precise measurement of Tl isotopic compositions by MC-ICPMS: application to the analysis of geological materials and meteorites. Geochimica et Cosmochimica Acta, v. 63, p. 935-944.

Rehkamper, M., Frank, M., Hein, J.R., Porcelli, D., Halliday, A., Ingri, J., and Liebetrau, V., 2002, Thallium isotope variations in seawater and hydrogenetic, diagenetic, and hydrothermal ferromanganese deposits. Earth and Planetary Science Letters, v. 197, p. 65-81.

Rouxel, O.J., Bekker, A., and Edwards, K.J., 2005, Iron isotope constraints on the Archean and Paleoproterozoic ocean redox state. Science, v. 307, p. 1088-1091.

Siebert, C., Nagler, T.F., and Kramers, J.D., 2001, Determination of molybdenum isotope fractionation by double-spike multicollector inductively coupled plasma mass spectrometry. Geochemistry Geophysics Geosystems, v. 2, paper number 2000GC000124.

Smith, C.N., Klaue, B., Kesler, S.E., Rytuba, J.J. and Blum, J.D., 2004. Natural variations of mercury isotopic compositions in hydrothermal ore deposits. Eos: Transactions, American Geophysical Union, v. 85, p. 799.

Smith, C.N., Kesler, S.E., Klaue, B. and Blum, J.D., 2005. Mercury isotope fractionation in fossil hydrothermal systems. Geology, v. 33, p. 825-828.

Smith, C.N., Kesler, S.E., Blum, J.D., and Rytuba, J.J., 2008. Isotope Geochemistry of Mercury in Source Rocks, Mineral Deposits and Spring Deposits of the California Coast Ranges, USA. Earth and Planetary Science Letters, v. 269, p. 399-407.

Varekamp, J.C. and Buseck, P.R., 1984. The Speciation of Mercury in Hydrothermal Systems, with Applications to Ore Deposition. Geochimica et Cosmochimica, v. 48, p. 177-186.

Walder, A.J. and Furuta, N., 1993. High-precision lead-isotope ratio measurement by inductively-coupled plasma multiple collector mass-spectrometry. Analytical Sciences, v. 9, p. 675-680.

Welz, B., 1985. Atomic Absorption Spectrometry. VCH, New York, p. 506.

White, W.M., Albarede, F. and Telouk, P., 2000. High-precision analysis of Pb isotope ratios by multi-collector ICP-MS, Chemical Geology, v. 167, p. 257-270.

Wiesli, R.A., Beard, B.L., Taylor, L.A. and Johnson, C.M., 2003. Space weathering processes on airless bodies: Fe isotope fractionation in the lunar regolith, Earth and Planetary Science Letters, v. 216, p. 457-465.

Wombacher, F., Rehkamper, M. and Mezger, K., 2004. Determination of the mass-dependence of cadmium isotope fractionation during evaporation. Geochimica et Cosmochimica Acta, v. 68, p. 2349-2357.

Xie, Q., Lu, S.Y., Evans, D., Dillon, P. and Hintelmann, H., 2005. High precision Hg isotope analysis of environmental samples using gold trap-MC-ICP-MS, Journal of Analytical Atomic Spectrometry. v. 20, p. 515-522.

Zadnik, M.G., Specht, S. and Begemann, F., 1989. Revised isotopic composition of terrestrial mercury, International Journal of Mass Spectrometry and Ion Processes, v. 89, p. 103-110.

# CHAPTER III.

# MERCURY ISOTOPE FRACTIONATION IN FOSSIL HYDROTHERMAL SYSTEMS


## Abstract

The Hg isotopic compositions of samples throughout the vertical extent of two fossil hydrothermal systems were analyzed by multicollector inductively coupled plasma–mass spectrometry (MC-ICP-MS). Results show greater than 5‰ ($\delta^{202}Hg/^{198}Hg$; relative to NIST 3133) fractionation, more than 50 times greater than the 0.1‰ ($2\sigma$) external reproducibility of the analyses. Hg isotope compositions from both hydrothermal systems can be grouped by dominant mineralogy and position; $\delta^{202}Hg/^{198}Hg$ values at the tops of the systems are –3.5‰ to –0.4‰ in cinnabar-dominant sinter and –0.2‰ to +2.1‰ in metacinnabar-dominant sinter, and the underlying veins have $\delta^{202}Hg/^{198}Hg$ values of –1.4‰ to +1.3‰. These differences probably resulted from the combination of boiling of the hydrothermal fluid, oxidation near the surface, and kinetic effects associated with mineral precipitation. The natural variation in Hg isotopic compositions observed in this study is higher than that expected from the trend of decreasing mass-dependent fractionation with increasing mass extrapolated from stable isotope systems up to Z = 26 (Fe), confirming that even the heaviest elements undergo significant stable isotope fractionation in hydrothermal systems.


## 1. Introduction

Hydrothermal processes cause mass-dependent isotope fractionation in light stable elements (e.g., C, O, H, S) and should produce similar, but smaller, mass-dependent variations in the isotopic composition of heavy elements such as Hg (see review by Johnson et al., 2004). Better information on the nature and magnitude of isotopic fractionation for Hg in hydrothermal systems is needed if isotope compositions are to be used to determine the source areas and migration processes of Hg in the crust.

## 2. Analysis of Hg Isotopes

Properties of Hg that could contribute to isotope fractionation include its high volatility, large mass range of stable isotopes (196, 198, 199, 200, 201, 202, 204 amu), multiple common redox states, and covalent bonding (O'Neil, 1986). Fractionation of Hg isotopes was produced in laboratory experiments by early investigators (Brönsted and von Hevesy, 1920), but analytical limitations delayed recognition of smaller natural variations (Nier, 1950). Later analyses using gas source mass spectrometry reported variations in isotopic compositions of Hg in cinnabar (Obolenskii and Doilnitsyn, 1976), but are of uncertain significance because of low analytical precision (Koval et al., 1977).

Precise isotope ratio measurement of Hg is hindered by its volatility and high first ionization potential, which make it unsuitable for thermal ionization mass spectrometry. Recent studies, including this one, have employed multicollector inductively coupled plasma–mass spectrometry (MC-ICP-MS), which effectively ionizes Hg in an argon plasma source. Results show that Hg isotopic compositions are constant within analytical uncertainty in carbonaceous chondrites (Lauretta et al., 2001), but vary in terrestrial

geologic materials including hydrothermal ore deposits (Klaue et al., 2000; Hintelmann and Lu, 2003).

### 3. Stable Isotope Fractionation in Hydrothermal Systems

Growing evidence suggests that heavy stable isotopes undergo fractionation in hydrothermal systems. Larson et al. (2003) found fractionations of 1‰–2‰ ($\delta^{65}Cu/^{63}Cu$) in hypogene sulfides from skarn and porphyry base metal deposits that formed at 350–550 ºC. Graham et al. (2004) reported values of –3.0‰ to +1.6‰ ($\delta^{57}Fe/^{54}Fe$) in pyrite and chalcopyrite from the Grasberg Igneous Complex and associated Cu-Au skarns, which also formed at these high temperatures. In a study of seafloor hydrothermal sulfides, Rouxel et al. (2004) reported $\delta^{57}Fe/^{54}Fe$ values as low as –3.2‰ in sulfides precipitated at ~200 °C, and compositions of ~0‰, near basaltic values, for sulfides precipitated at ~300 °C.

Isotopic fractionation can be caused by redox, mineral precipitation, and boiling reactions, all of which are common in hydrothermal systems. Differences in bond strengths among sulfur compounds with different redox states, for example, cause fractionations of 20‰–35‰ ($\delta^{34}S/^{32}S$) between aqueous $H_2S$ and $SO_4^{2-}$ at 200–350 ºC (Ohmoto and Rye, 1979). Sphalerite-galena pairs that precipitated together from hydrothermal fluids show temperature-dependent equilibrium fractionation of 1‰–4‰ between 150 and 350 ºC. In active geothermal systems at Wairakei, New Zealand, and The Geysers, California, condensation of steam rising from boiling deep reservoirs yields water with lighter O and H isotopic compositions than those in the reservoir (Giggenbach and Stewart, 1982). Native sulfur deposited from $H_2S$ gas issuing from fumaroles at

Yellowstone National Park, Wyoming, is as much as 5.5‰ ($\delta^{34}S/ {}^{32}S$) lighter than the deep fluid source composition (Schoen and Rye, 1970; Truesdell et al., 1978). Similar processes in submarine hydrothermal vent fluids have been suggested to cause fractionation of B isotopes (Leeman et al., 1992).

## 4. Mercury in the Epithermal Environment of Hydrothermal Systems

The greatest variety of hydrothermal processes that might fractionate isotopes, including boiling, is found in epithermal systems, which consist of aqueous fluids circulating in the upper 1-2 km of the crust at temperatures of 150–300 ºC (Cooke and Simmons, 2000). Many systems of this type are found in volcanic regions and are covered by sinter terraces and hot springs. Epithermal Au-Ag deposits, which are fossil analogues of these hydrothermal systems, consist of quartz veins with minor but economically important amounts of Au-Ag as electrum, along with small amounts of sulfides, selenides, and tellurides containing Au and Ag, as well as Cu, Zn, Pb, Hg, As, Sb, and Tl. These deposits are divided into high-sulfidation deposits that form from acidic, sulfur-rich fluids, and low-sulfidation deposits that form from near-neutral, sulfur-poor fluids (Sillitoe and Hedenquist, 2003), which show abundant evidence of boiling, including vapor-rich fluid inclusions and bladed calcite pseudomorphed by quartz (Simmons and Christenson, 1994).

In low-sulfidation deposits (Fig. 3-1A), which are the focus of this study, Hg can be sourced either from a magma or surrounding country rock. In the reduced, low-sulfur fluids typical of such deposits, $Hg^0_{aq}$ is more abundant than $Hg^{2+}_{aq}$ and behaves like a dissolved gas (Varekamp and Buseck, 1984). As the fluid ascends along open fractures it

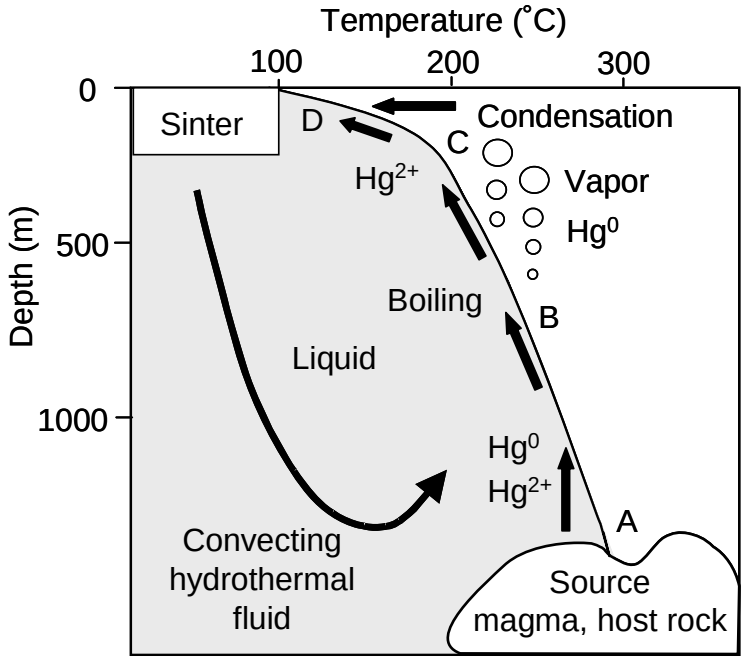


Figure 3-1. Boiling-point curve for $H_2O$ under hydrostatic conditions. Figure shows processes (A–D) involved in formation of epithermal mineral deposits that may fractionate Hg isotopes (adapted from Haas, 1971).

cools and begins to boil (Fig. 3-1B), and $Hg^0_{aq}$ is partitioned into the vapor phase (Christenson and Mroczek, 2003). In the boiling fluid, diffusion of Hg between the liquid and the vapor bubbles may be expected to enrich the vapor in light isotopes. Loss of $H_2S$ to the vapor during boiling will cause reduction of $Hg^{2+}$ in dissolved complex ions, such as:

$$HgS(H_2S)_2^0 + H_2^0 \rightarrow Hg^0_g + 3H_2S_{(g)}, \quad (1)$$

forming more $Hg^0_g$ (Christenson and Mroczek, 2003); a step that may also favor lighter isotopic compositions in the vapor. These combined effects are postulated to produce a vapor containing isotopically light Hg and a residual liquid at depth containing isotopically heavy Hg.

Hg-bearing minerals are precipitated in two parts of these hydrothermal systems. At depth, isotopically heavy Hg in the liquid is deposited in solid solution in electrum, sulfosalts, and sulfides. Near the surface, isotopically light $Hg^0$ in the vapor can mix with oxygenated groundwater, where it is oxidized to $Hg^{2+}$ and reacts with $H_2S$ in the vapor to precipitate cinnabar in the silica-rich sinter (Fig. 3-1C). If deep hydrothermal fluid escapes to the surface it can also react with $H_2S$ to form cinnabar or metacinnabar that may become enriched in heavy Hg isotopes (Fig. 3-1D).

## 5. Geologic Setting of Fossil Hydrothermal Systems

In order to test these predictions about the isotopic composition of Hg in epithermal systems, samples must be obtained from deposits that preserve both the sinter on the paleosurface and the underlying veins at depth. Most epithermal deposits consist of veins from which overlying sinter has been removed by erosion, and most sinter

deposits have not undergone enough erosion to expose any underlying veins. Two unusual epithermal mineral deposits in the National and Ivanhoe mining Districts of northern Nevada preserve both sinter and underlying vein material.

In the National District (Fig. 3-2A), Hg-bearing siliceous sinter and epiclastic sediments at the summit of Buckskin Mountain are underlain by the Bell vein (Vikre, 1985). The sinter consists of thin layers of chalcedony and opal with cinnabar and metacinnabar, and displays desiccation cracks indicative of deposition in shallow water at the paleosurface; the underlying vein contains fluid inclusions that preserve evidence of boiling (Vikre, 1985). Samples of the Bell vein collected 290 m below the sinter contain banded quartz with Ag-selenides, sulfosalts, base metal sulfides, and electrum; Hg is in solid solution in electrum, arsenopyrite, stibnite, and tetrahedrite in amounts of up to 1 wt% (Table 3-1). In the sinter, Hg is found in red cinnabar that contains 2-3 wt% Cl, and in black metacinnabar, which has as much as 12 wt% Se (Appendix A).

In the Ivanhoe District (Fig. 3-2B), the west-northwest–striking Clementine vein system cuts Paleozoic sedimentary and overlying silicified Tertiary volcaniclastic rocks, which are covered by a 3 $km^2$ cap of Hg-mineralized silica sinter. Alternating quartz-adularia layers, bladed calcite, and vapor-rich fluid inclusions indicate that the vein-forming fluids boiled (Peppard, 2002). The paleosurface beneath which the veins formed, which forms the present surface, contains abundant silica sinter with desiccation cracks, cinnabar and metacinnabar. A vein sample from 275 m below the sinter consists of alternating quartz and adularia layers with Ag selenides, sulfosalts, base metal sulfides, and electrum (Table 3-1). Samples from the surface include a fracture-filling with froth-

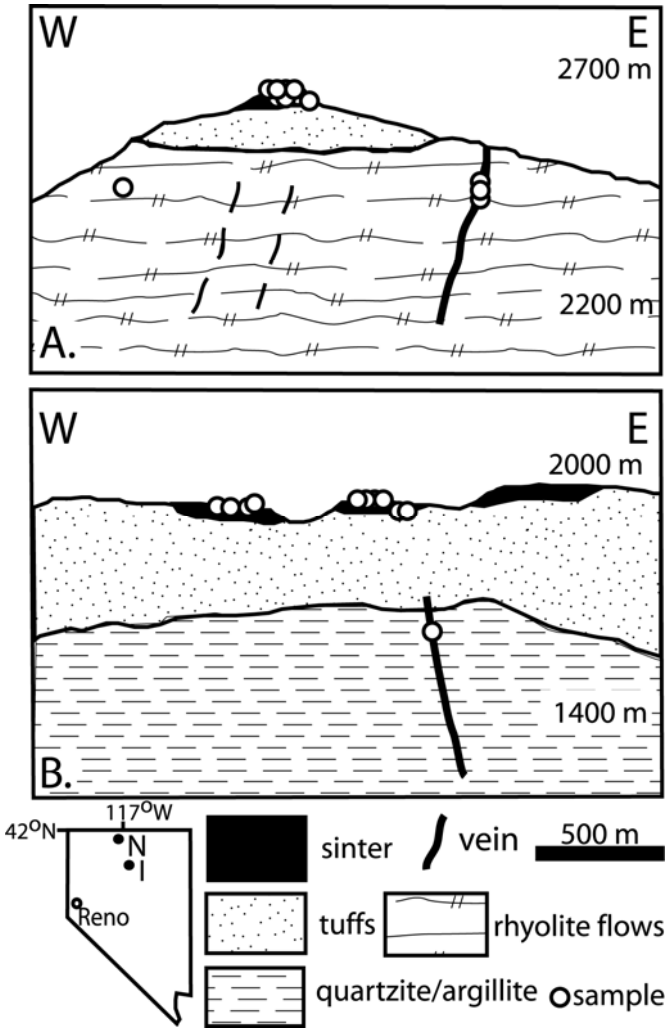


Figure 3-2. Geologic cross sections through fossil hydrothermal systems with schematic locations of samples. A: Buckskin Mountain, National District (N), northern Nevada, showing relation between silica sinter and silicified epiclastic sediments at summit and in underlying Bell vein (modified from Vikre, 1985). B: Ivanhoe District (I), northern Nevada, showing relative positions of Clementine vein /fault and overlying sinters (modified from Peppard, 2002).

Table 3-1: Analytical Results For Epithermal Deposit Samples

| Sample Name | Type* | Description | Method | $\delta^{202}$Hg |
|---|---|---|---|---|
| National | | | | |
| BN-5 352† | Vein | Drusy quartz veinlet w/ stibnite | leach | -0.1 |
| BM-9 | MC | Blk metacinnabar layers in sinter | leach | -0.2 |
| BM-10 | Cinn | Red cinnabar layers in sinter | leach | -2.3 |
| BM-11 | Cinn | Red cinn in sinter w/ mudcrack textures | leach | -3.0 |
| BM-12 | Cinn | Red cinn in sinter, taken from open cut at summit | leach | -1.4 |
| BM-13 | Cinn | Silicified, bedded epiclastic sediments w/ red cinn | leach | -0.4 |
| BM-14 | Vein | Banded qtz vein, elec, Ag-selenides, tetra, py | leach | 0.5 |
| BVPD03-1§ | Vein | Banded qtz vein, sulfides, selenides | pyrolysis | -1.4 |
| BVPD03-2§ | Vein | Banded qtz vein, sulfides, selenides | pyrolysis | 1.3 |
| BNMS-D§ | Cinn | Bedded sinter, red cinn bands w/ brown detritus | pyrolysis | -1.6 |
| BNMS-E§ | Cinn | Finely laminated sinter, red cinn bands | pyrolysis | -3.5 |
| BUCK02-1A1§ | MC | Chalcedonic sinter w/ clots, diss. of blk metacinn | pyrolysis | 0.4 |
| BUCK02-1A2§ | MC | Sinter w/ mixed blk metacinn and red cinn | pyrolysis | 2.1 |
| BUCK02-1A3§ | MC | Sinter w/blk metacinn bands,clots w/ red cinn clots | pyrolysis | 0.3 |
| BUCK02-5§ | MC | Blk porous metacinn bed in clastic sinter | pyrolysis | 1.9 |
| Ivanhoe | | | | |
| IH76-902# | Vein | Qtz vein and qtz cemented bx, py, selenides | leach | -0.6 |
| VL-1 | Cinn | Frothy silica sinter replacing lithic tuff and seds | leach | -0.8 |
| VL-2 | Cinn | Alternating gry bands of silica and clastic layers | leach | -1.2 |
| VL-3 | Cinn | White silicified tuff | leach | -0.5 |
| VL-10# | Cinn | White silicified tuff | leach | -0.5 |
| BU-1 | Cinn | Sinter w/ red cinn, dessication cracks | leach | -0.9 |
| BU-2 | Cinn | Sinter w/ red cinn, open cut | leach | -0.9 |
| KA-2 | Cinn | Sinter w/ red cinn, dessication cracks | leach | -0.9 |
| CLEM-1# | Fault | Frothy silica, red cinn | leach | -0.4 |
| CLEM-2# | Fault | Frothy silica, silica cemented bx, red cinn | leach | -0.4 |

Note: All $\delta^{202}$Hg values are reported relative to the NIST 3133 Hg standard. Errors on $\delta^{202}$Hg are ±0.1‰ (2σ) based on external reproducibility of natural ore samples.
*MC = metacinnabar-bearing sinter, Cinn = cinnabar-bearing sinter
†Access to drill core provided by R. Hatch.
§Powdered splits provided by P.G. Vikre.
#Samples provided by B. Peppard.

textured silica, clay and silica collected at the surface 200 m above the Clementine vein and sinter samples with cinnabar and minor metacinnabar in fractures and layers.

## 6. Analytical Methods

Approximately 100 mg of material was handpicked from each crushed and sieved sample. Samples were prepared by acid leaching in closed PFA beakers with aqua regia at ~90 °C for 24 h. For vein samples with high concentrations of elements known to produce chemical interferences with cold vapor (CV) generation (e.g., Se, Au, or Ag; Welz, 1985), Hg was isolated by pyrolysis of the samples at 800 ºC in Ar, followed by combustion of the pyrolysis gases in $O_2$ at 1000 ºC, and liquid trapping of the combustion gases in an oxidizing $KMnO_4/H_2SO_4$ solution (Liang et al., 2003; EPA methods 101A and 7473; Chapter II).

The prepared samples were diluted to 40 ± 4 ppb Hg and introduced into a Nu Plasma MC-ICP-MS, using continuous-flow cold vapor generation with $Sn(II)Cl_2$ as the reducing agent. For mass bias correction and internal standardization, an external Tl spike (NIST 997) was introduced into the cold vapor stream by a desolvating nebulizer (Lauretta et al., 2001). This method of sample introduction allows online, selective, and quantitative chemical separation of the $Hg^0$ vapor from the sample matrix, thus eliminating matrix effects because only Hg, and minor amounts of $H_2O$ and HCl vapor enter the plasma (Chapter II). There is no variation in the compounds entering the plasma, thus fractionation effects due to the sample matrix are unlikely and could only be caused by nonquantitative reduction of the $Hg^{2+}$.

Isotopic fractionation was measured relative to the NIST 3133 Hg standard, which was run before and after each sample. All of the Hg isotopes except for $^{199}$Hg were routinely measured and fractionation was observed to be mass-dependent. Data are presented as $\delta^{202}$Hg/$^{198}$Hg (hereafter $\delta^{202}$Hg), because this ratio has the best balance between precision of measurement and mass difference. Typical in-run precision of better than ±0.05‰ (2σ), based on the deviation between bracketing standard runs, was achieved on a daily basis. The average $\delta^{202}$Hg value and external reproducibility of NIST 3133 and our laboratory standard (elemental Hg from Almadèn, Spain) was –0.55 ± 0.08‰ (2σ, $n$ = 43), based on repeated measurements during this study. The 2σ reproducibility for multiple analyses of 3 natural ore specimens ranged between ±0.06 and ±0.09‰ ($n$ = 60) (Chapter II), and the maximum value was used as a conservative estimate of the external reproducibility for this study. Blanks and sample introduction memory effects were monitored after each standard and sample run. A calibrated $^{199}$Hg spike was used to test for quantitative Hg extraction by isotope dilution and to confirm the observed isotopic fractionation by introducing 2‰ isotopic shifts of the $^{202}$Hg/$^{199}$Hg ratio of natural samples.

**7. Analytical Results**

The isotopic composition of Hg in samples from the National and Ivanhoe epithermal deposits range from –3.5‰ to +2.1‰ $\delta^{202}$Hg, a range 56 times greater than the 0.1‰ (2σ) external reproducibility of our measurements, and provide evidence for significant fractionation of Hg isotopes in hydrothermal systems (Fig. 3-3; Table 3-1). Fractionation is systematic with respect to position in the deposit and mineralogy. At

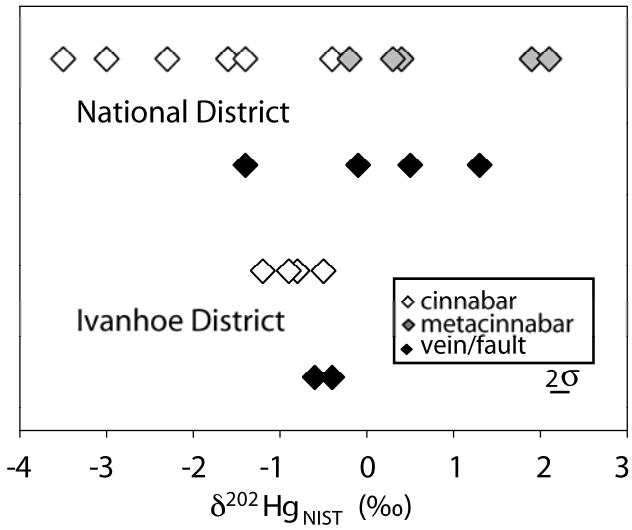


Figure 3-3. $\delta^{202}$Hg of samples from the National and Ivanhoe Districts. Variation in $\delta^{202}$Hg values (relative to NIST 3133 Hg standard) of vein/fault and sinter samples shown as a function of dominant mineralogy (Table 3-1).

National, $\delta^{202}$Hg values range from –3.5‰ to –0.4‰ in cinnabar-bearing sinter compared to –1.4‰ to +1.3‰ in the underlying veins. Sinter containing abundant metacinnabar has $\delta^{202}$Hg values that range from –0.2‰ to +2.1‰, overlapping most of the range of values observed for the veins. At Ivanhoe, $\delta^{202}$Hg values of sinter above the Clementine vein range from –1.2‰ to –0.5‰, compared to –0.6‰ to –0.4‰ for samples from the Clementine vein and a near-surface fault above it.

## 8. Discussion

These results are in general agreement with our prediction that Hg in the upper part of epithermal hydrothermal systems should be isotopically light relative to that in the lower part. The significantly lighter $\delta^{202}$Hg values of cinnabar-sinter likely reflect the contribution of isotopically light Hg transported to the surface in the vapor phase. The difference between average isotopic compositions of cinnabar-sinter Hg and vein-fault Hg is much greater at National than at Ivanhoe. The National District contains a considerably larger ore resource than Ivanhoe (Vikre, 1985; Peppard, 2002) and was probably larger and longer-lived than the Ivanhoe system, a difference that could have produced larger degrees of fractionation in the National District.

The high $\delta^{202}$Hg values in sinter containing metacinnabar from National, which do not agree with our prediction, probably reflect incursions of deep fluid into the shallow, sinter environment. Deep vein fluids reach the surface of epithermal hydrothermal systems intermittently and account for at least part of the trace metals that are deposited in sinter. Metacinnabar is enriched in Se which is not commonly transported by the vapor phase in epithermal systems, indicating that it probably had a

larger input of elements from deep vein fluids, including isotopically heavy Hg (Fig. 3-1, step D). The wide range of isotopic compositions in metacinnabar-bearing sinter probably reflects variable degrees of mixing between these two Hg reservoirs.

Boiling of the hydrothermal fluid was probably the most important cause of the extensive fractionation observed in fossil epithermal deposits. Compared to the 5‰ range of $\delta^{202}$Hg values observed here for epithermal deposits, other low-temperature deposits in which boiling is not common have ranges of only +0.4‰ to –1.5‰ (Almadèn standard) (Klaue et al., 2000) and 0.0‰ to –1.3‰ (NIST SRM 1641d) (Hintelmann and Lu, 2003). The apparent importance of boiling to fractionation of Hg in epithermal systems is further supported by the relatively narrow (~0.8‰) range of $\delta^{202}$Hg values measured in sphalerite from Mississippi Valley–type deposits, which formed without boiling (Smith et al., 2004).

8.1 Isotopic Fractionation of Hg Compared to that of Other Heavy Isotope Systems

The large range of Hg isotope compositions in hydrothermal ore deposits is greater than might be expected for such a heavy element. The maximum natural stable isotope variation observed for each element that has been investigated in hydrothermal ore deposits is plotted in Figure 3-4. For elements up to Fe (Z = 26) the decrease in maximum isotopic variation decreases with increasing mass over three orders of magnitude. Extrapolation from these light elements predicts that mass-dependent fractionation would be below the analytical resolution of 0.01‰ $amu^{-1}$ above Z ~ 50. Recent measurements of isotopic compositions in heavier isotope systems do not follow this predicted decrease however. Instead, isotopic fractionations in hydrothermal systems for elements ranging from Fe to Hg show a similar range ~1 ± 0.5‰ $amu^{-1}$ (Fig. 3-4).

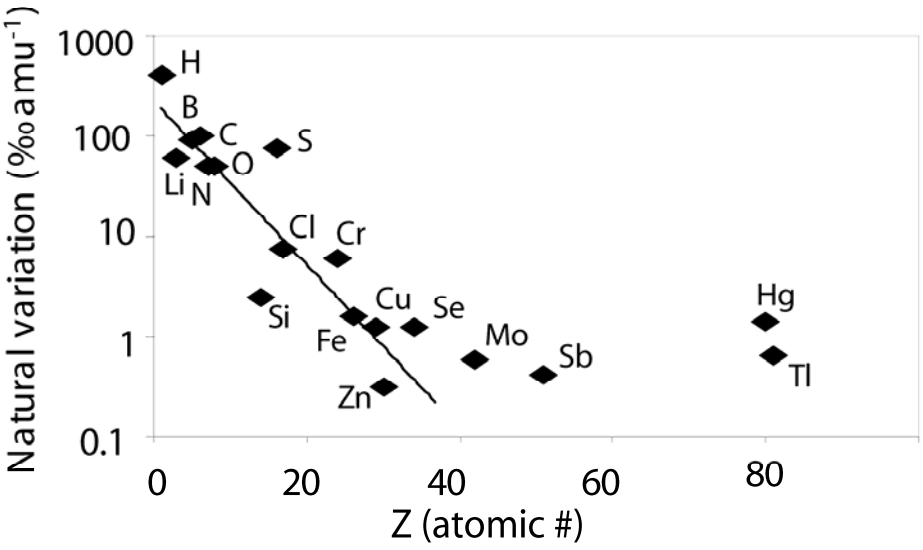


Figure 3-4. Plot of estimated maximum natural variation in isotope compositions (‰) normalized per amu of mass span of the ratio of interest. All data for heavier elements ($Z \geq 26$) are from hydrothermal ore deposits (Larson et al., 2003; Rouxel et al., 2003; Wieser and de Laeter, 2003; Anbar, 2004; Graham et al., 2004; Hoefs, 2004). Line is an exponential extrapolation of decrease in fractionation with increasing mass based on trend of light elements ($Z \leq 26$).

The similar and larger magnitude of isotopic fractionation for the heavier elements may be due to a predominance of kinetic effects with increasing mass. For most transition elements, redox reactions are the major agents of fractionation (Anbar, 2004; Johnson et al., 2004). This is evident when contrasting the maximum fractionation of Cu, $\delta^{65}Cu/^{63}Cu \sim 1.2‰$, which has two oxidation states, with Zn, $\delta^{66}Zn/^{64}Zn \sim 0.3‰$, which has only one common oxidation state and lies below the extrapolated trend (Fig. 3-4) (Marechal et al., 1999). All of the elements between Fe and Hg that exhibit higher degrees of fractionation have multiple oxidation states, although the amount of data available for these systems is quite limited and the full extent of fractionation present in nature may not yet have been observed. Hg is the only metal to vaporize during boiling in low-temperature hydrothermal systems (Spycher and Reed, 1989). The position of Hg slightly above the trend of isotopic fractionation between Fe and Tl shown in Figure 3-4 may be due to its susceptibility to fractionation by both redox and vaporization reactions, whereas only redox reactions are important fractionation mechanisms for most of the other transition metals. Consequently, the unique property of vapor transport at low temperatures appears to have a substantial effect on Hg isotopic composition in the geologic environment. Detailed field and experimental observations will be needed to determine whether boiling is the dominant cause of fractionation in Hg isotopes. If this is correct, the use of Hg isotopes as tracers will be most useful in hydrothermal systems that have not boiled.

**Acknowledgments**

This study was supported by grant EAR-01-06730 from the National Science Foundation to Stephen E. Kesler and Joel D. Blum, and grant ES07373-06 from the National Institute of Environmental Health Sciences to Joel D. Blum. Field work was supported by a Hugh E. McKinstry grant from the Society of Economic Geologists and a University of Michigan Scott Turner Award to the author. R. Hatch provided access to drill core from the National District, and B. Peppard is thanked for additional samples from the Ivanhoe District. A field visit to the National District with P. Vikre and subsequent discussions with him greatly benefited the authors' understanding of the geology of this site. Eric Essene, Gerald Keeler, Stuart Simmons, Johan Varekamp, and Bruce Wilkinson are thanked for their review of this work.

## References Cited


Anbar, A.D., 2004. Iron stable isotopes: Beyond biosignatures. Earth and Planetary Science Letters, v. 217, p. 223–236.

Brönsted, J.N., and von Hevesy, G., 1920. The separation of mercury isotopes. Nature, v. 106, p. 144–147.

Christenson, B.W., and Mroczek, E.K., 2003. Potential reaction pathways of Hg in some New Zealand hydrothermal environments, *in* Simmons, S.F., and Graham, I., eds., Volcanic, geothermal and ore-forming processes; rulers and witnesses of processes within the Earth: Society of Economic Geologists Special Publication 10, p. 111–132.

Cooke, D.R., and Simmons, S.F., 2000. Characteristics and genesis of epithermal gold deposits, *in* Hagemann, S.G., and Brown, P.E., eds., Gold 2000: Reviews in Economic Geology, v. 13, p. 221–244.

Giggenbach, W.F., and Stewart, M.K., 1982. Processes controlling the isotopic composition of steam and water discharges from steam vents and steam-heated pools in geothermal areas. Geothermics, v. 11, p. 71–80.

Graham, S., Pearson, N., Jackson, S., Griffin, W., and O'Reilly, S.Y., 2004. Tracing Cu and Fe from source to porphyry: In situ determination of Cu and Fe isotope ratios in sulfides from the Grasberg Cu-Au deposit. Chemical Geology, v. 207, p. 147–169.

Haas, J.L., Jr., 1971. Effect of salinity on maximum thermal gradient of a hydrothermal system at hydrostatic pressure. Economic Geology, v. 66, p. 940–946.

Hintelmann, H., and Lu, S.Y., 2003. High precision isotope ratio measurements of mercury isotopes in cinnabar ores using multi-collector inductively coupled plasma mass spectrometry. Analyst, v. 128, p. 635–639.

Hoefs, J., 2004. Stable isotope geochemistry: Berlin, Springer-Verlag, 201 p.

Johnson, C.M., Beard, B.L., and Albarede, F., 2004. Overview and general concepts, *in* Johnson, C.M., et al., eds., Geochemistry of non-traditional stable isotopes: Reviews in Mineralogy and Geochemistry, v. 55, p. 1–24.

Klaue, B., Kesler, S.E., and Blum, J.D., 2000. Investigation of natural fractionation of stable mercury isotopes by inductively coupled plasma mass spectrometry, *in* Proceedings of the International Conference on Heavy Metals in the Environment, Ann Arbor, Michigan, Contribution 1101 (CD-ROM).

Koval, N.A., Zakharchenko, V.V., Savin, O.R., Vinogradov, V.I., Shkurdoda, V.A., and Simonovskii, V.I., 1977. Problem of natural fractionation of mercury isotopes. Doklady Akademii Nauk SSSR, v. 235, p. 936–938.

Larson, P.B., Maher, K., Ramos, F.C., Chang, Z.S., Gaspar, M., and Meinert, L.D., 2003. Copper isotope ratios in magmatic and hydrothermal ore-forming environments. Chemical Geology, v. 201, p. 337–350.

Lauretta, D.S., Klaue, B., Blum, J.D., and Buseck, P.R., 2001. Mercury abundances and isotopic compositions in the Murchison (CM) and Allende (CV) carbonaceous chondrites. Geochimica et Cosmochimica Acta, v. 65, p. 2807–2818.

Leeman, W.P., Vocke, R.D., and McKibben, M.A., 1992. Boron isotopic fractionation between coexisting vapor and liquid in natural geothermal systems, Proceedings of the International Symposium on Water-Rock Interaction, v. 7, p. 1007–1010.

Liang, L., Horvat, M., Li, H., and Pang, P., 2003. Determination of mercury in minerals by combustion/trap/atomic fluorescence spectrometry. Journal of Analytical Atomic Spectrometry, v. 18, p. 1383–1385.

Marechal, C.N., Telouk, P., and Albarede, F., 1999. Precise analysis of copper and zinc isotopic compositions by plasma-source mass spectrometry. Chemical Geology, v. 156, p. 251–273.

Nier, A.O., 1950. A redetermination of the relative abundances of the isotopes of neon, krypton, rubidium, xenon, and mercury. Physical Review, v. 79, p. 450–454.

Obolenskii, A.A., and Doilnitsyn, E.F., 1976. Natural fractionation of mercury isotopes. Doklady Akademii Nauk SSSR, v. 230, p. 701–704.

Ohmoto, H., and Rye, R., 1979. Isotopes of sulfur and carbon, *in* Barnes, H.L., ed., Geochemistry of Hydrothermal Ore Deposits, 2nd edition: New York, John Wiley & Sons, p. 509-567.

O'Neil, J.R., 1986. Theoretical and experimental aspects of isotopic fractionation, *in* Valley, J.W., et al., eds., Stable isotopes in high temperature geological processes: Reviews in Mineralogy, v. 16, p. 1–40.

Peppard, B., 2002. Geology and geochemistry of the Ivanhoe vein system, Elko, Nevada [M.Sc. thesis]: Ann Arbor, University of Michigan, 67 p.

Rouxel, O., Dobbek, N., Ludden, J., and Fouquet, Y., 2003. Iron isotope fractionation during oceanic crust alteration. Chemical Geology, v. 202, p. 155–182.

Rouxel, O., Fouquet, Y., and Ludden, J.N., 2004. Subsurface processes at the Lucky Strike hydrothermal field, Mid-Atlantic Ridge: Evidence from sulfur, selenium, and iron isotopes I. Geochimica et Cosmochimica Acta, v. 68, p. 2295–2311.

Schoen, R., and Rye, R.O., 1970. Sulfur isotope distribution in solfataras: Yellowstone National Park. Science, v. 170, p. 1082–1084.

Sillitoe, R.H., and Hedenquist, J.W., 2003. Linkages between volcanotectonic settings, ore-fluid compositions, and epithermal precious metal deposits, *in* Simmons, S.F., and Graham, I., eds., Volcanic, geothermal and ore-forming processes; rulers and witnesses of processes within the Earth: Society of Economic Geologists Special Publication 10, p. 315–343.

Simmons, S.F., and Christenson, B.W., 1994. Origins of calcite in a boiling geothermal system. American Journal of Science, v. 294, p. 361–400.

Smith, C.N., Klaue, B., Kesler, S.E., Rytuba, J.J., and Blum, J.D., 2004. Natural variations of mercury isotopic compositions in hydrothermal ore deposits. Eos (Transactions, American Geophysical Union), v. 85, p. 799.

Spycher, N.F., and Reed, M.H., 1989. Evolution of a Broadlands-type epithermal ore fluid along alternative *P-T* paths; implications for the transport and deposition of base, precious, and volatile metals. Economic Geology and the Bulletin of the Society of Economic Geologists, v. 84, p. 328–359.

Truesdell, A.H., Rye, R.O., Whelan, J.F., and Thompson, J.M., 1978. Sulfate chemical and isotopic patterns in thermal waters of Yellowstone Park, Wyoming. U.S. Geological Survey Open-File Report 78-0701, p. 435–436.

Varekamp, J.C., and Buseck, P.R., 1984. The speciation of mercury in hydrothermal systems, with applications to ore deposition. Geochimica et Cosmochimica Acta, v. 48, p. 177–185.

Vikre, P.G., 1985. Precious metal vein systems in the National District, Humboldt County, Nevada. Economic Geology , v. 80, p. 360–393.

Welz, B., 1985. Atomic absorption spectrometry: Weinheim, VCH, 506 p.

Wieser, M.E., and de Laeter, J.R., 2003. A preliminary study of isotope fractionation in molybdenites. International Journal of Mass Spectrometry, v. 225, p. 177–183.

# CHAPTER IV.

# ISOTOPE GEOCHEMISTRY OF MERCURY IN SOURCE ROCKS, MINERAL DEPOSITS AND SPRING DEPOSITS OF THE CALIFORNIA COAST RANGES, USA


## Abstract

We present here the first study of the isotopic composition of Hg in rocks, ore deposits and spring precipitates in The Geysers-Clear Lake area of the northern California Coast Ranges, a region that is host to numerous fossil and active Hg-rich hydrothermal systems. Mineralization in the region is related to increased heat flow and volcanism caused by the migration of the Mendecino Triple Junction through the region beginning at 2.3 Ma. There are two types of mercury deposits present in the area, hot-spring deposits that form at shallow depths (<300 m) and silica-carbonate deposits that extend to depths of 1000 m. Active springs and geothermal areas continue to precipitate Hg and Au and are analogues to the fossil hydrothermal systems preserved as ore deposits.

The hydrothermal systems of The Geysers-Clear Lake area are mainly hosted by the Mesozoic Franciscan accretionary wedge and Great Valley Sequence forearc sedimentary rocks, which have median Hg concentrations of 51 and 64 ppb respectively. Mafic and felsic rocks of the latest Tertiary Clear Lake Volcanic Field, which erupted to cover and intruded into the Mesozoic basement rocks, have lower median Hg concentrations of 27 ppb. The mean Hg isotopic compositions of the rocks in the Great

Valley Sequence (-0.63‰ $\delta^{202}$Hg, n = 19), Franciscan Complex (-0.43‰ $\delta^{202}$Hg, n = 11) and Clear Lake Volcanic Field (-0.54‰ $\delta^{202}$Hg, n = 10) are similar (one way analysis of variance, $p<0.05$) although there is significant variance among $\delta^{202}$Hg values of the Franciscan Complex. Hot spring and silica carbonate ore deposits have similar mean Hg isotopic compositions to the potential source rocks, but there is more variability in the isotopic compositions of the ore deposits, which range from +0.55 to -3.88‰ $\delta^{202}$Hg. Active hot springs in the region precipitate sulfidic mud that contains up to 4890 ppm Hg and 14 ppm Au. The Hg isotopic compositions of these precipitates range from -0.21 to -3.42‰ $\delta^{202}$Hg, and are in, general, lighter than ore deposits and host rocks in the region.

Hg isotopic compositions presented here suggest that processes that leach and transport Hg from source rocks cause very little isotopic fractionation (< ± 0.5‰). Significant isotopic fractionation occurs in the near-surface zones of hydrothermal systems. Boiling of hydrothermal fluids or separation of a mercury-bearing $CO_2$-rich vapor is likely the most important process causing the observed Hg isotope fractionation. This should result in the release of mercury with low $\delta^{202}$Hg values into the atmosphere from the top of these hydrothermal systems. Estimates of mass balance indicate that only a small amount of Hg (< 3.5%) leaves active ore-forming systems and residual Hg reservoirs are not measurably enriched in heavy Hg isotopes as a result.

## 1. INTRODUCTION

Presented here is the first study of Hg isotopes in the California Coast Ranges, an area with widespread evidence of Hg mobilization and mineralization. The goal of this work is to assess Hg isotope ratios as tracers of metal source, examine how low-

temperature geochemical processes fractionate Hg isotopes, and gain insight into the biogeochemical cycling of this toxic element in areas of Hg enrichment and anthropogenic disturbance.

The Geysers-Clear Lake area offers a unique natural environment for this study. The area is host to the northernmost of a chain of Hg and Au ore deposits that extends south along the San Andreas Fault for 400 km (Fig. 4-1). The largest ore deposits in the chain, New Almaden and New Idria, produced nearly 70 000 metric tons of Hg (2 million flasks, 1 flask = 76 lb), and are the fourth and fifth largest Hg deposits in the world (Rytuba, 2003). This belt of mineralization is related to the tectonic evolution of the North American Plate boundary from a subduction to transform margin after the impingement of the Mendecino Triple Junction on the North American plate at 29 Ma (Atwater, 1970). The northward migration of the Mendecino triple junction exposed the lower crust to the shallow aesthenosphere through a slab-less window along the southern edge of the northward moving Gorda plate (Dickinson and Snyder, 1978). This effect caused an increase in heat flow along the San Andreas transform boundary that resulted in widespread hydrothermal activity that formed the multitude of ore deposits along the California Coast Ranges (Benz, 1992; Rytuba, 1995). This transient heat flux is reflected in the ages of volcanic centers in the California Coast Ranges that decrease from 15 Ma in the south to 0.01 Ma in the Gyesers-Clear lake area (Fig. 4-1) (Fox et al., 1985; Wagner et al., 2005).

The Geysers-Clear Lake area is well suited for a study of Hg isotope geochemistry because it is possible to sample in detail active and fossil hydrothermal systems that have continuously deposited Hg over the last 2.3 Ma. The area is host to

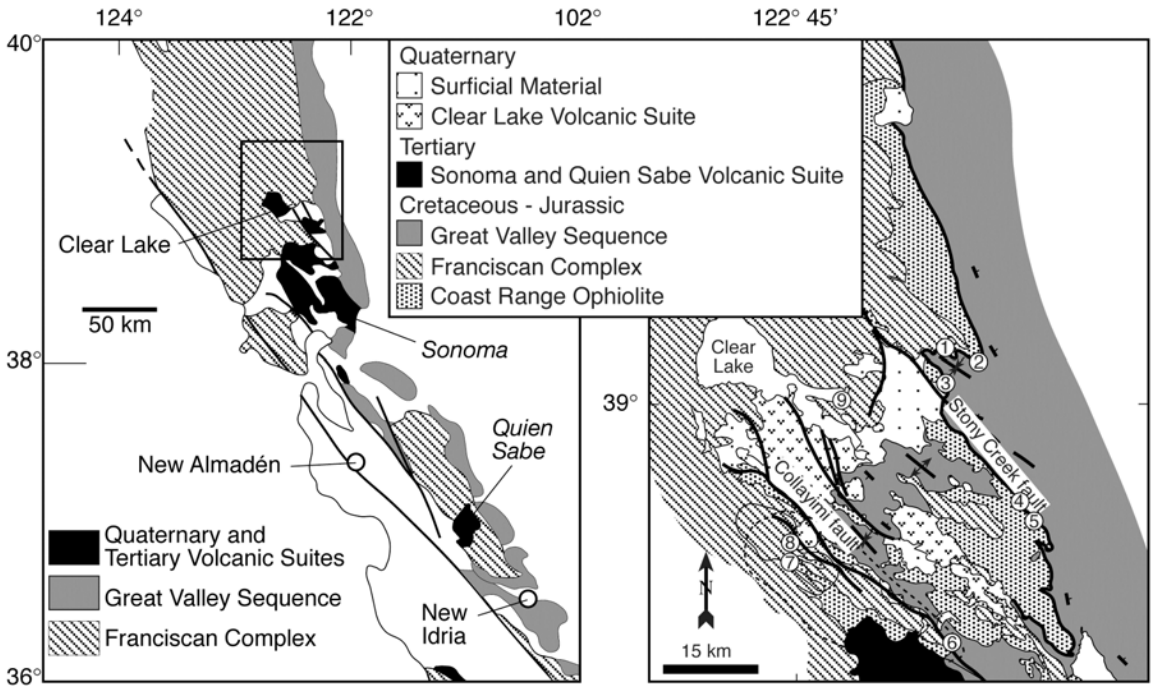


Figure 4-1. A. Regional geologic map of the California Coast Ranges showing the location of major lithologic units and mercury deposits. Inset shows location of map in 1B B. Generalized geologic map of the Clear Lake district showing location of deposits and other features discussed in the text. 1 – Elgin, 2 – Blanc, Jones, Elbow, Manzanita, Wideawake, Wilbur, 3 – Abbott, Turkey Run, 4 –Baker, Harrison, Manhattan, Reed, 5 – Knoxville, McLaughlin, 6 – Aetna, Corona, Oat Hill, 7 – Contact, Culver-Baer, 8 – Anderson, Schwartz. The Geysers geothermal area is inside the dashed zone that includes points 6,7 and 8.

numerous Hg and Au-Hg ore deposits, some with clear links to volcanic activity including active hot springs precipitating Hg and Au minerals today, and others with a more enigmatic connection to local volcanic activity, which include the serpentinite-hosted silica-carbonate type. This study also includes data from the massive Hg deposits at New Almaden and New Idria, which lie to the south of the main study area (Fig. 4-1A), for purposes of comparison. Excellent surface exposures of possible source rocks for the abundant metals in the region include Mesozoic forearc and back arc assemblages of the Franciscan Complex, Coast Range Ophiolite and Great Valley sequence, as well as the Neogene volcanic rocks of the area.

From field exposures of the Hg mineralization, source rock and geothermal systems throughout the Clear Lake region it is possible to obtain samples that test:

1) The Hg isotopic signatures of possible source rocks.
2) Magmatic (Sherlock, 2005) and amagmatic (Moiseyev, 1971) genetic models of Hg mineralization.
3) Evolution of Hg isotopic compositions over a period of 2.3 Ma.
4) The role of physical and chemical processes that formed the Hg mineralization.

## 2. GEOLOGY OF THE GEYSERS-CLEAR LAKE AREA

The geology of northern California in the Geysers-Clear Lake area is characterized by a Mesozoic paleosubduction zone complex overlain by Tertiary and Quaternary volcanic and shallow marine sedimentary rocks. The paleosubduction zone is preserved in three tectonostratigraphic units; the Franciscan Complex accretionary

wedge, the overthrust Coast Range Ophiolite, and the time-equivalent forearc rocks of the Great Valley Sequence (Fig. 4-1). The Great Valley Sequence and Coast Range Ophiolite were thrust over the coeval Franciscan Complex during continental accretion and subsequently disssected by north- and northwest-, trending strike-slip, normal and reverse faults related to the San Andreas transform fault system. These rocks were later covered by the Sonoma and Clear Lake volcanic fields of late Tertiary to Holocene age.

## 2.1 Country Rocks

The Franciscan Complex is a classic fossil subduction-zone accretionary wedge (Bailey et al., 1964; Ernst, 1970; Wakabayashi, 1999). It is comprised of a volumetrically small percentage of 1-300 m tectonic blocks of eclogite, amphibolite and blueschist in a matrix of lower grade meta-sedimentary rock and serpentine. The matrix of the unit contains weakly metamorphosed sections of sandstone, mudstone, chert and mafic rock structurally interleaved with other sections that have been metamorphosed to a maximum grade of prehnite-pumpellyite facies (T~250˚C) (Ernst et al., 1970). The terrigenous sedimentary rocks are interpreted to be similar to those of the Great Valley Sequence (see below) and are likely derived, at least in part, from a similar source (Jayko and Blake, 1984).

The Coast Range Ophiolite is exposed mainly in a narrow zone between the forearc rocks of the Great Valley Sequence to the east and the Franciscan mélange to the west and as tectonic slices within the Franciscan Complex (Fig. 4-1). The contact between these units has been modified by numerous episodes of faulting since accretion and the current high-angle fault boundary may have strike-slip as well as thrust components (Unruh, 1995). The rocks of the Coast Range Ophiolite consist of mafic lava

flows and serpentine, often in tectonic slivers (Shervais, 1990). This study sampled both large blocks of the ophiolite at the fault boundary and small slivers in the Franciscan.

The Great Valley Sequence was deposited in a Cretaceous forearc basin in-board of the Franciscan accretionary wedge. The unit is composed of sandstone, mudstone and conglomerate that was shed off the Klamath-Sierra arc and has a maximum thickness of 15 km. The early Cretaceous depositional environment evolved from a slope setting to a broad bathyl forearc basin with extensive turbidite deposits as the basin widened in response to eastward migration of the arc and westward thickening of the accretionary prism (Ingersoll, 1979). Reports of the metamorphic grade of the Great Valley Sequence vary with thickness and location. In general the unit is weakly metamorphosed to zeolite facies (< 250 ˚C) (Blake et al., 1988) and oxygen isotope evidence suggests that a maximum temperature of 175 ˚C was attained (Sucheki and Land, 1983), corresponding to conditions of burial metamorphism.

The Late Tertiary to Quaternary Sonoma and Clear Lake volcanic sequences intrude and overlie the Mesozoic units. These volcanic fields are the youngest and northernmost of a series of Cenozoic volcanic fields related to magmatism initiated by the northward migration of the Mendocino Triple Junction and the accompanying slab window (Dickinson and Snyder, 1979; Benz et al., 1992; Brady and Spotila, 2005). The Sonoma Volcanic field ranges in age from 8.2 to 2.5 Ma and the Clear Lake Volcanic field ranges from 2.1 Ma to 10 ka (Hearn et al., 1981; Donnelly-Nolan et al., 1981; Wagner et al., 2005). Geothermal activity at The Geysers and elsewhere in the Clear Lake region is related to this later phase of volcanic activity.

In the Clear Lake Volcanic field, early widespread flows of basaltic andesite were followed by more localized rhyodacite and dacite flows as the center of volcanism moved northward with time (Hearn et al., 1981). The presence of silicic intrusions in the Clear Lake area has been confirmed by drilling at The Geysers geothermal field, which lies above a 1.1-1.2 Ma (Dalrymple et al., 1999) composite intrusion of granite, granodiorite and microgranite porphyry referred to as The Geysers "felsite" (Hulen et al., 1993). The presence of other magma chambers in the area still in the process of crystallization has been inferred from high $^{3}He/^{4}He$ ratios in gases from the Northwest Geysers (Kennedy and Truesdell, 1996). Sr and Nd isotopic analyses suggest that silicic magmas of the Clear Lake Volcanic field (CLVF) are a mixture of mantle-derived basalt with as much as 40% partial melting of the crust (Hammersley and DePaolo, 2006).

## 2.2 Ore Deposits of the California Coast Ranges

The Geysers-Clear Lake area contains three types of ore deposits: hot spring Au-Hg, hot spring Hg and silica-carbonate Hg (Rytuba, 1995) (Table 4-1)(Fig. 4-2). All deposits have been proposed to have formed from a similar connate fluid source (Peters, 1990; 1991), but vary in deposit type and metal content according to host rock type, dilution of the ore fluid with meteoric water and local thermal gradient. In general, economic concentrations of Hg, but not Au, formed from cool (~50 to 150 ˚C) and often dilute mixtures of connate and meteoric waters (Barnes et al., 1973; Peters, 1993). Where these fluids reacted with serpentinite, silica-carbonate Hg deposits formed and where these fluids boiled near the surface, hot spring Hg deposits formed in the vapor-rich vadose zone. Au ore deposits formed in areas of high heat flow in structural settings that

Table 4-1. Ore deposit descriptions by district (Rytuba, 1995).

| Name | Deposit Type | Alteration | Age (Ma) |
|---|---|---|---|
| **Maycamas District** | | | |
| Culver-Baer | Silica-Carbonate Hg | Silica-Carbonate | |
| Contact | Silica-Carbonate Hg | Silica-Carbonate | |
| Socrates | Silica-Carbonate Hg | Silica-Carbonate | |
| Schwartz | Silica-Carbonate Hg | Kaolinite | |
| Big Chief | Silica-Carbonate Hg | Kaolinite | |
| Corona | Silica-Carbonate Hg | Silica-Carbonate | |
| Oat Hill | Hot Spring Hg | Kaolinite-Quartz | |
| **Sulphur Bank** | Hot Spring Hg | Alunite-Kaolinite | <0.044 |
| **Wilbur Springs District** | | | |
| Turkey Run | Silica-Carbonate Hg | Silica-Carbonate | |
| Abbott | Silica-Carbonate Hg | Silica-Carbonate | |
| Wideawake | Silica-Carbonate Hg | Silica-Carbonate | |
| Elgin | Silica-Carbonate Hg/ Hot Spring Hg (?) | Silica-Carbonate/ Kaolinite-Quartz | |
| Manzanita | Hot Spring Au-Hg | Adularia | |
| In-Between | Hot Spring Au-Hg | Adularia | |
| Cherry Hill | Hot Spring Au-Hg | Adularia | 0.56±0.14 |
| **Knoxville District** | | | |
| McLaughlin | Hot Spring Au | Alunite | 0.75 |
| Manhattan | Hot Spring Hg | Quartz-Chalcedony | |
| Knoxville | Silica-Carbonate Hg | Silica-Carbonate | |
| Reed | Silica-Carbonate Hg | Silica-Carbonate | |
| Soda Springs Prospect | Silica-Carbonate Hg | Silica-Carbonate | |

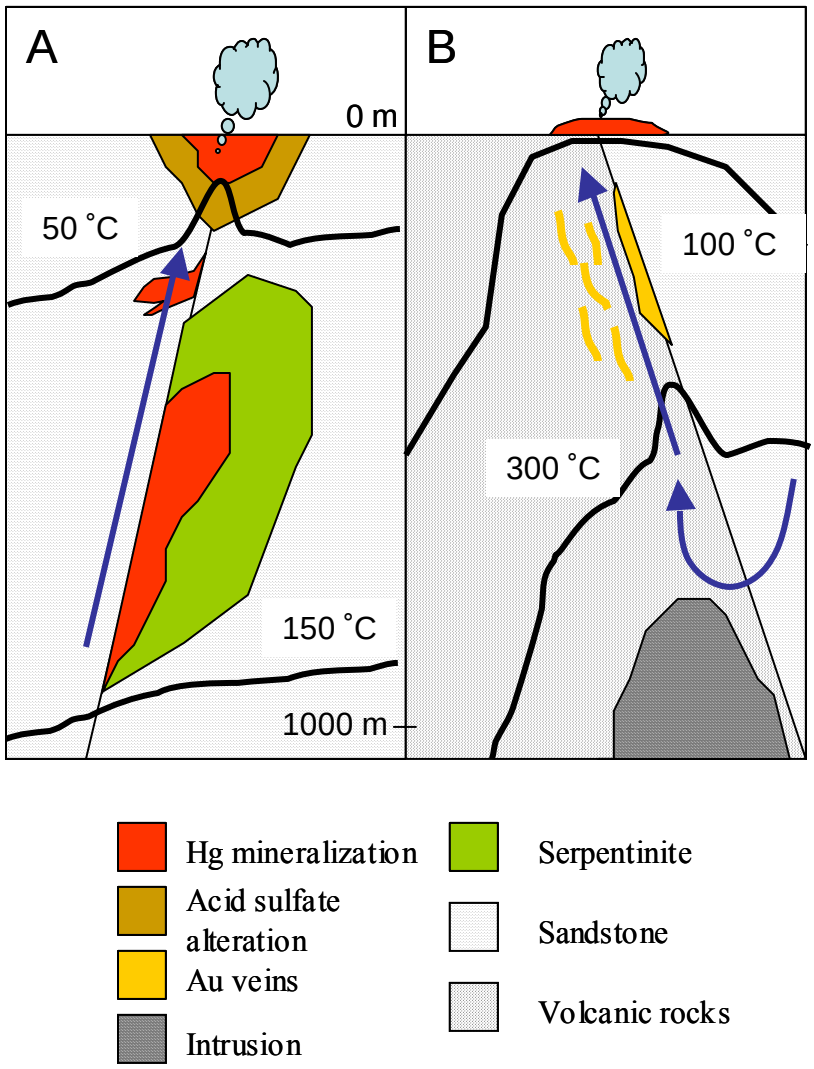


Figure 4-2. Schematic model for the formation of the different ore deposit types present in the California Coast Ranges. All deposits types are proposed to formed from similar hydrothermal fluids with a significant connate component, but vary according to host rock and local thermal gradient. Silica-carbonate Hg deposits form from cool (~150 ˚C), reduced fluids that reacted with serpentinite (Rytuba, 1995). Where similar fluids interact with sandstone, hot spring Hg deposits form. Hot spring Au-Hg deposits form from higher temperature (200 – 250 ˚C), $H_2S$-rich fluids that deposit quartz and precious metals in veins at depth and Hg in silica sinter at the paleosurface (Sherlock et al., 1995).

focused connate fluids in narrow zones where the fluids boiled and deposited quartz and precious metals in veins at depth and that reached the surface locally to form silica sinter containing Hg (Sherlock et al., 1995). These deposits required higher temperatures (200 – 250 ˚C) and less dilute connate fluids to form Au bisulfide complexes in economic concentrations.

Silica-carbonate-type deposits consist of cinnabar and $Hg^0$ associated with amorphous silica and Mg-carbonate minerals that replace serpentinite host rock. The largest examples of this class, New Almadèn (Bailey and Everheart, 1964) and New Idria (Linn, 1968), are associated with regional-scale antiformal structures that trapped ore-forming fluids. The Geysers-Clear Lake area, where this study is centered, contains much more numerous, but smaller silica-carbonate type deposits, and is of greater interest because the deposits are spatially associated with active hot springs. These deposits formed from low temperature (<120 ˚C) $CO_2$-$CH_4$-$H_2S$-rich fluids similar in composition to oil and gas field brines along fault contacts with serpentinite blocks and many of these deposits contain liquid and solid hydrocarbons (e.g. Peters, 1991; Peabody and Einaudi, 1992; Sherlock et al., 1993).

Hot spring Hg deposits consist largely of disseminated cinnabar in a shallow zone of acid sulfate-type alteration of wallrock consisting of kaolinite and alunite or in silica sinter. A few of these systems such as the Sulphur Bank Hg deposit, which began to form as recently as 44 k.y. ago (Fig. 4-1B, site 9), are still actively depositing Hg sulfides from hydrothermal fluids at the surface (White and Roberson, 1962). These deposits preserve evidence of shallow depths of formation that include cinnabar “paint” along fractures, a

feature that formed from condensed Hg-rich vapor above a boiling hydrothermal system (e.g. Rytuba and Heropolous, 1992).

A few hot spring-type deposits in The Geysers-Clear Lake area also contain Au in veins that formed 100's of m below the paleosurface. The largest of these is McLaughlin (Fig. 4-1, site 5), which consists of electrum (Au-Ag alloy) and sulfides in quartz veins and Hg in silica sinter that was deposited at the paleosurface (Sherlock et al., 1995). In the Wilbur Springs District (Fig. 4-1, site 2), electrum, sulfides and hydrocarbons were deposited in quartz-carbonate-adularia (K-feldspar) veins at the Cherry Hill and Manzanita mines, associated with argillic alteration of the Great Valley Sequence host rock (Pearcy and Petersen, 1990). Evidence from fluid inclusions indicates that these formed at moderate temperatures (185-260 ˚C) from low salinity (<2.4 wt% NaCl eq.) hydrothermal fluids (Pearcy and Petersen, 1990; Sherlock et al., 1995) consisting of a mixture of connate water from the Great Valley Sequence diluted with meteoric and possibly magmatic waters (Peters, 1991).

It is not clear from field relations and geochemical evidence whether the low temperature silica-carbonate deposits represent an earlier, cooler stage of regional heating and the hot springs deposits a later period of higher heat flow (cf. Rytuba, 1995) or are more representative of a spatial relation to volcanic centers and the specific alteration types associated with the host rocks in the area. The magnesite-chalcedony alteration assemblage that identifies silica-carbonate type deposits will only form in serpentinite host rock (Sherlock et al., 1993). Hot spring deposits are restricted to sedimentary and volcanic rock hosts that contain feldspars, which are altered to an assemblage of kaolinite, alunite and silica at shallow depths (Yates and Hilpert, 1946; White and

Roberson, 1962). In the Knoxville District, silica-carbonate Hg deposits surround the McLaughlin hot spring Au-Hg deposit. Within the McLaughlin deposit higher temperatures are recorded in fluid inclusions in deeper vein samples and cooler temperatures are observed in shallow samples, near the Hg-rich sinter that lies on the top of the deposit (Sherlock et al., 1995). This relation of deeper, hotter and distal, cooler zones may also be reflected in the distribution of silica-carbonate type Hg deposits that surround McLaughlin.

2.3 Active Springs

Active hydrothermal systems are discharging moderately saline, isotopically modified waters at springs throughout The Geysers-Clear Lake area that have been interpreted to be mixtures of meteoric and connate fluids analogous to the ore fluids that formed the Hg and Au-Hg deposits of the region (Barnes, 1970; Barnes et al., 1973; White et al., 1973; Peters, 1991, 1993). There is a large body of geochemical evidence in the literature that supports the involvement of connate fluids from and water-rock interaction with the Great Valley Sequence in the active and fossil hydrothermal systems of the California Coast Ranges (Barnes, 1970; White et al., 1973; Peters, 1991, 1993; Donnelly-Nolan et al., 1993; Rytuba, 1993; Sherlock, 1995, 2005). The nature of this connate fluid has been a matter of debate with various compositions proposed from trapped Cretaceous seawater in pore fluids based on $^{129}I$ and $^{36}Cl$ isotopes (Fehn et al., 1992) to highly exchanged meteoric water with Great Valley Sequence rock based on evidence from O isotopes (Sherlock, 2005). Peters (1993) proposed a mixing model based on the stable isotope geochemistry of active springs where hot connate fluids were

progressively diluted with cooler meteoric fluids. All of these scenarios require the interaction of the hydrothermal fluid with the Great Valley Sequence.

Springs in the area can be grouped into: 1) cooler, and more dilute mineral springs transporting minor amounts of Hg and no Au, 2). hot springs that are precipitating significant amounts of Au and Hg. The springs range in temperature from about 28 to 99ºC and in pH from about 6.2 to 8.4 and both variables show a strong positive correlation with the mercury content of these waters (Figure 4-3). Mineral springs discharge cool (< 30 ˚C), gas-rich ($CO_2$, $CH_4$) fluids and have lower Hg contents and no Au (Peters, 1993). Baker Soda Springs is a cool, mineral spring that discharges from a travertine terrace immediately adjacent to the Baker silica-carbonate Hg mine. Grayish precipitates from the springs contain Hg and the chloride content of the spring water (2985 ppm) is similar to other minerals springs in the region that are fed by a mixture of meteoric water and saline, connate fluids derived from the Great Valley sequence (Peters, 1993). Mineral springs discharging from the Turkey Run mine are relatively low in Hg and have salinity similar to that of Baker Soda Springs. Precipitates sampled from a groundwater monitoring well at the McLaughlin mine, southeast of Baker Soda Springs, contain up to 261 ppm Hg and the water has a low salinity typical of meteoric derived fluids.

Hot springs of the Wilbur Springs district in the Sulfur Creek basin are spatially related to several hot spring-type Au-Hg deposits, and unlike the cooler mineral springs, are currently precipitating significant Hg and economic amounts of Au (Fig. 4-1, site 2). The spring fluids are geochemically distinct from the cooler springs and contain less metoric component and a greater connate fluid signature with heavier $\delta^{18}O$ and higher

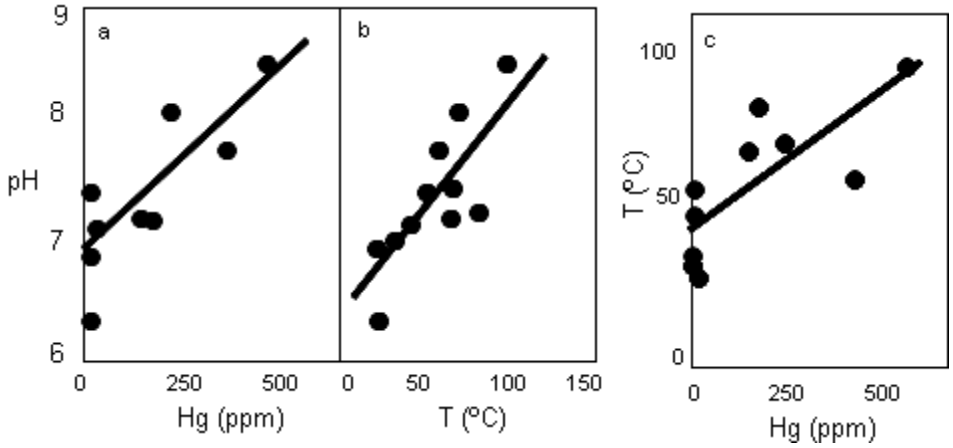


Figure 4-3. Concentrations of Hg in spring precipitates correlates positively with a) pH and c) temperature of the discharging spring waters confirming that $Hg^0_{aq}$ solubility is enhanced by higher pH and temperature (Varekamp and Buseck, 1984). Water pH decreases as: 1) springs lose $CO_2$ to the atmosphere and/or 2) precipitate carbonates, which is consistent with the correlation between temperature and pH (b). Lower temperature waters indicate dilution with cool, near neutral meteoric water and/or conductive cooling and degassing of deep fluids near the surface. Data reported in Table 4-4.

chlorinity. Elbow Springs (Fig. 4-1, site 2) discharges at about 70 ˚C, is chloride-rich (12,000 ppm) and precipitates in the spring contain cinnabar and native Au. Less than 200 m away, Jones' Fountain of Life discharges $CO_2$ and $CH_4$-rich water at about 60 ˚C and spring precipitates there also contain cinnabar and Au as do light gray precipitates from nearby Blanck Springs. Four kilometers northwest of the Au-Hg depositing springs of Sulfur Creek, Elgin Spring discharges fluids similar in temperature, chloride and sulfate content (Fig. 4-1, site 1; Table 4-4). Here the active spring precipitates black sulfidic mud that contains microcrystalline cinnabar and native Au and is associated with hot spring-type Hg mineralization that has over-printed earlier silica-carbonate alteration.

Hot springs depositing Hg, but not Au, are associated with The Geysers steam field, which is one of the largest vapor-dominated geothermal reservoirs in the world (Fig. 4-1); it produced 2000 MW at its peak in the 1960's and currently produces about 1000 MW. The reservoir is hosted in a series of imbricated thrust sheets comprised of Franciscan greenstone, greywacke and serpentinite that are cut by high-angle faults that compartmentalize the reservoir (Thompson, 1992). Underlying the field is The Geysers "felsite", a large concealed silicic intrusive body. The felsite has metamorphosed adjacent sedimentary rocks to biotite-tourmaline hornfels and produced weak base metal mineralization (Hulen et al., 1993). High $^{3}He/^{4}He$ ratios in well samples from the Northwest Geysers indicate that a younger, crystallizing intrusion in the northwest Geysers area supplies heat and some chemical components to the current steam reservoir (Kennedy and Truesdell, 1996).

The Geysers steam field is thought to have begun as a liquid-dominated reservoir that persisted from 1 Ma to 0.25 Ma and to have undergone a catastrophic

depressurization event followed by boiling that created the present day vapor-dominated reservoir (Hulen et al., 1997). Studies of fluid inclusions and oxygen isotopes have shown that fluid in the reservoir is largely connate in origin, diluted to various extents with slightly exchanged meteoric water, much like the other thermal springs in the region (Moore and Gunderson, 1995). Steam escaping from the vapor reservoir has caused regional argillic alteration of the host rock and manifestations at the surface include areas of steaming ground, native S mounds and mudpots. Escaping steam deposits Hg and hydrocarbons at the present surface in The Geysers geothermal system. Along the margins of the steam reservoir are the Culver-Baer, Socrates, Anderson and other slica-carbonate Hg ore deposits of the Western Maycamas District (Fig. 4-1).

## 3. ANALYTICAL METHODS

### 3.1 Sample Preparation

Ore and rock (from mine workings and outcrop) and hot and mineral spring precipitates were collected during the 2002 and 2005 field seasons. Additional samples were provided from the extensive collections of E.H. Bailey and J.J. Rytuba of the U.S. Geological Survey and the National Museum of Natural History (NMNH). For geochemical analyses, rock samples were broken with a steel hammer and fresh pieces were crushed to a powder in a stainless steel disc mill and stored in plastic bags. Ore mineral (cinnabar) separates were hand-picked under a binocular microscope for most samples, with the exception of very fine-grained samples that were crushed in a steel mortar and analyzed in bulk. Spring precipitates were collected with spring water in pre-cleaned borosilicate glass jars with PFA lined lids (I-Chem®) and stored at 4 ˚C. In

preparation for digestion, spring precipitates were dried on filter paper in a HEPA filtered laminar flow hood and stored in plastic bags.

Samples were decomposed for analysis using either acid dissolution or pyrolysis, depending on the matrix composition and concentration of Hg in the sample. Mineral separates and spring precipitates (~0.05 - 0.30 g) were weighed into 15 mL PFA vessels and 4 mL of a 3:1 mixture of concentrated ultrapure $HCl/HNO_3$ was added (Lechler et al., 1997). The vessels were capped tightly and placed on a 90 °C hot plate overnight, and then opened and diluted with DDI water. The acidic solution was centrifuged and the supernatant was removed from the insoluble residues, which typically consisted of silicate and oxide minerals. The digested samples were stored in borosilicate glass vials with PFA lined caps to retain the Hg in solution.

Rock powders (~1-2 g) were weighed into glazed ceramic boats and loaded into a two-stage pyrolysis-combustion apparatus described in Chapter II and Smith et al. (2005). The samples were step-heated to 750 ˚C under a flow of Ar for 17 minutes, which released all Hg from the samples. The Ar stream flowed into a second chamber, held at 1000 ˚C, and combusted with a stream of $O_2$. The gas flow was then bubbled through an impinger into an oxidizing solution of 1% $KMnO_4$ (w/v) where Hg was effectively trapped in solution as $Hg^{2+}$. Procedural blanks and sample recoveries were determined for samples and standards. The 1% $KMnO_4$ solution was reduced with hydroxylamine hydrochloride to dissolve any precipitated $MnO_2$ solids resulting in a clear solution ready for dilution and analysis. This technique of liquid trapping is a common method for sampling flue gases with relatively high concentrations of Hg in industrial settings (EPA 7470).

## 3.2 Hg Elemental and Isotopic Compositions

All Hg elemental and isotopic analyses were performed on a Nu Plasma multi-colector inductively-coupled-plasma mass-spectrometer (MC-ICP-MS) at the University of Michigan, Ann Arbor. The Hg concentration of each sample was determined by MC-ICP-MS detection employing a standard calibration curve (Yoshinaga and Morita, 1997). Relative error of the Hg concentrations is estimated to be ±5% (1σ).

Samples were analyzed for Hg isotopic composition using the analytical procedures described in Smith et al. (2005) and Chapter II. For samples with Hg concentrations above ~1 ppm, digests were diluted to 20 ± 1 ppb Hg. Samples processed by pyrolysis typically produced solutions with concentrations ranging from 2-10 ppb and were matched to standards with similar (±5%) concentrations. The sample was introduced into the MC-ICP-MS, using continuous-flow, cold-vapor generation in a gas-liquid separator with $Sn(II)Cl_2$ as the reducing agent. Instrumental mass-bias was corrected using: 1) an internal thallium (Tl) spike (NIST 997) introduced as an aerosol to the gas flow by a Cetac Technologies Airdus desolvator employing a MCN-2 microconcentric nebulizer and 2) sample-standard bracketing using a NIST 3133 solution matched in concentration and matrix to each sample (Smith et al., 2005; Chapter 2). Cold vapor generation allows quantitative chemical separation of the $Hg^0$ vapor from the sample matrix, thus eliminating matrix effects because only Hg and minor amounts of $H_2O$ and HCl vapor enter the plasma. Chemical purification by cold-vapor generation is quantitative and much simpler than chromatographic methods where the possibility of fractionation during separation of the element of interest is much greater.

Isotopic fractionation was measured relative to the NIST 3133 Hg standard, which was analyzed before and after each sample. All of the Hg isotopes except for $^{199}$Hg were measured routinely and fractionation was observed to be mass-dependent. Hg isotope compositions are reported in delta notation as $\delta^{202}$Hg in permil (‰), referenced to NIST 3133, because this ratio has the best balance between precision of measurement and mass difference. $\delta^{202}$Hg values are calculated as:

$$\delta^{202}\text{Hg} = 1000*\{[(^{202}\text{Hg}/^{198}\text{Hg})_{\text{sample}}]/[(^{202}\text{Hg}/^{198}\text{Hg})_{3133}]\text{-}1\}.$$

Typical internal precision was better than ±0.05‰ (2SE) on a daily basis. The average $\delta^{202}$Hg value and external reproducibility of NIST 3133 and our laboratory standard (elemental Hg from Almadèn, Spain) was –0.55 ± 0.08‰ (2σ, $n$ = 43), based on repeated measurements during this study. The 2σ reproducibility for multiple analyses of 3 natural ore specimens ranged between ±0.06 and ±0.09‰ ($n$ = 60), and ±0.1 ‰ was used as a conservative estimate of the external reproducibility for this study. Blanks and sample introduction memory effects were monitored after each standard and sample run and were < 1% of the total signal.

## 4. RESULTS

### 4.1 Hg Concentrations

#### 4.1.1 California Coast Range Rocks

Hg concentrations for samples from the Clear Lake Volcanic suite range from 16 to 288 ppb by weight ($\bar{x}$ = 66, M = 25 ppb) (Fig. 4-4) (Table 4-2). In the rocks of the Franciscan Complex and Coast Range Ophiolite, Hg concentrations range from 21 to 88 ppb ($\bar{x}$ = 52, M = 51 ppb) (Fig. 4-4). Sedimentary rocks from the Great Valley Sequence range from 32 to 154 ppb Hg ($\bar{x}$ = 71, M = 64 ppb) (Fig. 4-4). Mercury concentrations

are highest in Franciscan and Great Valley sedimentary rocks, especially fine-grained varieties, and lowest in igneous and metamorphic rocks, with all but 4 samples have <100 ppb Hg. These total concentrations and general abundances by rock type are comparable to literature values (see reviews by Wedepohl, 1995 and Rytuba, 2005). None of the rock types has sufficient Hg enrichment to dominate the Hg geochemistry of the study area or be considered an enriched Hg source.

The Great Valley mudstones have higher Hg concentrations than the sandstone samples, and form distinct groups ($p$ = 0.04) according to Hg content by lithology, similar to analyses of these rock types reported in the literature (e.g. McNeal and Rose, 1974; Peck, 1975) (Table 4-3). The Hg content of the mudstones does not appear to correlate to the organic content of the rock ($R^2$ = 0.01). The relationship between organic matter and Hg content is obscured in the smaller sandstone sample population due the low total organic carbon (TOC) content of the sandstones and the resolution of the TOC analyses (± 0.17 wt%, 1SE).

Table 4-2. Analytical results for The Geysers-Clear Lake area rock samples.

| Sample No. | Description | $\delta^{202}$Hg | Hg (ppb) | TOC (wt%) | $^{87}Sr/^{86}Sr$[a] | εNd[a] |
|---|---|---|---|---|---|---|
| 98HCL11 | GV sandstone collected near Loch Lomond | -0.53 | 40.8 | 0.10 | 0.70702 | -2.64 |
| GVBC-1 | Fe-Ox stained mudstone | -0.85 | 85.0 | 1.24 | | |
| GVBC-2 | mudstone, near base of Knoxville Fm | -0.93 | 69.2 | 1.91 | | |
| GVBC-6 | thinly bedded mudstone | -0.50 | 63.1 | 0.36 | | |
| GVBC-7 | mudstone | -0.27 | 121.9 | 1.15 | | |
| GVSC-1 | shale at intersection of Hwy 20 and Bear Cr. Rd. | -0.81 | 50.6 | 0.08 | | |
| GVSC-2 | silty mudstone | -0.68 | 154.2 | 0.10 | | |
| GVSC-3 | mudstone w/ black organic-rich layers | -0.59 | 83.9 | 0.58 | | |
| GVSC-5 | sandstone | -0.57 | 48.4 | 0.10 | | |
| GVSC-6 | silty mudstone | -0.63 | 37.9 | 0.83 | | |
| GVSC-7 | sandstone w/ black plant hash | -0.34 | 41.7 | 0.08 | | |
| GVSC-8 | thinly bedded mudstone, near mouth of canyon | -0.17 | 64.1 | 0.10 | | |
| GVSC-9 | Fe-Ox stained mudstone | -0.68 | 109.9 | 0.10 | | |
| KF-1 | cg poorly sorted sandstone near Reed Mine | -0.91 | 31.5 | 0.09 | | |
| KF-2 | fg sandstone and mudstone | -0.93 | 65.0 | 0.35 | | |
| | | | | | | |
| 98HCL17 | Mt. Konocti sequence dacite of Wright Peak (dwp) | -0.25 | 21.7 | | | |
| 98HCL12 | Cobb Mtn sequence - rhyodacite of Cobb Mtn - dcf | -0.69 | 86.8 | | 0.70437 | 2.43 |
| 97HCL8 | Dacite of Konocti Bay - dkb | -0.74 | 92.2 | | 0.70352 | 1.94 |
| SB-16 | Early basaltic andesite - cinder cone on Hwy 20 - beu | -1.20 | 287.7 | | 0.70470 | 0.12 |
| 98HCL4 | Early basaltic andesite flow - Schoolteacher Hill - beu | -0.60 | 16.7 | | 0.70470 | 0.11 |
| 98HCL14 | Ford Flat Road - rhyodacite of Alder Creek - raf | -0.56 | 25.3 | | | |
| 98HCL2 | High Valley basaltic andesite - bhvfl | -0.57 | 17.2 | | 0.70390 | 0.10 |
| 98HCL13 | Cobb Mtn sequence - dacite of Cobb Valley - dcv | -0.49 | 16.5 | | 0.70518 | -0.04 |
| 01HCL01 | Roundtop mountain basalt - brp | -0.46 | 28.2 | | 0.70369 | 0.26 |
| | | | | | | |
| CR-1 | metabasalt of Coast Range ophiolite, Geysers rd. near cold Spr. | -0.65 | 21.3 | 0.08 | | |
| F1 | serpentine, Hwy 29 near Lake County line | -0.71 | 24.3 | 0.09 | | |
| F2 | lt. brown sandstone (greywacke) | -1.21 | 88.0 | 0.09 | | |
| F3 | blueschist, Geysers Rd. | -0.11 | 50.9 | 0.08 | | |
| F4 | Greywacke of Sulphur Cr. Unit | -0.43 | 86.3 | 0.08 | | |
| F5 | cherty mudstone, silica veining | -0.32 | 68.1 | 0.09 | | |
| F6 | greywacke | -0.88 | 61.0 | 0.10 | | |
| F7 | Blueschist, intersection of Clear Cr. Rd. and Cinnabar Rd. | 0.20 | 35.4 | 0.09 | | |
| SB-1 | Greywacke near Borax lake | 1.61 | 60.0 | 0.08 | | |
| SB-2 | Greywacke 0.75 mi. SSE Sulphur bank pit | -0.58 | 40.0 | 0.09 | | |
| Serp. Reiff Rd. | Serpentine outcrop at Yolo County line | -1.70 | 33.3 | 0.09 | | |

[a] From Hammersley and dePaolo, 2006

The Hg concentrations of the Great Valley sandstone samples average 46 ppb Hg, within the range of sandstones analyzed by Peck (1975) and Mc Neal and Rose (1974). The Hg concentrations of Great Valley Sequence mudstones average 84 ppb Hg, very close to the concentrations reported for the USGS Sco-1 Cody shale standard (Table 4-3) and the shales analyzed by Peck (1975) and Mc Neal and Rose (1974). Samples of the Great Valley Sequence with abundant Fe-oxide staining have Hg concentrations slightly greater than the mean (Table 4-2). The low TOC of both Great Valley sandstone and mudstone most likely indicates that sulfides, and possibly clays, rather than organic matter, are important Hg hosts in both rock types.

In the Franciscan, greywacke sandstone samples range from 40 to 88 ppb Hg, while tectonic blocks of blueschist contain between 35 and 51 ppb Hg. Serpentinite and metabasalt of the Franciscan and CRO have between 21 and 33 ppb Hg, similar to the mafic rocks of the Clear Lake Volcanic field. The metamorphosed sandstones of the Franciscan average 67 ppb Hg, slightly higher than the sandstone of the Great ValleySequence. Both the serpentinite of the CRO and metabasalt of the Franciscan have concentrations slightly higher than the concentrations reported for ultramafic rocks, typically < 7 ppb, but within the range reported for basalts

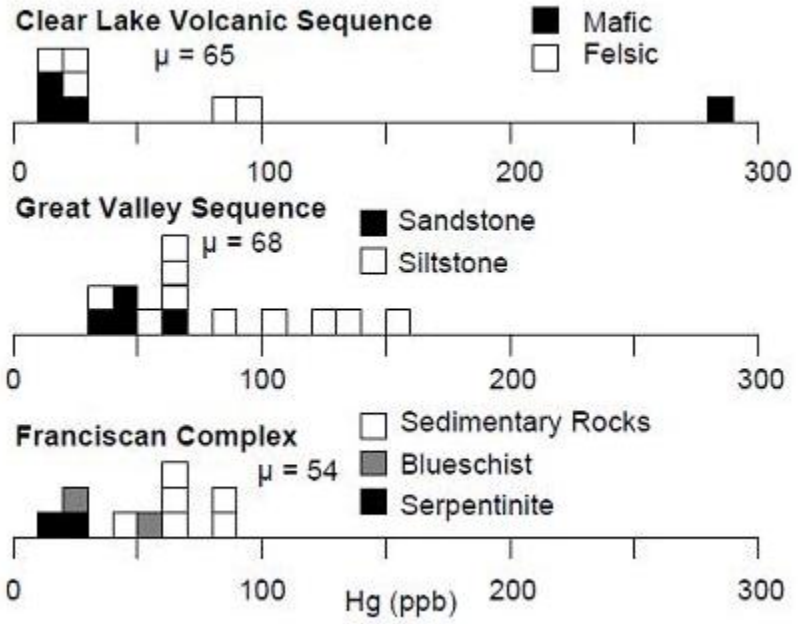


Figure 4-4. Hg concentrations of rock samples from the Franciscan Complex, Coast Range Ophiolite and Great Valley sequence by lithology.

Table 4-3. Hg concentrations for geostandards.

| Rock Type | Sample Name | Hg (ppb) | Description |
|---|---|---|---|
| ***Igneous, Mafic*** | | | |
| Basalt | JB-1 | 30[1], 28[2], 29.9[3] | |
| Andesite | JA-1 | 15[1], 11.7[3] | |
| | JA-2 | 1.8[1], 1.8[3] | |
| | DVA | 17[1] | |
| | DVB[1] | 15[1] | Basltic andesite |
| Peridotite | JP-1 | 6.5[1], 5.3[3] | |
| | PCC-1 | 9.7[7], | |
| Gabbro | JGb-1 | 6.8[1], 4.2[3], 2.1[2] | |
| | GPMA203 | 1.5[1] | Gabbronorite |
| Dunite | DTS-1 | 7[2], 7.7[7] | Dunite |
| ***Igneous, Felsic*** | | | |
| Dacite | DVD | 15[1] | |
| Rhyolite | JR-1 | 2.2[1], 8[4], 3.4[3] | |
| | JR-2 | 0.9[1], 0.9[3] | |
| Granodiorite | JG-1 | 19[1], 16.5[3] | |
| | JG-1a | 3.5[1], 4.1[3] | |
| Granite | JG-2 | 3.3[1], 3.3[3] | |
| | GPMA401 | 2.4[1] | Alaskite granite |
| | G-2 | 51[2], 40[5], 42[7] | |
| | GPMA402 | 2.7[1] | Biotitic granite |
| | GPMA403 | 3.8[1] | |
| | GPMA404 | 1.9[1] | Plagiogranite |
| ***Sedimentary*** | | | |
| Sandstone | GSR-4 | 8.4[2] | |
| Shale | Sco-1 | 73[1], 70[5], 71.5[6] | Cody shale |
| | SGR-1 | 305[1], 313[2] | Green River oil shale |
| | SDO-1 | 190[2] | Ohio shale |
| Limestone | JLs-1 | 5.6[1] | |
| | GSR-6 | 16[2] | |
| Chert | JCh-1 | 5.3 | |
| Marine Mud | MAG-1 | 59[1], 56.6[6] | |
| Marine Sediment | MESS-2 | 92[2] | Beaufort Sea |
| Silt | OOPE201 | 22[1] | Volcanoclastic |
| | OOPE402 | 12[1] | Siliceous |
| Clay | OOPE101 | 264[1] | Terrigenous |
| | OOPE501 | 93[1] | Red Clay |

All samples analyzed by CV-AAS. [1]Tershima (1994) [2]Govindaraju (1994)
[3]Imai (1995) [4]Ando et al. (1989) [5]Elrick and Horowitz (1986)
[6]Chan and Bina (1989) [7]Peck (1975)

. Blueschist samples are well within the broad range of values reported for metamorphic rocks and close to the values of a typical sandstone protolith (Mc Neal and Rose, 1974). Heating during metamorphism has been shown to mobilize and redistribute Hg in metamorphic rocks (Pitcairn et al., 2003), although the low grade metamorphosed rocks of the Franciscan and CRO have Hg contents very similar to that expected for their protolith.

The mafic and felsic volcanic rocks of the CLVF fall within the ranges reported for mafic igneous and felsic intrusive rocks world wide, typically between 3 to 30 ppb, (Table 4-3). Most of the Clear Lake Volcanic rock samples have Hg concentrations similar to those of other igneous rocks (Table 4-3). One CLVF sample, SB-16, has an anomalously high Hg content in comparison to all rock types (288 ppb), suggesting possible contamination of the sample by hydrothermal or anthropogenic Hg sources. Although there was widespread hydrothermal activity in the area (Donnelly-Nolan et al., 1993), the sample appears fresh and unaltered. It is possible that airborne particulates rich in Hg from the Sulphur Bank mine superfund site < 2km southwest contaminated the sample. Therefore, with few exceptions, the Hg concentrations of the rocks of the study area do not appear to be anomalous above the background expected.

4.1.2 Precipitates from Active Springs

Hg concentrations of mineral and hot springs in the study area range from 0.3 to 489 ppm, far greater than the country rock of the region (Table 4-4). Precipitates from the cool, mineral springs discharging from the Turkey Run Hg mine adit contain 0.3 ppm Hg,

Table 4-4. Geochemical and isotopic data from mineral springs and hot springs.

| Sample | Location | $\delta^{202}$Hg | Hg (ppm) | Au (ppm) | T (˚C) | pH | Flow (l/min) | Sulfate | Chloride |
|---|---|---|---|---|---|---|---|---|---|
| BSS-1 | Baker Soda Spring | -2.11 | 2.2 | 0.001 | 25 | 6.8 | 1 | 0.25 | 2985 |
| TRS-1 | Turkey Run adit | -1.37 | 0.34 | b.d. | 28 | 6.8 | 57 | 5310 | 1145 |
| ELB-1 | Elbow | -1.60 | 225.2 | 12.10 | 72 | 8.0 | 0.5 | 200 | 11390 |
| WS-1 | Elbow | -1.20 | | | | | | | |
| WS-1 | Elbow | -1.39 | | | | | | | |
| Jones' Ftn.-1 | Jones | -1.50 | 364.3 | 3.70 | 58 | 7.7 | 0-95 | 220 | 11860 |
| Blanck-1 | Blanck | -2.04 | 15.2 | 2.75 | 44 | 7.0 | 12 | 292 | 8510 |
| WS-3 | Wilbur Springs | -0.95 | 8.2 | 4.35 | 54 | 7.3 | 7 | 187 | 10910 |
| ELG-1 | Elgin | -3.03 | | 0.82 | 67 | 7.4 | 22.4 | 262 | 11480 |
| ELG-2 | Elgin | -3.42 | 113.3 | | | | | | |
| 99MPS02 | McLaughlin monitoring well | -0.48 | 81.9 | | | | | | |
| 99MPS02b | McLaughlin monitoring well | -0.21 | 261.4 | | | | | | |
| Geysers-1 | The Geysers | -1.18 | 15.0 | | | | | | |
| Geysers-2 | The Geysers | -0.70 | 66.5 | | | | | | |
| 99SM1s | Schwartz Mine adit | -0.85 | 7.5 | | 22 | 6.2 | | | |
| AHS-1 | Anderson Hot Springs | -1.56 | 141.3 | | 68 | 7.1 | | | |
| AHS-2 | Anderson Hot Springs | -1.02 | 163.8 | | 84.9 | 7.1 | | | |
| AHS-5 | Anderson Hot Springs | -0.98 | 489.5 | | 99.5 | 8.4 | | | |

the lowest concentration of the spring precipitates sampled. Baker Soda Springs is also a cool, mineral spring immediately adjacent to the Baker silica-carbonate Hg mine. Grayish precipitates from the springs contain 2 ppm Hg. Precipitates sampled from a groundwater monitoring well at the McLaughlin mine contain up to 261 ppm Hg, which is probably related to the presence of Au-Hg mineralization at the mine.

In the Sulfur Creek basin, springs are spatially related to several hot spring-type Au-deposits, and unlike the cooler mineral springs, are currently precipitating significant Hg and economic amounts of Au from saline waters (Fig. 4-1, site 15). Spring temperature and the Hg content of the spring precipitates vary considerably in the small (< 1 $km^2$) basin. Elbow springs precipitates contain 225 ppm Hg and 12.1 ppm Au and less than 200 m away, Jones' Fountain of Life spring precipitates contain 364 ppm Hg and 3.7 ppm Au. Blanck's spring is approx. 450 m SW from Jones' and is considerably lower in Hg concentration (15.2 ppm) as is Wilbur Springs (8.2 ppm), approx. 350 m NE from Elbow. Elbow and Jones' have much higher Hg concentrations than Blanck and Wilbur, although all springs contain considerable Au. Wilbur Springs is located in a streambed and is potentially diluted with groundwater during periods of increased runoff.

Elgin spring discharges fluids similar in temperature, chloride and sulfate content to the Sulfur Creek springs located 4 km SE (Fig. 4-1, site 14; Table 4-4). Here the spring is overprinting silica-carbonate alteration with hot spring-type Hg mineralization. The spring precipitates black sulfidic mud that contains 113 ppm Hg and 1.1 ppm Au.

Springs in and adjacent to The Geysers steam field discharge fluids derived from interaction of the vapor reservoir with local groundwater (Janik et al., 1999). Fluids from the North Central and Northwest Geysers have higher steam fractions (Y = 0.1-1.0) than

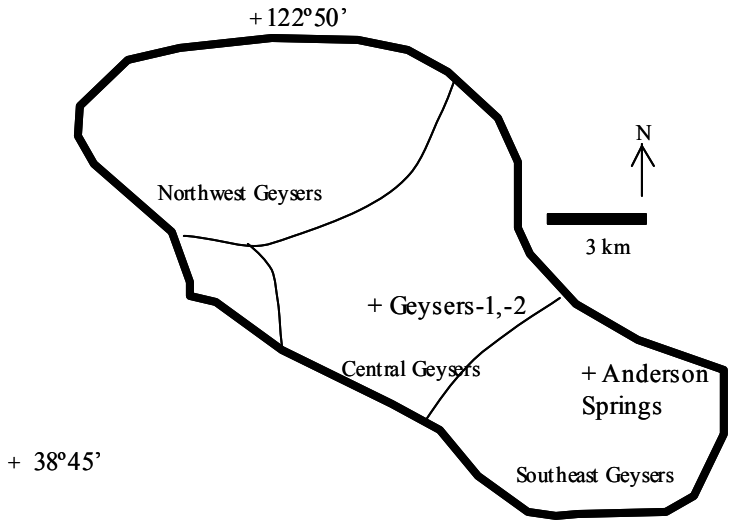


Fig. 4-5. The Geysers sample locations (modified from Lowenstern et al., 2003).

the Southeast Geysers (Y = 0.01–0.05) (D'Amore and Truesdell, 1985) and enriched $\delta^{18}O$ and δD isotopic values that indicate a greater component of connate fluid (Fig. 4-5). Boiling mudpots in the North Central Geysers area precipitate mud with a Hg content of 66 ppm. Precipitates sampled from a small thermal spring and associated steaming ground contained 15 ppm Hg. In the Southeast Geysers at Anderson Hot Springs a new spring has formed in 1998, possibly due to steam extraction in the Southeast Geysers (Janik et al., 1999). The main historically active spring at Anderson continues to precipitate black mud that contains 141 ppm Hg and grey mud from a neighboring fumarole contains 163 ppm Hg. Precipitates from the new spring contain 489 ppm Hg, the highest Hg content for a spring precipitate measured in this study. Gases from the new spring are higher in $H_2S$ and $NH_3$ than the older springs at the site (Janik et al., 2000). Fluid temperatures close to 100 ˚C at the new spring indicate that these fluids boiled within a few meters of the surface. Spring precipitates in fluids issuing from the neighboring Schwartz Hg mine adit contain 7 ppm Hg.

## 4.2 Hg Isotopic Compositions

### 4.2.1 California Coast Range Rocks

The Hg isotopic compositions of California Coast Range rocks are summarized in Table 4-3. The $\delta^{202}Hg$ values of the Great Valley Sequence sedimentary rocks vary from -0.17 to -0.93‰, tightly clustered about a mean value of -0.63‰ (Fig. 4-6). The $\delta^{202}Hg$ values of the Clear Lake Volcanic rocks also fall within a range between -0.25 and 1.20‰ with a mean of -0.62‰. More variation in isotopic composition is found in the rocks of the Franciscan Complex, where $\delta^{202}Hg$ ranges from 1.61 to -1.71‰ with a mean of -0.43‰.

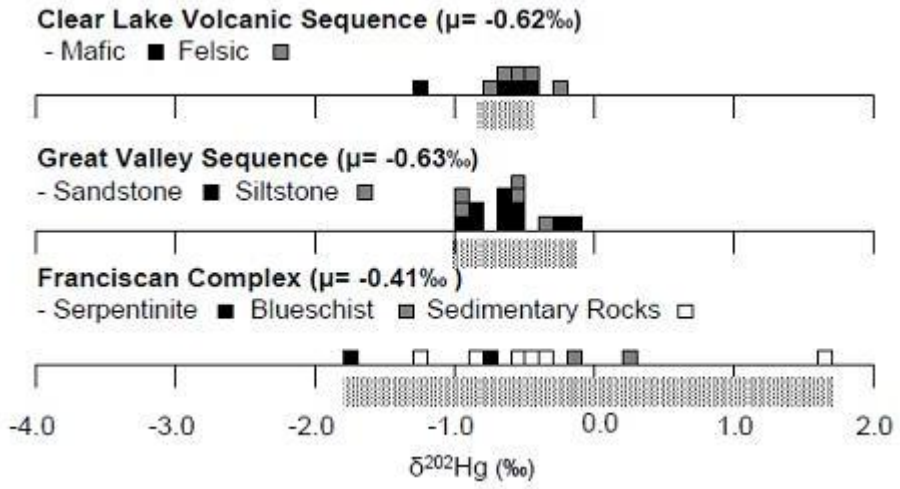


Figure 4-6. $\delta^{202}$Hg values for Clear Lake Volcanic sequence, Great Valley sequence and Franciscan Complex/Coast Range Ophiolite rock samples by lithology. Error bars (2σ) are smaller than the histogram bins.

The differences among the mean isotopic compositions of the three groups are not statistically significant (one way analysis of variance, $p < 0.05$), but the variance of the values within the Franciscan Complex compared to the other two groups is significant. As noted above, the Franciscan sample group is more heterogeneous in terms of lithology than the other groups and has been metamorphosed, and the observed variability probably reflects these factors.

In the Franciscan Complex/Coast Range Ophiolite and the Clear Lake Volcanics, there appears to be a correlation between increased Hg concentration and isotopic composition for several of the lowest $\delta^{202}$Hg samples. In the Franciscan group this is apparent for the sample of serpentinite at the Reiff Rd. location, where there is a strong possibility of hydrothermal Hg contamination as the sample site lies on the boundary of the highly mineralized Knoxville mining district and near the extensive mine dumps and open pit at the McLaughlin mine. The Reiff Rd. sample also has an elevated Hg content (33.3 ppb), several times higher than expected for an ultramafic rock. The highest $\delta^{202}$Hg value in the Franciscan (1.61 ‰) shows no unexpected Hg enrichment relative to the metasedimentary group and may represent a primary isotopic signature (Fig. 4-7). In the Clear Lake Volcanics one mafic and two felsic rocks with relatively high mercury contents and low $\delta^{202}$Hg values fall along a trend towards lower $\delta^{202}$Hg with increasing Hg content (Fig. 4-7). The lightest sample has a Hg content > 260 ppb higher than expected for a mafic rock and as discussed earlier, may be contaminated with isotopically light hydrothermal Hg from the open pit and mine dumps at the neighboring Sulphur Bank mine. If so, original Clear Lake rocks likely had $\delta^{202}$Hg values between about -0.2 and -0.6 ‰, and between 0.2 and –1.2 ‰ in the Franciscan/Coast Range Ophiolite as

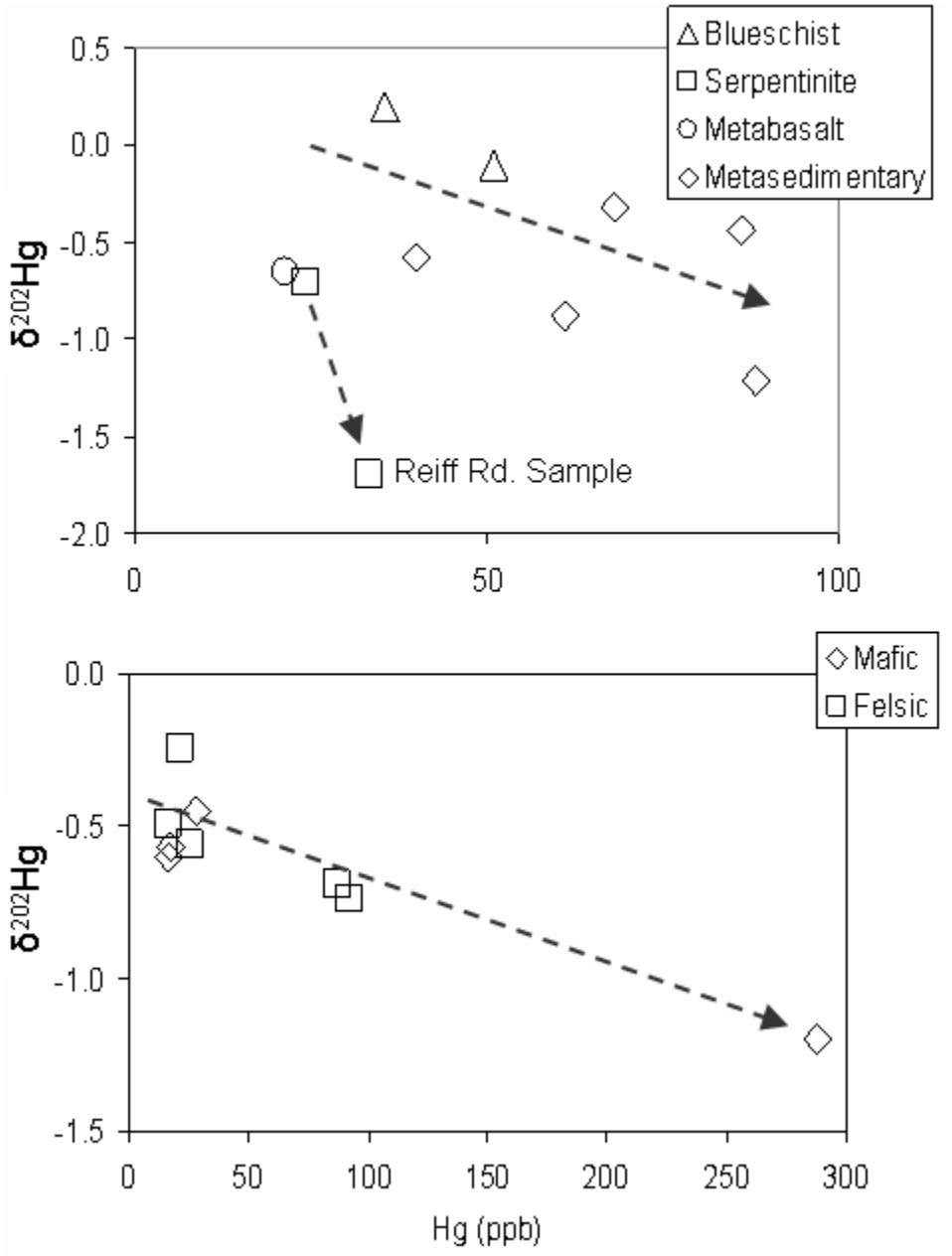


Figure 4-7. Plots of Hg concentration vs. $\delta^{202}$Hg to illustrate potential contamination by addition of low $\delta^{202}$Hg hydrothermal Hg. Franciscan/Coast Range Ophiolite (top) samples show enrichment trends for serpentinite samples and to a lesser extent, metasedimantary rocks. Clear Lake Volcanic samples (bottom) show potential contamination in one mafic sample.

shown by the shaded zone in Figure 4-6. The lowest $\delta^{202}$Hg values appear to reflect contamination by hydrothermal activity and possibly anthropogenic disturbance related to mining activities.

Samples from the Great Valley sequence show a relatively small spread of $\delta^{202}$Hg values with no systematic difference in isotopic composition of mudstones and sandstones, and no relation between mercury contents and $\delta^{202}$Hg values ($R^2 = 0.01$).

4.2.2 Precipitates from Active Springs

The $\delta^{202}$Hg values for all precipitates from mineral springs and hot springs range from -0.21 to -3.42‰, a far greater span of values than that of the surrounding rocks. The $\delta^{202}$Hg values of precipitates from The Geysers and adjacent Anderson Hot Springs vary over a narrower range from -0.70 to -1.56‰ (Table 4-4). Precipitates at the North Central Geysers have $\delta^{202}$Hg values within the range of Franciscan reservoir rocks, -0.7 to –1.18‰, which is also reflected in the gas chemistry from wells in this area (Lowenstern et al., 1999). Precipitates at the Anderson Springs in Southeast Geysers have $\delta^{202}$Hg values that are lower (-0.98 to –1.56‰) and similar in range to the ore deposit related Wilbur Springs precipitates. Spring precipitates in the Wilbur Springs and Knoxville Districts to the east of The Geysers have isotopic compositions that vary over the entire range noted above (-0.21 to -3.42‰) (Fig. 4-1). In the Wilbur Springs District, spring precipitates from the Elgin Hg mine are much lighter than the majority of springs in the district (4 km south of Elgin), which, cluster between -1.20 to -2.04‰ (Table 4-4). Samples from the cool, mineral springs at Turkey Run (-1.37‰) and Baker Soda Springs (-2.11‰) have relatively low $\delta^{202}$Hg values, possibly influenced by detrital mineralization at the sampling site. Precipitates from a groundwater monitoring well at the McLaughlin mine

in the Knoxville District are isotopically heavier than all other mineral or hot spring precipitates, and almost identical to the mean $\delta^{202}$Hg value of Great Valley Sequence rocks.

4.2.3 Ore deposits

The Hg isotopic compositions of ore deposits in the Geysers-Clear Lake area are similar among the various mining districts and deposit types (Table 4-5). The mean $\delta^{202}$Hg values of samples from the Wilbur Springs, Maycamas, Knoxville Districts and the Sulphur Bank mine, -0.45, -0.50, -0.77, and -0.65 respectively, do not differ significantly ($p < 0.05$). These values are close to the isotopic compositions of the Great Valley sequence (-0.63 ‰), Franciscan and Coast Range Ophiolite (-0.43 ‰), and Clear Lake Volcanic Field rocks (-0.54 ‰), which host these deposits.

The $\delta^{202}$Hg values range from 0.55 to -3.88‰ in the Maycamas District, from 0.07 to -2.53‰ in the Knoxville District, and from 0.21 to -1.78‰ in the Wilbur Springs District (Fig. 4-9). Ore deposits adjacent to The Geysers steam field are isotopically heavier compared to deposits further to the east away from The Geysers. $\delta^{202}$Hg values greater than 0 are observed mainly in silica-carbonate deposits of the Western Maycamas district as well as New Almaden and New Idria. The Franciscan, which hosts these deposits, is the only potential source rock to have $\delta^{202}$Hg values significantly greater than 0.

The isotopic compositions of Hg in the Elgin Hg ore deposit and Elgin hot spring precipitates are much lighter than that other ore deposits in the Wilbur Springs District, and the other districts of the region. The $\delta^{202}$Hg values of the Sulphur Bank deposit, one

Table 4-5. Analytical results from ore deposit samples in The Geysers-Clear Lake area.

| Sample No. | Location | Description | $\delta^{202}$Hg |
|---|---|---|---|
| USGS-ABT-1 | Abbott Mine | | -0.21 |
| CS0505 | Manzanita (In-Between) | | -0.34 |
| CS0503 | Turkey Run Mine | | -1.12 |
| CS0504 | Wideawake Mine | petroliferous | -0.01 |
| MZ-1 | Manzanita Mine | cinnabar in gouge | -1.12 |
| MZ-2 | Manzanita Mine | cinnabar on fractures in silicified mudstone | 0.04 |
| MZ-3 | Manzanita Mine | cinnabar in bleached mudstone | -0.13 |
| MZ-5 | Manzanita Mine | cinnabar in veinlet w/ powdery white selvage | -0.06 |
| MZ-6 | Manzanita Mine | cinnabar in fracture, disseminated in sandstone | -1.78 |
| MZ-7 | Manzanita Mine | quartz after calcite vein w/ cinn | 0.21 |
| MZ-8 | Manzanita Mine | cinnabar in white powdery altn | -0.47 |
| USGS-MAN-4 | Manhattan Mine | cinnabar in brecciated sinter | 0.00 |
| USGS-MAN-5 | Manhattan Mine | cinnabar layers in white sinter w/ punky bands | -0.65 |
| USGS-MAN-6 | Manhattan Mine | punky altered green bx, cinn? | -0.78 |
| USGS-MAN-8 | Manhattan Mine | cinnabar in black sinter | -0.28 |
| USGS-MAN-1 | Manhattan Mine | cinnabar paint on fracture surfaces | 0.07 |
| USGS-MAN-9 | Manhattan Mine | | -0.25 |
| USGS-MAN-7 | Manhattan Mine | silica-carb bx with cinn | -0.90 |
| USGS-BAK-1 | Baker Mine | gray acid sulphate altn, diss cinn in mudstone | -1.05 |
| USGS-HAR-1 | Harrison Mine | cinnabar concentrate from ore | -0.46 |
| USGS-HAR-2 | Harrison Mine | native S and cinnabar | -0.22 |
| CS0514 | McLaughlin | travertine terrace w/ sulfosalts | -0.36 |
| CS0513 | McLaughlin | travertine terrace w/ sulfosalts | -1.58 |
| KM-1 | Knoxville Mine | | -0.42 |
| KM-2 | Knoxville Mine | | -1.32 |
| KM-3 | Knoxville Mine | | -0.68 |
| KM-4 | Knoxville Mine | | -0.35 |
| KM-5 | Knoxville Mine | | -0.42 |
| KM-6 | Knoxville Mine | | -1.18 |
| RM-10 | Reed Mine | Andalusia pit | -1.63 |
| RM-4 | Reed Mine | cinn filling voids in silica-carb ore | -0.93 |
| RM-5 | Reed Mine | silica-carb alteration | -1.30 |
| RM-7 | Reed Mine | | -1.16 |
| RM-8 | Reed Mine | | -0.66 |
| RM-9 | Reed Mine | | -0.22 |
| SS-3 | Reed Mine | small prospect on road to Reed from McL pit | -2.53 |

Table 4-5 continued. Analytical results from ore deposits.

| Sample No. | Location | Description | $\delta^{202}$Hg |
|---|---|---|---|
| CS0507 | Elgin Mine | diss cinn in silica carb | -2.34 |
| CS0508 | Elgin Mine | py>cinn in silica-carb | -0.55 |
| CS0509 | Elgin Mine | fg cinn in acid sulphate altered host | -3.69 |
| CS0510 | Elgin Mine | cinnabar diss in silica-carb | -3.54 |
| CS0511 | Elgin Mine | cinn w/ botroydal silica in blk silica carb | -0.75 |
| USGS-BC-1 | Big Chief Mine | cinnabar>native Hg | 0.55 |
| USGS-BC-2 | Big Chief Mine | cinn in gray altd rock | -0.33 |
| USGS-SCHTZ-2 | Schwartz (Anderson) | | 0.38 |
| USGS-SCHTZ-1 | Schwartz (Anderson) | | 0.09 |
| USGS-AET-1 | Aetna Mine | | -0.51 |
| USGS-AET-2 | Aetna Mine | | -1.00 |
| USGS-CB-2 | Culver-Baer Mine | | -0.31 |
| CB-3 | Culver-Baer Mine | | -0.91 |
| CB-4 | Culver-Baer Mine | | -0.45 |
| CB-5 | Culver-Baer Mine | | -0.75 |
| CB-6 | Culver-Baer Mine | | -0.68 |
| CM-1 | Corona Mine | | -0.37 |
| CM-3 | Corona Mine | | -0.80 |
| CM-4 | Corona Mine | | -0.77 |
| CTC-1 | Contact Mine | | 0.65 |
| CTC-2 | Contact Mine | | 0.67 |
| OH-1 | Oat Hill Mine | | -1.02 |
| OH-2 | Oat Hill Mine | | -0.27 |
| OH-4 | Oat Hill Mine | | -3.88 |
| OH-6 | Oat Hill Mine | | -0.31 |
| SB-4 | Sulphur Bank | Fe-oxide+cinn vein | -0.51 |
| SB-5 | Sulphur Bank | Purplish metacinn? In clay altn | -1.19 |
| SB-6 | Sulphur Bank | Cinn-limonite in clay altn | -0.70 |
| SB-7 | Sulphur Bank | Cinn-limonite in clay altn | -0.79 |
| SB-10 | Sulphur Bank | Cinn-limonite in clay altn | -0.96 |
| SB-12 | Sulphur Bank | | -0.53 |
| SB-13 | Sulphur Bank | | -0.21 |
| USGS-SB-1 | Sulphur Bank | Cinn surrounding clasts of GV congl w/ gyp(?) | -0.18 |
| CS0516 | Sulphur Bank | Native S and cinn in wht bleached andesite | -0.59 |
| CS0517 | Sulphur Bank | Wht kaol-native S-cinn vein in bleached andesite | -0.88 |
| NMNH-98582-2 | New Idria | | -1.44 |
| NMNH-98582 | New Idria | | -1.26 |
| NMNH-98583-5 | New Idria | | 0.18 |
| NMNH-66782 | New Idria | | -0.33 |
| NMNH-66783 | New Idria | | -0.31 |
| NMNH-66784 | New Idria | | -0.12 |
| NMNH-98579-2 | New Idria | | -0.19 |
| NMNH-98583-2 | New Idria | | -0.55 |
| NMNH-15107-1 | New Almaden | | -1.19 |
| NMNH-15107-2 | New Almaden | | -1.27 |
| NMNH-51621-3 | New Almaden | | -0.01 |
| NMNH-51621-4 | New Almaden | | -0.11 |
| NMNH-51621-5 | New Almaden | | -0.06 |
| NMNH-51621-7 | New Almaden | | -0.12 |
| NMNH-66441 cinn | New Almaden | Cinnabar | 0.79 |
| NMNH-66441 nat ] | New Almaden | Native Hg | 0.47 |
| NMNH-66444 | New Almaden | | -0.57 |
| NMNH-98616-3 | New Almaden | | 0.87 |
| NMNH-98616-2 | New Almaden | | -0.92 |
| NMNH-98617-1 | New Almaden | | -0.30 |

of the few deposits hosted in volcanic rocks, vary over a relatively narrow range from -0.18 to -1.19‰, similar in distribution to the CLVF and Great Valley Sequence rocks.

In general, the isotopic compositions of the ore deposits are similar to the surrounding country rock, but heavier than the spring precipitates deposited from active hydrothermal systems. Vein samples from Manzanita and In-between are heavier than the adjacent springs at Jones' Fountain of Life, Blanck, Elbow and Wilbur Springs.

## 5. DISCUSSION

### 5.1 Hg Isotopes as a Tracer of Source

The $\delta^{202}$Hg values of the Franciscan, Clear Lake Volcanic and Great Valley units exposed in The Geysers-Clear Lake area are clustered about a similar mean Hg isotopic composition although samples from the Franciscan Complex have a wider range of values (Fig. 4-8). Ore deposits have a similar mean $\delta^{202}$Hg value compared with the potential source rocks, but with a greater range of $\delta^{202}$Hg values. Hot spring and mineral spring precipitates have much lower $\delta^{202}$Hg values than the ore deposits and host rocks of the region.

Given the relatively uniformity of Hg isotopic compositions of the host rocks in the Clear Lake area, variability of $\delta^{202}$Hg in ore deposits and hot springs must be caused by processes that occurred during hydrothermal transport and ore-formation. Smith et al (2005) summarized the chemical and physical processes in hydrothermal systems that might lead to mercury isotope fractionation in systems of this type, including: 1) liberation of $Hg^{2+}$ from country rock and solution as $Hg^0_{aq}$, 2) partitioning of $Hg^0$ into the vapor phase either by direct boiling or separation of a $CO_2$ phase, and 3) oxidation of $Hg^0_v$ by surface waters and reaction with $H_2S$ to form cinnabar precipitates. The presence

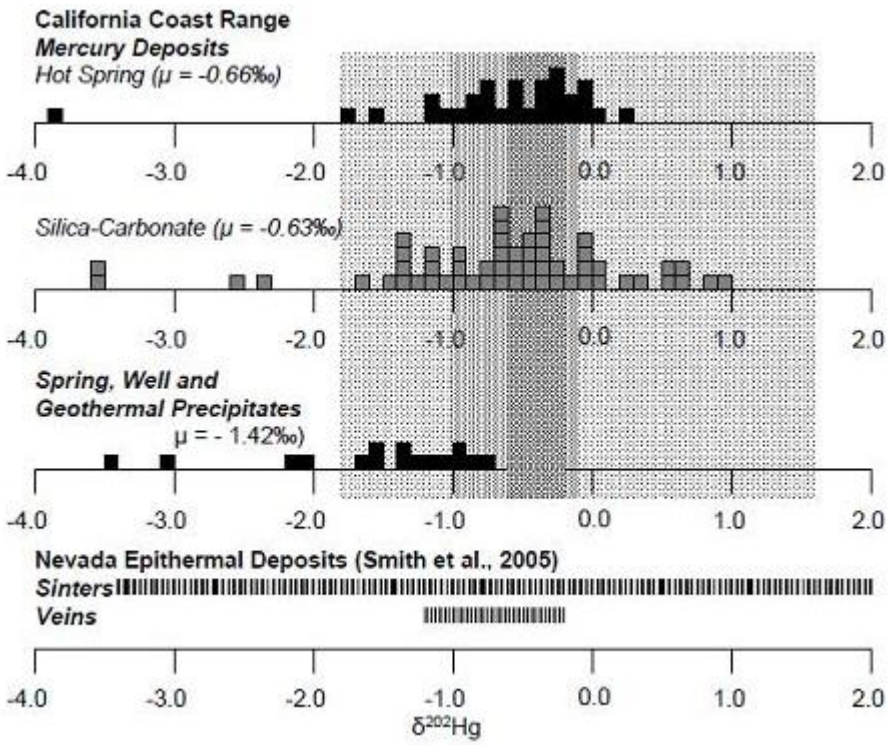


Figure 4-8. Summary of $\delta^{202}$Hg values for ore deposits, springs, well and geothermal area precipitates. Data from Nevada epithermal deposits presented for purposes of comparison. Note the wide range of $\delta^{202}$Hg values measured in shallow, sinter deposits compared with deeper vein samples (Smith et al., 2005).

of hydrocarbons in the rocks, ore deposits, and active hydrothermal systems of the study region will also be important to Hg geochemistry.

The metallogenesis of Hg ore deposits has been related to these environments of formation: 1) direct input of Hg from a magmatic source; and 2) release of Hg from sedimentary basins during regional heating (Moiseyev, 1971; Peabody and Einaudi, 1992). The similar average isotopic composition of Hg among the possible sedimentary and igneous source rock units and the ore deposits does not allow us to evaluate this hypothesis directly, but it does indicate that large fractionation (>±0.5‰) in the isotopic composition of Hg during its liberation from any of the possible source rocks is unlikely. Franciscan and Great Valley sedimentary rocks are the most likely sources rocks for the deposits because of their higher average Hg contents (Varekamp and Buseck, 1984).

5.2 Mechanisms of Fractionation in the Release, Transport and Deposition of Hg

In the sedimentary and meta-sedimentary rocks of the Great Valley Sequence and the Franciscan Complex, Hg can be present in sulfide minerals; adsorbed onto clays, micas and organic matter; dissolved in hydrocarbon fluids; and combined with organic matter to form Hg complexes such as methyl-Hg. Hg begins to be released from clay particles and organic matter at temperatures as low as 60 ˚C, primarily in the form of $Hg^0$, and continues to be released until about 150 ˚C (McNerney and Buseck, 1973). Hydrocarbons also form in this temperature range and under the reducing conditions buffered by these hydrocarbon-forming reactions Hg is present as $Hg^0$. Evidence for these organic reactions related to thermal maturation of sedimentary rocks in The Geyser-Clear Lake area come from $NH_3$ and B found in gases at The Geysers and in neighboring hot springs (Donnelly-Nolan et al., 1993). Under these conditions mercury would be liberated

as $Hg^0$ species in fluids with even moderate levels of S (< $10^{-2}$ m) (Varekamp and Buseck, 1984).

The limited fractionation (< ±0.5‰) observed in the source region within sedimentary basins may occur from several mechanisms related to the processes detailed above including: 1) Hg-organic complex→$Hg^0$; 2) $Hg^{2+}_{sulfide}$→$Hg^0$; 3) Hg-hydrocarbon→$Hg^0$. Of these reactions, the release of Hg from sulfides and organic compounds probably accounts for most of the Hg reduction and any accompanying isotopic fractionation. The magnitude of fractionation between sulfide and elemental Hg is expected to be minor, as evidenced by the 0.2-0.3 ‰ fractionation between co-existing cinnabar and native Hg measured from Hg ore deposits (cf. Chapter 2). Fractionation between Hg-organic compounds and $Hg^0$ may also be negligible if the breakdown of organic compounds is quantitative or nearly quantitative, which it is assumed to be the case at temperatures above 200 ˚C. A similar case can be argued for the release of Hg from petroleum, although this process may not be quantitative at temperatures below 175 ˚C. Therefore, Hg release from the various forms in the host rock may not significantly fractionate the isotopic composition of the rock reservoir.

Most fractionation probably occurs during deposition of Hg in shallow hydrothermal systems. In the shallow crust (<~300 m), the physical and chemical environment of the hydrothermal system differs greatly from at depth. At depth, Hg is transported by $H_2O$-$CO_2$-$H_2S$-$CH_4$ bearing reduced fluids as $Hg^0_{aq,}$ $Hg(HS)_2$ or other bisulfide complexes. Convection of the hydrothermal fluid along a thermal gradient transports Hg from depth to the shallow crust where ore deposits form and hot springs discharge at the surface. Hg is favored to be in solution at temperatures above 150 ˚C and

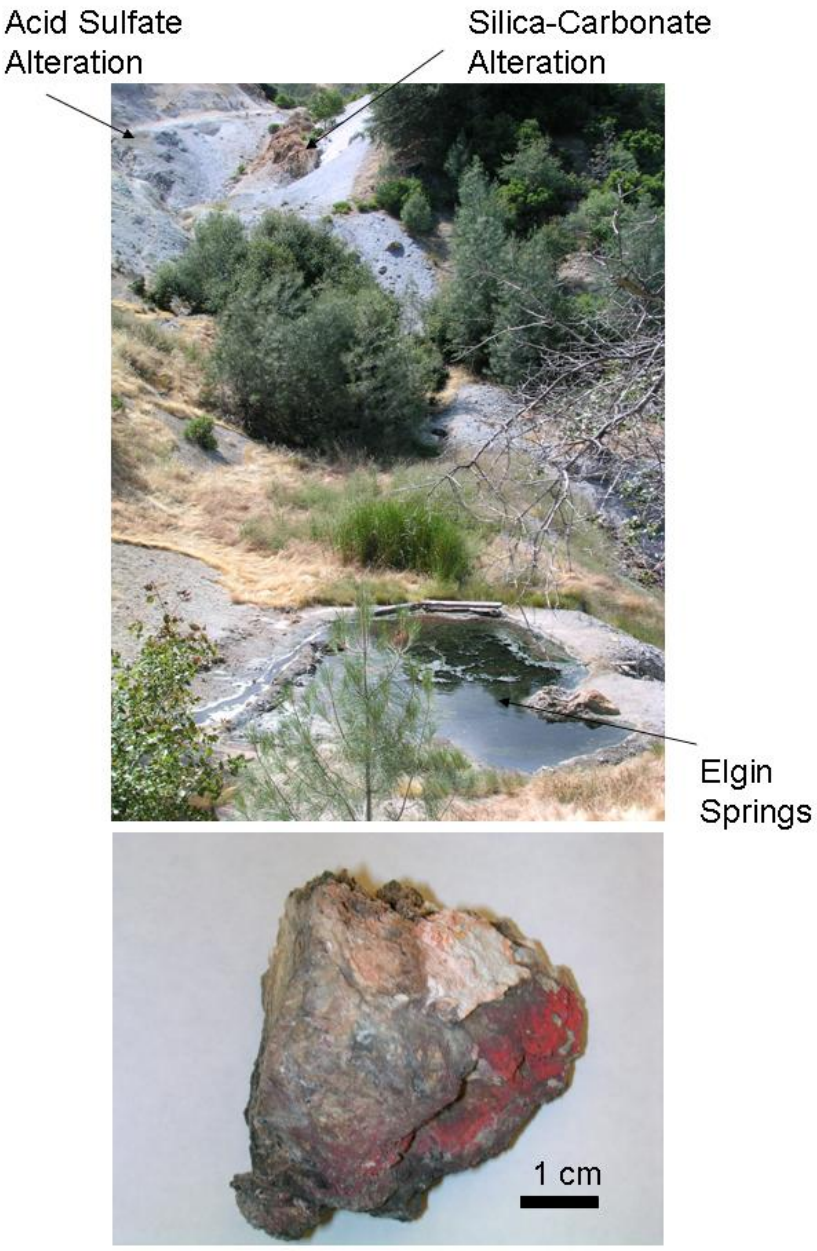


Figure 4-9. Top: Elgin Hg deposit with acid sulfate alteration superimposed on silica-carbonate alteration. Hot springs actively precipitating Au and Hg in the foreground. Bottom: Cinnabar "paint" along fracture surfaces in silica-carbonate ore from Elgin.

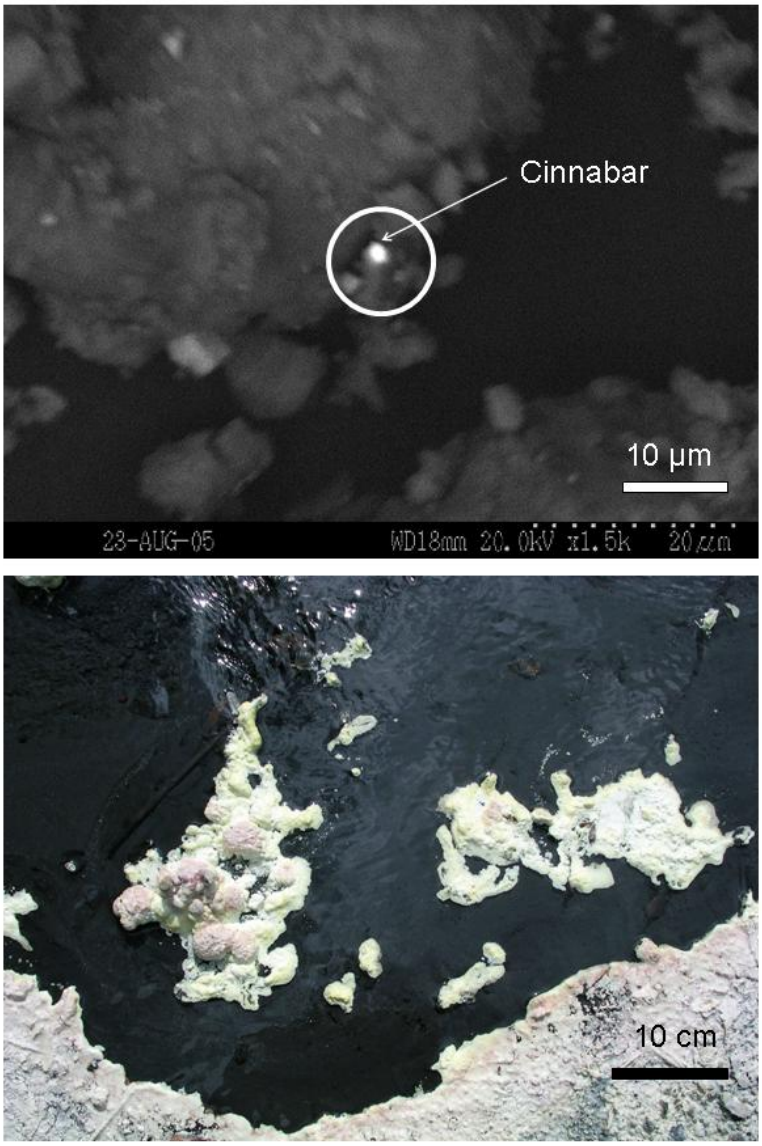


Figure 4-10. Top: BSE image of microcrystalline cinnabar (circled) in an amorphous Na-Si-Al-Fe-S-K phase (Janik et al., 1994) from Blanck springs. Bottom: Black, sulfidic mud containing Au and cinnabar precipitates at Elgin with native S crust.

(Krupp, 1988), it is not adsorbed onto organic residues at this temperature. Also, Hg is heat labile above 150 ˚C and condensation of $Hg^0$ from the transported Hg reservoir is not possible, although Hg would be incorporated in any sulfides that were precipitated (Moore et al., 1982; Christenson and Mroczek, 2003). At shallower depths, the confining pressure decreases and the ascending hydrothermal fluids boil and separate a gas phase. Addition of shallow groundwater also oxidizes the fluid. Thus, once in solution above 150 ˚C, Hg is highly mobile and not likely to fractionate during transport, until boiling and sulfide precipitation, oxidation or other ore-forming process occurs.

Fractionation could occur by several mechanisms during ore formation including: oxidation, precipitation of minerals that incorporate Hg, and Hg-organic reactions, but boiling accompanied by the release of $Hg^0_g$ will likely be the dominate process (Smith et al., 2005). In hot spring-type Au systems, phase separation and boiling occurs at depths between 1000 to 300 m as evidenced by quartz pseudomorphing platy calcite and fluid inclusions in hydrothermal minerals with variable liquid:vapor ratios (Simmons and Christenson, 1994). Hot spring Hg deposits display characteristics of formation at very shallow depths (<300m) (Rytuba, 1993), which include: widespread acid-sulfate alteration caused by acidic vapors that formed from the oxidation of $H_2S$ near the surface (Figs. 4-9,-10) and active thermal springs precipitating Hg at the surface today. Ore textures including cinnabar “paint” on fractures (Fig. 4-9) (Yates and Hilpert, 1946) as well as chemically pure cinnabar from these deposits (Peabody and Einaudi, 1992; Rytuba and Heropolous, 1992) suggest they were precipitated from $Hg^0_g$ reacting with $H_2S$ in shallow groundwater.

In hydrothermal systems above 200 ˚C, $Hg^0_{aq}$ can be abundant relative to other Hg species. Increasing pH and temperature and decreasing total S and $pO_2$ caused by boiling can enhance the stability of the $Hg^0_{aq}$ species (Varekamp and Buseck, 1984). Experimental calculations show that upon boiling aqueous $Hg^0$ strongly partitions to the vapor phase (Spycher and Reed, 1989) and $Hg^0_g$ has been reported in steam emissions from The Geysers (Robertson et al., 1977). Under these conditions, separation of a mercury-bearing vapor phase should deposit mercury with anomalously low $\delta^{202}$Hg values in the uppermost, gas-rich parts of the deposits. This process has been proposed to cause the ~4‰ difference between $\delta^{202}$Hg values of Hg in veins at depth and sinter near the surface at Buckskin Mountain, Nevada (Smith et al., 2005; Chapter III). A similar process probably accounts for the much lower $\delta^{202}$Hg values in the Elgin and Oat Hill hot spring Hg deposits, which differ by up to ~3‰ $\delta^{202}$Hg compared to the inferred source rock $\delta^{202}$Hg.

Active springs in the Coast Ranges have been described as cooler, more dilute, examples of the hydrothermal systems that formed the Hg and Au deposits of the region (Barnes et al., 1973; White, 1981; Pearcy, 1989; Peters, 1991, 1993; Sherlock, 1995, 2005). The springs display characteristics of both vapor- and liquid-dominated systems (White et al., 1971). The tops of many mercury deposits have been removed by erosion but the active springs represent this environment. Under these conditions, Hg isotopic fractionation related to boiling should be a significant fractionation mechanism. The near surface environment of hot springs is gas-rich and commonly enriched in isotopically light, vapor-transported Hg isotopes (cf. Smith et al., 2005; Chapter III). The near surface is also much cooler than the deeper ore-forming environments allowing $Hg^0$ to condense

by conductive cooling (Christenson and Mroczek, 2003), a process that should preserve low $\delta^{202}$Hg values. A comparison of the $\delta^{202}$Hg values active springs to hot spring- and silica-carbonate-type $\delta^{202}$Hg values reveals that spring precipitates have lower $\delta^{202}$Hg values than hot spring-type deposits, which are in turn, are lower in general than $\delta^{202}$Hg values for silica-carbonate-type deposits (Fig. 4-8).

Ore deposits that form at depth typically show a lesser range of $\delta^{202}$Hg values similar to the limited fractionation of isotopes that occurred during the leaching and transport of Hg at depth (Smith et al., 2005). Silica-carbonate type Hg deposits typically form at depths of 200 to 1000 m, while hot spring-type Hg deposits form at or very near the surface (0 to 300 m) and active springs precipitate Hg at the surface (Peabody and Einaudi, 1992; Sherlock et al., 1995) (Fig. 4-2). This vertical zonation is clearly illustrated in a comparison of $\delta^{202}$Hg values among the deposit types (Fig. 4-8).

5.3 Estimates of Mass Balance

Boiling hydrothermal systems may lose sufficient light Hg isotopes such that an isotopically heavy reservoir is left behind. This investigation does not find evidence for an isotopically heavy reservoir among the source rocks, ore deposits and active hydrothermal systems of The Geysers-Clear Lake area, nor was such a reservoir found in the epithermal deposits of Nevada (Smith et al., 2005). It is possible to have a scenario in which only a small fraction of the total Hg exits the system as vapor, in which case the escaping fraction would vary greatly from the reservoir composition, but the reservoir composition would not be affected by the small amount of mass lost from the system (Criss, 1999).

Where estimates of mass balance can be made, vaporized mercury does appear to have made up a relatively small fraction of the total mercury endowment of the deposit. At Sulphur Bank there is an estimated Hg flux to the atmosphere from hydrothermal fluids of about 7-8 kg y-1 (Nacht et al., 2004). The age at Sulphur Bank is well constrained by $^{14}C$ dating of wood fragments directly beneath the andesite host of the deposit, with activity beginning at 44.5 ka and cinnabar deposition continuing today (White and Roberson, 1962; Varekamp and Waibel, 1987). Total mercury emissions to the atmosphere for this time would be about $3.12 \times 10^5$ kg. There is an estimated Hg production at SB of $8.9 \times 10^6$ kg and this number sets a lower limit for the size of the subsurface accumulation. White and Roberson (1962) estimated the total Hg deposition at Sulphur Bank to be $1.4 \times 10^7$ kg. Thus, only between 2.2 and 3.5% of the Hg was lost to the atmosphere during the period of ore formation. The resulting shift in the isotopic composition of the remaining Hg pool would be less than the analytical resolution (< 0.10 ‰) of our method given the $\alpha_{gas\text{-}liquid}$ determined by Zheng et al. (2007).

5.4 Relationship Between Hg Sources and Active Hydrothermal Systems

In The Geysers reservoir there is a geographic difference in the two reservoir composition end members present: 1) gas-rich, high steam fraction (Y = 0.1 to 1.0), water poor fluids related to the high temperature reservoir in the center and north of the field; 2) low gas, condensed water-rich (Y = 0.01 to 0.05) fluids associated with natural recharge and re-injection wells in the southeast field and Anderson Springs (Fig. 4-5)(Janik et al., 2000). Fluids from the North Central and Northwest Geysers, where Geysers-1 and-2 were sampled, have enriched $\delta^{18}O$ and $\delta D$ isotopic values that indicate a greater exchange with Franciscan reservoir rocks and higher $CH_4$, $NH_3$ and $N_2/Ar$ derived from the thermal

decomposition of organic matter in the Franciscan (Lowenstern and Janik., 2003). Thermal waters at Anderson Springs and the Schwartz Mine drainage are largely surface meteoric water with a small fraction of non-condensable gas from the steam reservoir including enrichment in $NH_3$ (Lowenstern and Janik, 2003).

Although significant differences are observed in the chemical and isotopic composition of compartmentalized fluids within The Geysers, there does not appear to be a similar grouping reflected in the Hg isotopic composition of the spring precipitates. The $\delta^{202}$Hg values of the three sites sampled at Anderson Springs do not vary considerably from the two sites sampled in the North Central Geysers. The least fractionated samples of the two groups are nearly identical within analytical resolution. The enrichment in $NH_3$ in gases from both sites is consistent with derivation from the Franciscan reservoir rocks and the Hg isotopic compositions from both sites are also in agreement for the range of $\delta^{202}$Hg values measured in the Franciscan. Hg vapor and $NH_3$, $N_2$, and $CH_4$ are removed from the Franciscan reservoir and transported to the surface in either gas-rich or condensed water-rich fluids without significant fractionation of Hg isotopes in the subsurface. Hg isotopic compositions of surface manifestations from the Southeast and North Central Geysers appear to reflect a common source region and are not affected by the different transport fluid compositions present at the two sites.

## 6. CONCLUSIONS

The results of this study show that significant mass dependent fractionation of Hg isotopes occurs in the near-surface zones of hydrothermal systems. This fractionation probably results largely from vaporization either by boiling or separation of a vapor

phase from the migrating hydrothermal solution. Processes that leach Hg from source rocks and transport Hg to the surface appear to cause minimal fractionation (< ±0.5‰). The similar range of $\delta^{202}$Hg values measured in potential igneous and sedimentary source rocks of The Geysers-Clear Lake area does not allow direct determination of the Hg source(s) to the region. The higher average Hg content of the sedimentary Great Valley and Franciscan rocks as well as Hg isotope and supporting chemical evidence presented from The Geysers geothermal reservoir suggests that Hg in the region was supplied by sedimentary rocks.

Springs at the top of active hydrothermal systems release some Hg to the atmosphere, but retain some Hg in near-surface spring precipitates and the majority in the subsurface reservoir. Estimates of Hg flux from the recently formed Sulphur Bank Hg deposit indicate that the release of Hg is small relative to the overall reservoir and measurable isotopic enrichment of the residual Hg is not expected given the α for $Hg_{liq}$-$Hg_{vap}$ determined experimentally by Zheng et al (2007). The overall effect of this process will be enrichment through geologic time of isotopically light mercury in spring deposits, sedimentary rocks and other surficial deposits that accumulate Hg from the atmosphere.

## ACKNOWLEDGMENTS

This work was supported by grant EAR-01-06730 from the National Science Foundation to Stephen Kesler and Joel Blum. Additional funding for field work was provided by a Hugh E. McKinstry grant from the Society of Economic Geologists and a University of Michigan Scott Turner Award to the author and the Volunteers in Aid program of the U.S. Geological Survey. James Rytuba is thanked for his guidance and

support in the field, as well as access to specimens from the U.S. Geological Survey collections. Eric Essene, Johann Varekamp, Gerald Keeler and James Rytuba are thanked for their reviews of this work.

## REFERENCES


Ando, A., Kamioka, H., Terashima, S., and Itoh, S., 1989, 1988 values for GSJ rock reference samples, "Igneous rock series". Geochemical Journal, v. 23, p. 143-148.

Atwater, T., 1970, Implications of plate tectonics for the Cenozoic tectonic evolution of western North America. Geological Society America Bulletin, v. 81, p.3513-3535.

Averitt, P., 1945, Quicksilver deposits of the Knoxville district, Napa, Yolo and Lake counties. California Division of Mines and Geology, v. 41, p. 65-89.

Bailey, E.H., and Everhart, D.L., 1964, Geology and quicksilver deposits of the New Almaden district, Santa Clara County, California, USA. U.S. Geological Survey Professional Paper 360, p. 1-206.

Bailey, E.H., Irwin, W.P., and Jones, D.L., 1964, Franciscan and related rocks, and their significance in the geology of western California. California Division of Mines Bulletin 183, p. 177.

Barnes, I., 1970, Metamorphic Waters from Pacific Tectonic Belt of West-Coast of United-States. Science, v. 168, p. 973-975.

Barnes, I., Hinkle, M.E., Rapp, J.B., Heropoulos, C., and Vaughn, W.W., 1973, Chemical Composition of Naturally Occurring Fluids in Relation to Mercury Deposits in Part of North-Central California. U.S. Geological Survey Bulletin 1382-A, p. 1-19.

Benz, H.M., Zandt, G., and Oppenheimer, D.H., 1992, Lithospheric Structure of Northern California from Teleseismic Images of the Upper Mantle. Journal of Geophysical Research-Solid Earth, v. 97, p. 4791-4807.

Brady, R.J., and Spotila, J.A., 2005, Southward-younging apatite (U-Th)/He ages in the northern California Coast Ranges due to a northward-migrating crustal welt. Earth and Planetary Science Letters, v. 235, p. 107-122.

Chan, C.C.Y. and Bina, S.A, 1989, Sensitive automated method for determination of mercury in geological materials by cold vapor atomic absorption. Geostandards Newsletter v. 13, p. 181-186.

Christenson, B.W., and Mroczek, E.K., 2003, Potential reaction pathways of Hg in some New Zealand hydrothermal environments, *in* Simmons, S.F., and Graham, I., eds., Volcanic, geothermal and ore-forming processes; rulers and witnesses of processes within the Earth: Society of Economic Geologists Special Publication, Volume 10, p. 111-132.

Cooke, D.R., and Simmons, S.F., 2000, Characteristics and genesis of epithermal gold deposits, *in* Hagemann, S.G., and Brown, P.E., eds., Gold 2000, Reviews in Economic Geology, Volume 13, p. 221-244.

Cox, M.E., 1984, Controls on the Distribution of Hg in Geothermal Wells from Ngawha, New Zealand and Puna, Hawaii: Proceedings of the 6th New Zealand Geothermal Workshop, p. 145-150.

Criss, R.E., 1999, Principles of Stable Isotope Distribution. Oxford University Press: New York, 264 p.

D'Amore, F. and Truesdell, A.H., 1985, Calculation of geothermal reservoir temperatures and steam fractions from gas compositions. In 1985 Internation Symposium on Geothermal Energy: Geothermal Resources Council Trans., v. 9, p. 305-310.

Dalrymple, G.B., Grove, M., Lovera, O.M., Harrison, T.M., Hulen, J.B., and Lanphere, M.A., 1999, Age and thermal history of The Geysers plutonic complex (felsite unit), Geysers geothermal field, California; a $^{40}Ar/^{39}Ar$ and U-Pb study. Earth and Planetary Science Letters, v. 173, p. 285-298.

Dickinson, W.R., and Snyder, W.S., 1979, Geometry of subducted slabs related to San Andreas transform. Journal of Geology, v. 87, p. 609-627.

Donnelly-Nolan, J.M., Burns, M.G., Goff, F.E., Peters, E.K., and Thompson, J.M., 1993, The Geysers-Clear Lake area, California; thermal waters, mineralization, volcanism, and geothermal potential. Economic Geology, v. 88, p. 301-316.

Donnelly-Nolan, J.M., Hearn, B.C., Jr., Curtis, G.H., and Drake, R.E., 1981, Geochronology and evolution of the Clear Lake Volcanics. U.S. Geological Survey Professional Paper 1141, p. 47-60.

Elrick, K.A., and Horowitz, A.J., 1986, Analysis of rocks and sediments for mercury by wet digestion and flameless cold vapor atomic absorption. USGS Open File Report 86-596, 5 p.

Ernst, W.G., 1970, Tectonic contact between the franciscan melange and the great valley sequence - crustal expression of a late mesozoic benioff zone. Journal of Geophysical Research, v. 75, p. 886-901.

Ernst, W.G., Seki, Y., Onuki, H., and Gilbert, M.C., 1970, Comparative study of low-grade metamorphisms in the California Coast Ranges and the outer metamorphic belt of Japan. Memoir - Geological Society of America, Volume 124, p. 276.

Fehn, U., Peters, E.K., Tullai-Fitzpatrick, S., Kubik, P.W., Sharma, P., Teng, R.T.D., Gove, H.E., and Elmore, D., 1992, $^{129}I$ and $^{36}Cl$ concentrations in waters of the eastern Clear Lake area, California; residence times and source ages of hydrothermal fluids. Geochimica et Cosmochimica Acta, v. 56, p. 2069-2079.

Fox, K. F., Fleck, R.J., Curtis, G.H., and Meyer, C.E., 1985, Implications of the northwestwardly younger age of the volcanic-rocks of west-central California. Geological Society of America Bulletin**,** v. 96, p. 647-654.

Govindaraju, K., 1994, Compilation of working values and sample description for 383 geostandards. Geostandards Newsletter, v. 18, Special Issue, p. 1-158.

Hammersley, L., and dePaolo, D., 2006, Isotopic and geophysical constraints on the structure and evolution of the Clear Lake volcanic system. Journal of Volcanology and Geothermal Research, v. 153, p. 331-356.

Hearn, B.C., Jr., Donnelly-Nolan, J.M., and Goff, F.E., 1981, The Clear Lake Volcanics; tectonic setting and magma sources.

Hulen, J.B., Heizler, M.T., Stimac, J.A., Moore, J.N., and Quick, J.C., 1997, New Constraints on the Timing of Magmatism, Volcanism, and the On-set of Vapor-Dominated Conditions at The Geysers Steam Field, California, 22nd Proceedings of the Workshop on Geothermal Reservoir Engineering: Stanford, California, p. 75-81.

Hulen, J.B., and Walters, M.A., 1993, The Geysers felsite and associated geothermal systems, alteration, mineralization, and hydrocarbon occurrences, *in* Rytuba, J.J., ed., Active geothermal systems and gold-mercury deposits in the Sonoma-Clear Lake volcanic fields, California, Volume 16: Economic Geology Guidebook Series, p. 141-152.

Imai, N., Terashima, S., Itoh, S. and Ando, A., 1994, Compilation of analytical data for minor and trace elements in seventeen GSJ geochemical reference samples, "igneous rock series".Geostandards Newsletter, v. 19, p. 135-213.

Ingersoll, R.V., 1979, Evolution of the Late Cretaceous forearc basin, northern and central California. Geological Society of America Bulletin, v. 90, p. I 813-I 826.

Janik, C.J., Goff, F., Rytuba, J.J., Counce, D., and Anonymous, 1994, Mercury in waters and sediments of the Wilbur hot springs area, Sulphur Creek mining district, California. Eos, Transactions, American Geophysical Union, v. 75, p. 243.

Janik, C.J., Goff, F., Sorey, M.L., Rytuba, J.J., Counce, E.M., Colvard, E.M., Huebner, M., White, L.D., and Foster, A., 1999, Physical, chemical, and isotopic data for samples from the Anderson Springs area, Lake County, California, 1998–1999. USGS Open File Report 99-585, 28 p.

Janik, C.J., Walter, S.R., Goff, F., Sorey, M.L., Counce, D., Colvard, E.M., 2000, Abrupt physical and chemical changes during 1992-1999, Anderson Springs, SE Geysers Geothermal Field, California. USGS Open File Report 00-037, 2 p.

Jayko, A.S., and Blake, M.C., Jr., 1984, Sedimentary petrology of graywacke of the the Franciscan Complex in the northern San Francisco Bay region, California: Field

Trip Guidebook - Pacific Section, Society of Economic Paleontologists and Mineralogists, v. 43, p. 121-133.

Kennedy, B.M., and Truesdell, A.H., 1996, The northwest Geysers high-temperature reservoir; evidence for active magmatic degassing and implications for the origin of the Geysers geothermal field. Geothermics, v. 25, p. 365-387.

Krabbenhoft, D.P., Wiener, J.G., Brumbaugh, W.G., Olson, M.L., DeWild, J.F., and Sabin, T.J., 1999, A national pilot study of mercury contamination of aquatic ecosystems along multiple gradients.

Krupp, R., 1988, Physicochemical Aspects of Mercury Metallogenesis. Chemical Geology, v. 69, p. 345-356.

Lauretta, D.S., Klaue, B., Blum, J.D., and Buseck, P.R., 2001, Mercury abundances and isotopic compositions in the Murchison (CM) and Allende (CV) carbonaceous chondrites. Geochimica et Cosmochimica Acta, v. 65, p. 2807-2818.

Linn, R. K., 1968, New Idria mining district, in ed. Ridge, J.D., Ore Deposits of the United States, v. 2, p. 1624-1647.

Lowenstern, J.B. and Janik, C.L., 2003, The Origins of reservoir liquids and and vapors from The Geysers geothermal field, California. Society of Economic Geologists Special Publication 10, p. 181-195.

McNeal, J.M. and Rose, A.W., 1974, The geochemistry of mercury in sedimentary rocks and soils in Pennsylvania. Geochimica et Cosmochimica, v. 38, p. 1759-1784.

McNerney, J.J., and Buseck, P.R., 1973, Geochemical Exploration Using Mercury Vapor. Economic Geology, v. 68, p. 1313-1320.

Moiseyev, A.N., 1971, Non-Magmatic Source for Mercury Ore Deposits. Economic Geology, v. 66, p. 591-&.

Moore, J.N., and Gunderson, R.P., 1995, Fluid inclusion and isotopic systematics of an evolving magmatic-hydrothermal system. Geochimica et Cosmochimica Acta, v. 59, p. 3887-3907.

Nacht, D.M., Gustin, M.S., Engle, M.A., Zehner, R.E., and Giglini, A.D., 2004, Atmospheric mercury emissions and speciation at the sulphur bank mercury mine superfund site, Northern California. Environmental Science & Technology, v. 38, p. 1977-1983.

Peabody, C.E., and Einaudi, M.T., 1992, Origin of petroleum and mercury in the Culver-Baer cinnabar deposit, Mayacmas District, California. Economic Geology, v. 87, p. 1078-1103.

Pearcy, E.C., 1989, The geology and evolution of the hot spring gold deposit at Cherry Hill, California [Ph.D. thesis], Harvard University, 248 p.

Pearcy, E.C., and Petersen, U., 1990, Mineralogy, geochemistry and alteration of the Cherry Hill, California hot-spring gold deposit. Journal of Geochemical Exploration, v. 36, p. 143-169.

Peck, E.S., 1975, Statistical study of the reported values of mercury in United States geological survey standard rocks. UCRL Report 51819, 30 p.

Peters, E.K., 1991, Gold-Bearing Hot-Spring Systems of the Northern Coast Ranges, California. Economic Geology, v. 86, p. 1519-1528.

—, 1993, $\delta^{18}O$ enriched waters of the Coast Range Mountains, Northern California; connate and ore-forming fluids. Geochimica et Cosmochimica Acta, v. 57, p. 1093-1104.

Pitcairn, I.K., Ashley, D.A.H., Teagle, D., Green, D.R.H., German, C.R., and Croudace, I.W., 2003, Mobility of Hg, As, Sb, S and C in a metamorphic belt: insights into the source of elements enriched in orogenic gold deposits, the Otago Schists, New Zealand, *in* Eliopoulos, D.G., ed., Proceedings of the Seventh Biennial SGA Meeting, Volume 2: Athens, Greece, p. 803-809.

Robertson, D.E., Crecelius, E.A., Fruchter, J.S., and Ludwick, J.D., 1977, Mercury emissions from geothermal power plants. Science, v. 196, p. 1094-1097.

Rytuba, J.J., 1993, Epithermal precious-metal and mercury deposits in the Sonoma and Clear Lake volcanic fields, California. Guidebook Series, v. 16, p. 38-51.

—, 1995, Cenozoic metallogeny of California, *in* Coyner, A.R.F., Patrick L, ed., Geology and ore deposits of the American Cordillera: Reno, NV, Geological Society of Nevada, p. 803-822.

Rytuba, J.J., and Heropoulos, C., 1992, Mercury; an important byproduct in epithermal gold systems. U. S. Geological Survey Bulletin 1877, p. D1-D8.

Rytuba, J.J., 2003, Mercury from mineral deposits and potential environmental impact. Environmental Geology, v. 43, p. 326-338.

Rytuba, J.J., 2005, Geogenic and mining sources of mercury to the environment, in eds. Parsons, M. and Percival, J. Mercury: Sources, measurements, cycles and effects. GAC Short Course v. 34, p. 21-41.

Schmitt, A.K., Romer, R.L., and Stimac, J.A., 2006, Geochemistry of volcanic rocks from the Geysers geothermal area, California Coast Ranges. Lithos, v. 87, p. 80-103.

Sherlock, R.L., 2005, The relationship between the McLaughlin gold-mercury deposit and active hydrothermal systems in the Geysers-Clear Lake area, northern Coast Ranges, California. Ore Geology Reviews, v. 26, p. 349-382.

Sherlock, R.L., Amelia, M., Logan, V., and Jowett, E.C., 1993, Silica carbonate alteration of serpentinite, implications for the association of precious metal and mercury mineralization in the Coast Ranges. Guidebook Series, v. 16, p. 90-116.

Sherlock, R.L., Tosdal, R.M., Lehrman, N.J., Graney, J.R., Losh, S., Jowett, E.C., and Kesler, S.E., 1995, Origin of the McLaughlin Mine sheeted vein complex; metal zoning, fluid inclusion, and isotopic evidence. Economic Geology, v. 90, p. 2156-2181.

Simmons, S.F., and Christenson, B.W., 1994, Origins of calcite in a boiling geothermal system. American Journal of Science, v. 294, p. 361-400.

Spycher, N.F., and Reed, M.H., 1989, Evolution of a Broadlands-Type Epithermal Ore Fluid Along Alternative P-T Paths - Implications for the Transport and Deposition of Base, Precious, and Volatile Metals. Economic Geology, v. 84, p. 328-359.

Suchecki, R.K., and Land, L.S., 1983, Isotopic geochemistry of burial-metamorphosed volcanogenic sediments, Great Valley Sequence, Northern California. Geochimica et Cosmochimica Acta, v. 47, p. 1487-1499.

Tershima, S., 1994, Determination of mercury in one hundred and eighteen geochemical reference samples by cold vapor atomic absorption spectrometry. Geostandards and Geoanalytical Research, v. 18, p. 199–202.

Thompson, R.C., 1992, Structural stratigraphy and intrusive rocks at The Geysers geothermal field: Special Report - Geothermal Resources Council, v. 17, p. 59-63.

Varekamp, J.C., and Buseck, P.R., 1984, The speciation of mercury in hydrothermal systems, with applications to ore deposition. Geochimica et Cosmochimica Acta, v. 48, p. 177-185.

Varekamp, J.C., and Waibel, A.F., 1987, Natural cause for mercury pollution at Clear Lake, California, and paleotectonic inferences. Geology, v. 15, p. 1018-1021.

Wagner, D.L., Fleck, R.J., McLaughlin, R.J., Sarna-Wojcicki, A., Clahan, K.B., and Bezore, S., 2005, New Constraints on the Age and Distribution of Cenozoic Volcanics North of San Pablo Bay, California: Implications for Displacement Along Faults Inboard of the San Andreas Fault. Geological Society of America Abstracts with Programs, v. 37, p. 83.

Wedepohl, K.H., 1995, The composition of the continental crust. Geochimica et Cosmochimica Acta, v. 59, p. 1217-1232.

White, D.E., 1981, Geothermal Systems and Hydrothermal Deposits. Economic Geology 75th Anniversary Volume, p. 392-423.

White, D.E., Barnes, I., and O'Neil, J.R., 1973, Thermal and Mineral Waters of Nonmeteoric Origin, California Coast Ranges. Geological Society of America Bulletin, v. 84, p. 547-559.

White, D.E., Muffler, L.J.P., and Truesdel, A.H., 1971, Vapor-dominated hydrothermal systems compared with hot-water systems. Economic Geology, v. 66, p. 75-97.

White, D.E., and Roberson, C.E., 1962, Sulphur Bank, California, a major hot-spring quicksilver deposit, Petrologic studies--A volume in honor of A. F. Buddington.

Yates, R.G., and Hilpert, L.S., 1946, Quicksilver deposits of the eastern Mayacamas District, Lake and Napa counties, California. California Journal of Mines and Geology, v. 42, p. 231-286.

Yoshinaga, J. and Morita, M., 1997, Determination of mercury in biological and environmental samples by inductively coupled plasma mass spectrometry with the isotope dilution technique. Journal of Analytical Atomic Spectrometry, v. 12, p. 417-420.

Zheng, W., Foucher, D., and Hintelmann, H., 2007, Mercury isotope fractionation during volatilization of Hg(0) from solution into the gas phase. Journal of Analytical Atomic Spectrometry, v. 22, p. 1097-1104.

# CHAPTER V.

# CONCLUSIONS

In this study, a novel method for measuring Hg isotope ratios in a variety of sample matrices was presented with the goal of measuring natural variations in Hg isotopes in terrestrial reservoirs. The data presented show that Hg isotopes can yield insight into the source and cycling of Hg in much the same way as other stable isotope systems.

A new method for obtaining high precision analyses of Hg isotopic compositions was developed by combining cold vapor ($Hg^0$) generation in a gas-liquid separator with new multiple collector inductively coupled plasma mass spectrometer technology (CV-MC-ICP-MS). Instrumental mass bias is corrected for by standard-sample bracketing and with the online addition of a Tl (NIST 997) aerosol as an external inter-element spike. The results of repeated analysis of NIST 3133 Hg standard and our laboratory standard, Almadèn elemental Hg show an external precision of better than ±0.08 ‰ $\delta^{202}Hg/^{198}Hg$ can be achieved ($\delta^{202}Hg$; relative to NIST 3133) (2σ, n=43). The external reproducibility of natural samples in a variety of inorganic and organic matrices is better than ±0.10 ‰ (2σ, n=64). Ore deposit samples from a variety of different deposits were analyzed and show a > 5 ‰ $\delta^{202}Hg$ range. Low temperature, inorganic geochemical processes can affect Hg isotope ratios within individual ore deposits as demonstrated by the isotopic variations within single deposits.

To test whether the unique volatility of Hg would be a factor in the fractionation of Hg isotopes, two fossil geothermal systems were selected for study where boiling and separation of $Hg^0$ vapor are known to have occurred. Modern geothermal systems discharge significant amounts of Hg to the atmosphere (Robertson, 1977; Coolbaugh et al., 2002). The Hg isotopic compositions of samples throughout the vertical extent of two fossil hydrothermal systems at the National and Ivanhoe mining districts in northern Nevada show greater than 5 ‰ $\delta^{202}$Hg fractionation, more than 50 times greater than the 0.1‰ ($2\sigma$) external reproducibility of the analyses. Hg isotope compositions from both hydrothermal systems can be grouped by dominant mineralogy and position; $\delta^{202}$Hg values at the tops of the systems are –3.5‰ to –0.4‰ in cinnabar-dominant sinter and –0.2‰ to +2.1‰ in metacinnabar-dominant sinter, and the underlying veins have $\delta^{202}$Hg values of –1.4‰ to +1.3‰. These differences are attributed to a combination of boiling of the hydrothermal fluid, oxidation near the surface, and kinetic effects associated with mineral precipitation.

The Geysers-Clear Lake area was selected to study the migration of Hg in the Earth's crust on a regional scale. The region hosts numerous Hg and Au-Hg ore deposits that have formed from 2.3 Ma, coinciding with the inception of volcanic activity in the area, until as recently as 44 ka, and continue today in hot springs actively precipitating Hg and Au. The region also contains The Geysers steam field, the largest actively producing geothermal area in North America, where Hg concentrations up to 12 ppm in steam emissions have been reported (Robertson et al., 1977) and numerous Hg deposits border on the geothermal area. The large number of Hg deposits in the region have formed from processes including boiling, gas transport, fluid mixing, cooling and

condensation in the shallow crust under varying redox conditions, temperatures and depths (Rytuba, 1996). Hot springs of the area also allow the analysis of Hg isotopes from active hydrothermal systems, thought to be analogous to the fossil hydrothermal systems preserved as ore deposits (White, 1981).

The concentration of Hg in fresh samples of the various rock types of the region was undertaken to determine if anomalously high or low Hg concentrations were present. The Mesozoic Franciscan Complex accretionary wedge and Great Valley Sequence forearc rocks which comprise the bedrock of the area contain similar clastic sedimentary rock types with similar concentrations of Hg (median values of 51 and 64 ppm respectively). Rocks of the Clear Lake Volcanic Field, which erupted to cover the Mesozoic basement, have lower Hg abundances (median of 27 ppm). These values are consistent with Hg concentration reported for these rock types in the literature.

The mean Hg isotopic compositions of the rocks of the Mesozoic Great Valley Sequence (-0.63‰ $\delta^{202}$Hg, n = 19), and Franciscan Complex (-0.43‰ $\delta^{202}$Hg, n = 11) and the Neogene Clear Lake Volcanic Field (-0.54‰ $\delta^{202}$Hg, n = 10) units are not statistically different (one way analysis of variance, $p<0.05$) suggesting a common source.

The Franciscan Complex and Great Valley Sequence contain clastic sedimentary rocks with higher concentrations of mercury than volcanic rocks of the Clear Lake Volcanic Field. Mean mercury isotope compositions for all three rock units are similar, although the range of values in Franciscan Complex rocks is greater than in either Great Valley or Clear Lake rocks. Hot spring and silica-carbonate mercury deposits have similar average mercury isotopic compositions that are indistinguishable from averages for the three rock units, although $\delta^{202}$Hg values for the mercury deposits have a greater

variance than the country rocks. Precipitates from spring and geothermal waters in the area have similarly large variance and a mean $\delta^{202}$Hg value that is significantly lower than the ore deposits and rocks.

These observations indicate that there is little or no isotopic fractionation during release of mercury from its source rocks into hydrothermal solutions. Isotopic fractionation does appear to take place during transport and concentration of mercury in deposits, however, especially in their uppermost parts. Boiling of hydrothermal fluids or separation of a mercury-bearing $CO_2$ vapor is likely the most important process causing of the observed Hg isotope fractionation. This should result in the release of mercury with low $\delta^{202}$Hg values into the atmosphere from the top of these hydrothermal systems. Preliminary estimates suggest that this process does not remove enough mercury to cause underlying deposits and crust to become enriched in isotopically heavy mercury.

The results of this study show that mass dependent fractionation of mercury isotopes reaches significant levels in the uppermost parts of geologic-hydrothermal systems that transfer mercury to the surface. This fractionation probably results largely from vaporization either by boiling or separation of a vapor phase from the migrating hydrothermal solution. Active springs at the top of these systems release some of this mercury to the atmosphere and retain some in near-surface spring precipitates. The overall effect of this process will be an enrichment through geologic time of isotopically light mercury in spring deposits, sedimentary rocks and other surficial deposits that accumulate Hg from the atmosphere.

## REFERENCES CITED

Coolbaugh, M.F., Gustin, M.S., and Rytuba, J.J., 2002, Annual emissions of mercury to the atmosphere from natural sources in Nevada and California. Environmental Geology, v. 42, p. 338-349.

Robertson, D.E., Crecelius, E.A., Fruchter, J.S., and Ludwick, J.D., 1977, Mercury emissions from geothermal power plants. Science, v. 196, p. 1094-1097.

Rytuba, J.J., 1996, Cenozoic metallogeny of California, *in* Coyner, A.R.F., Patrick L, ed., Geology and ore deposits of the American Cordillera: Reno, NV, Geological Society of Nevada, p. 803-822.

White, D.E., 1981, Geothermal Systems and Hydrothermal Deposits. Economic Geology 75th Anniversary Volume, p. 392-423.

# APPENDIX A.

# Hg IN EPITHERMAL MINERAL DEPOSITS

## Occurrence of Hg in Sinters

Silica sinters form from geothermal fluids supersaturated with silica that reach the surface and precipitate amorphous silica from the cooling fluid. Sinters are variably enriched in Hg, As, Sb, Tl and may also contain Au and Ag such as at Rotokawa, New Zealand (Krupp and Seward, 1990). These metals are transported to the surface from the depths of the hydrothermal system. In the sinter, Hg occurs in cinnabar (HgS), the HgS polymorph, metacinnabar and to a lesser extent, as tiemannite (HgSe), and corderoite ($Hg_3S_2Cl_2$).

Metacinnabar is formed metastably at temperatures below 374 ˚C at 1 atm (Dickson and Tunnell, 1958), possibly stabilized by the addition of trace impurities in its structure (Boctor et al., 1987). Metacinnabar shares the crystal structure of sphalerite (cubic) and like sphalerite, metacinnabar can accommodate an abundance of impurities. In the sinter deposits at Buckskin Mountain, National District, Nevada (Chapter III), the black internal reflections in metacinnabar are optically distinct from the red internal reflections of cinnabar when viewed in transmitted light (Figs.A-1-3). The two polymorphs are also compositionally distinct; metacinnabar contains up to 12 wt% Se whereas cinnabar contains no detectable

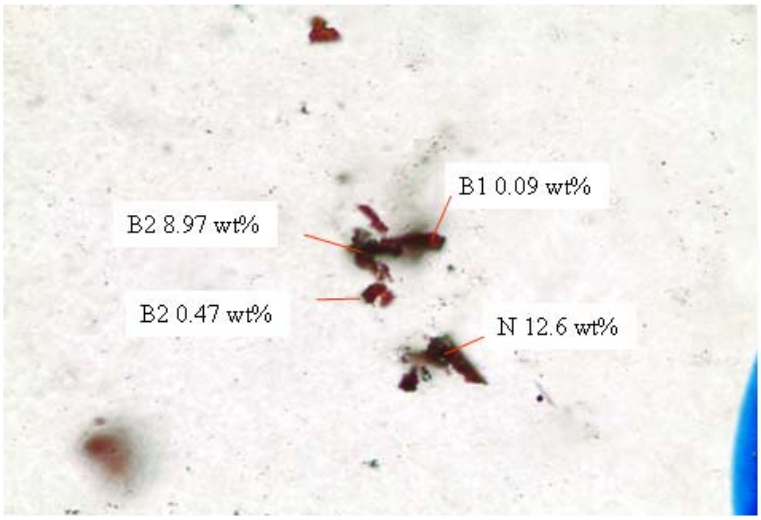


Figure A-1. Photomicrograph of BM-9 photo taken in PPL at 50 x magnification. The Se content in wt% measured by SEM-EDS is indicated at selected points.

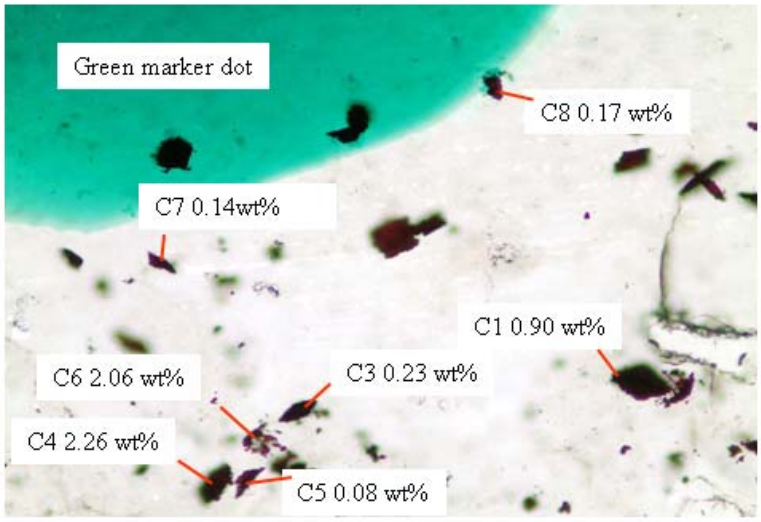


Figure A-2. Photomicrograph of BM-9 photo taken in PPL at 50 x magnification. The Se content in wt% measured by SEM-EDS is indicated at selected points.

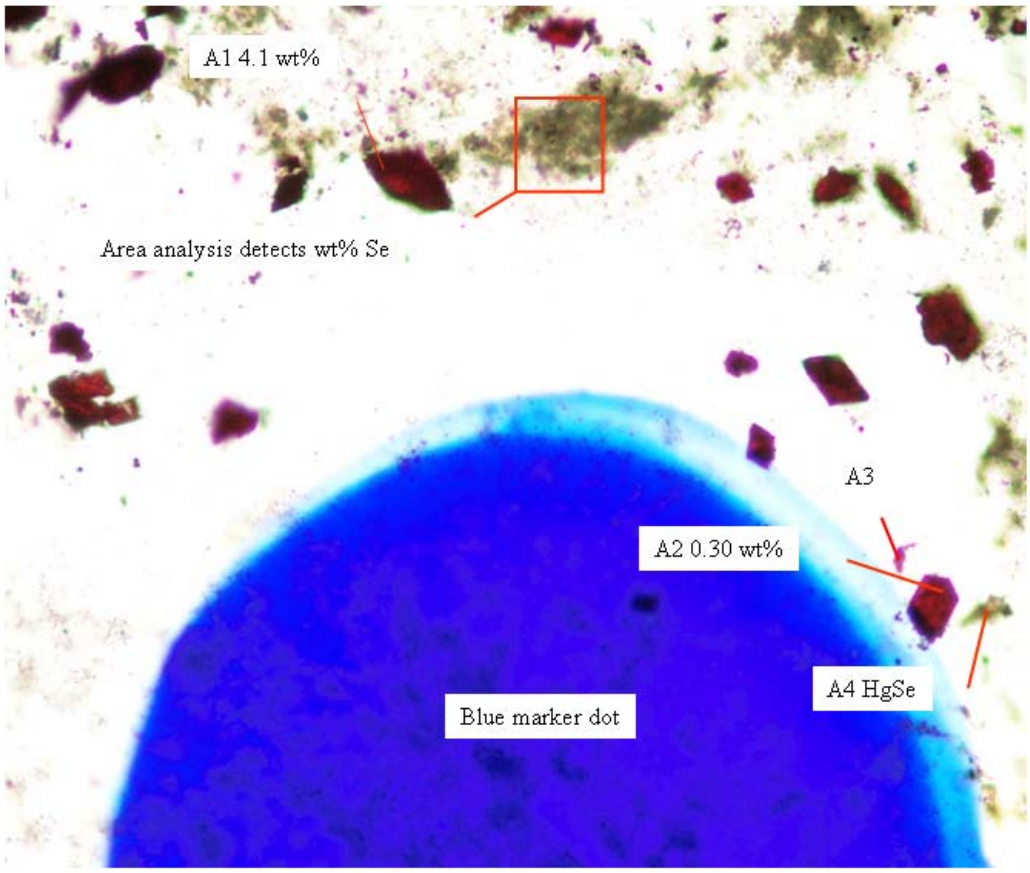


Figure A-3. Photomicrograph of BM-9 photo taken in PPL at 50 x magnification. The Se content in wt% measured by SEM-EDS is indicated at selected points.

Se, but has Cl contents ranging from 2 to 3 wt% (Table A-1; Fig. A-4). Rare tiemannite (HgSe) was also detected in one sample (BM-9; Fig. A-3).

Sinters may contain variable amounts of trace metal enrichment, determined by the relative input of geothermal fluid from depth. Those that form far above the water table contain only vapor transported contributions from the deeper hydrothermal system, typically Hg, Cl and S, forming relatively pure cinnabar as well as corderoite ($Hg_3S_2Cl_2$) and native S crusts at gas vents (Rytuba and Heropoulos, 1992). The sinter at Buckskin Mountain displays characteristics of both liquid and vapor contributions from the deep hydrothermal system, possibly originating from a fluctuating water table when the sinter formed. Red cinnabar is often chemically pure, interpreted by Rytuba and Heropoulos (1992) to indicate vapor deposition, wheras metacinnabar contains abundant Se, an element that is not transported in the vapor phase of epithermal fluids and must reflect the contribution of deep fluids.

Trace element analyses of the sinters at Buckskin Mountain reveal the presence of several elements, including Zn, Se, Sb and Sn, were transported to the sinter by hydrothermal fluid (Table A-2). The presence of both chemically pure cinnabar and trace metal-rich metacinnabar in close proximity on the same thin section suggests a complicated process of formation. These textures may be the result of a fluctuating water table and variable mixing of hydrothermal fluid and vapor with the groundwater table.

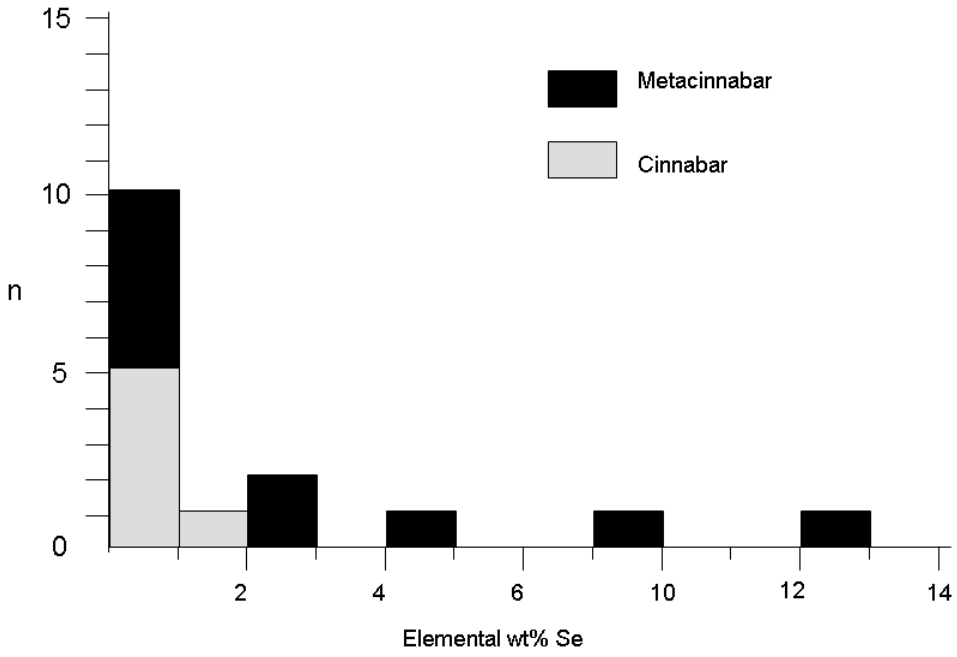


Figure A-4. Histogram comparing the Se content of metacinnabar and cinnabar. Values below 1 wt% should be considered below the detection limit of EDS analysis.

Table A-1. Se contnet of mineral grains in BM-9

| Point# | Mineral | Se (wt%) | Error (1SE) |
|---|---|---|---|
| A1 | Metacinnabar | 4.1 | 0.2 |
| A2 | Cinnabar | 0.3 | 0.1 |
| A3 | Cinnabar | 0.9 | 0.2 |
| A4 | Tiemannite? | 19.6 | 0.8 |
| | | | |
| B1 | Metacinnabar | 0.1 | 0.1 |
| B2 | Metacinnabar | 9.0 | 0.5 |
| B3 | Cinnabar | 1.3 | 0.2 |
| N | Metacinnabar | 12.6 | 0.6 |
| O | Metacinnabar | 0.4 | 0.1 |
| | | | |
| C1 | Metacinnabar | 0.9 | 0.2 |
| C2 | Metacinnabar | 0.3 | 0.1 |
| C3 | Metacinnabar | 0.3 | 0.1 |
| C4 | Metacinnabar | 2.3 | 0.2 |
| C5 | Cinnabar | 0.1 | 0.1 |
| C6 | Metacinnabar | 2.1 | 0.2 |
| C7 | Cinnabar | 0.1 | 0.1 |
| C8 | Cinnabar | 0.2 | 0.1 |

Table A-2. Results of trace element analyses by ICP-OES of selected sinter samples.

| Sample | Au (ppm) | Cu (ppm) | Mo (ppm) | Pb (ppm) | Sb (ppm) | Se (ppm) | Sn (ppm) | Zn (ppm) | Hg (ppm) |
|---|---|---|---|---|---|---|---|---|---|
| BM-9 | 14 | 3 | 16 | 0 | 0 | 76 | 611 | 15761 | 2586 |
| BM-10 | 42 | 36 | 63 | 3 | 2988 | 249 | 4770 | 89116 | 1706 |
| BM-11 | 7 | 0 | 16 | 2 | 287 | 54 | 844 | 23364 | 63 |
| BM-12 | 7 | 6 | 15 | 2 | 48 | 55 | 787 | 16804 | 1099 |
| BM-13 | 7 | 3 | 14 | 2 | 0 | 130 | 550 | 14264 | 3448 |

**Occurrence of Hg in Epithermal Veins**

Epithermal vein systems are the fossil analogue of the feeder zone in an active geothermal system. The veins are structurally controlled fluid conduits that were filled with quartz, carbonates, sulfides, selenides and tellurides during repeated boiling events (Cooke and Simmons, 2000). These veins systems typically formed at depths of 500-1500 m at temperatures ranging from 200-350 ˚C. In the vein Hg occurs chiefly in solid solution within the native elements, sulfides and selenides precipitated in the vein. The results of an investigation of the vein mineralogy of the Bell Vein, National District, Nevada, by petrographic microscope and SEM-EDS, are reported below.

**BM-14a**

This sample from the Bell vein dumps consists of alternating bands of quartz and sulfides+selenides. The sulfides and selenides occur in diffuse bands and in saginitic clots. Quartz bands alternate between finer and coarser grain size with minor sericite clots dispersed within. A small amount of bladed adularia (?) was observed in a coarse-grained quartz band. Naumannite-aguilarite ($Ag_2Se$-$Ag_2SeS$) solid solutions are common selenide phases present with most compositions averaging $Ag_2Se_{0.7}S_{0.3}$. A tetrahedrite group mineral with the approximate formula $(AgZnCu)_{0.47}(AsSb)_{0.15}(SeS)_{0.35}$ (giraudite ?) was observed in apparent equilibrium with naumannite-aguilarite (Figs.A-7, A-9, A-10). Galena with up to 19 atomic % Se (selenian galena) was often observed in equilibrium with naumannite-aguilarite in composite grains (Figs.A-5, A-7). Rare electrum occurs with the selenides and sulfides (Fig. A-6). Pyrite is the most common

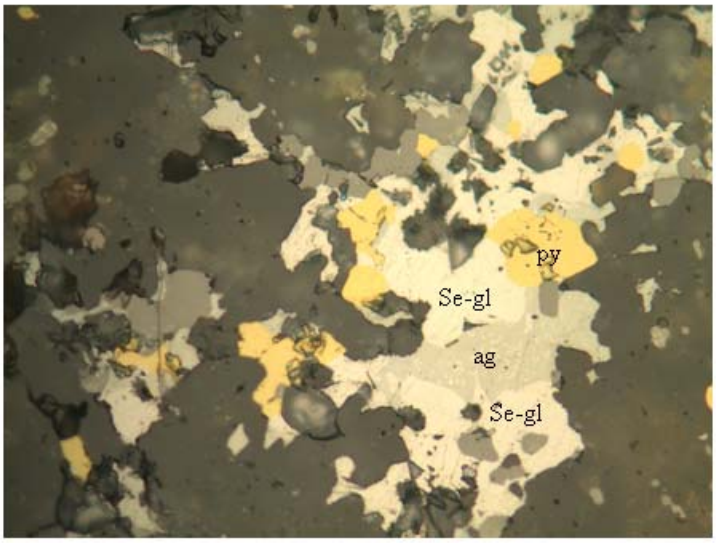


Figure A-5: Selenian galena(Se-gl), aguilarite (ag) and pyrite (py)
BM-14a, reflected light, FOV = 0.26 mm.

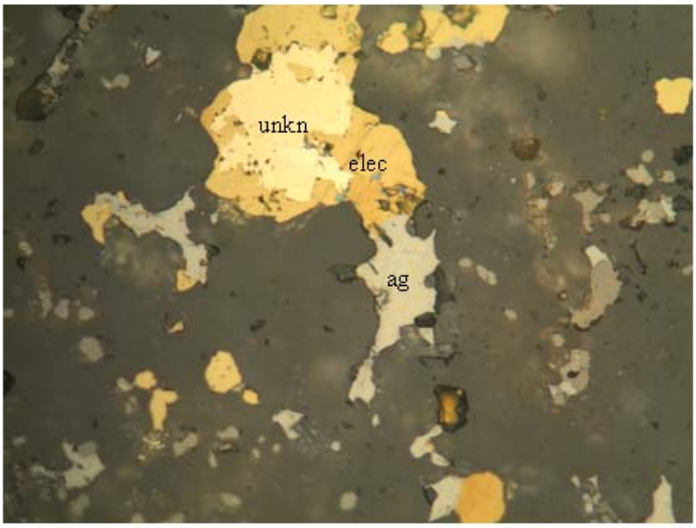


Figure A-6: Large electrum (elec) grain enclosing a creamy, pinkish unknown (unkn) with an adjacent aguilarite grain
BM-14a, reflected light, FOV = 0.26 mm

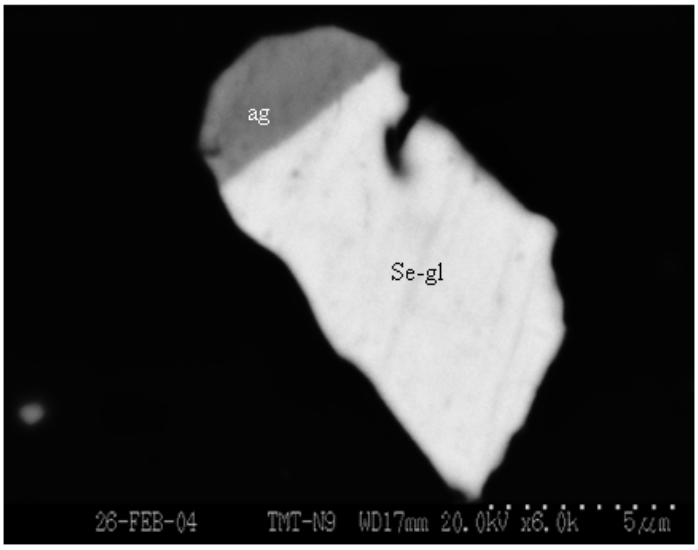


Figure A-7: Selenian galena ($PbSe_{0.18}S_{0.82}$) and aguilarite ($Ag_2Se_{0.70}S_{0.30}$) sharing a planar contact suggesting equilibrium, BM-14a, BSE

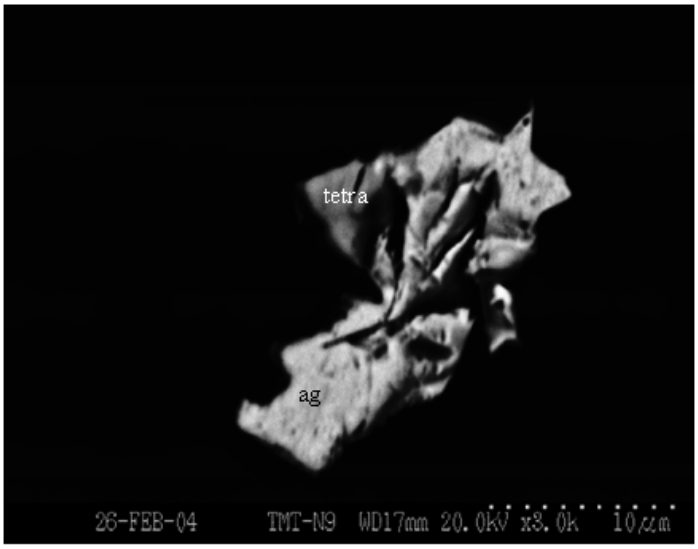


Figure A-8: Tetrahedrite group mineral (giraudite?) and aguilarite, BM-14a, BSE

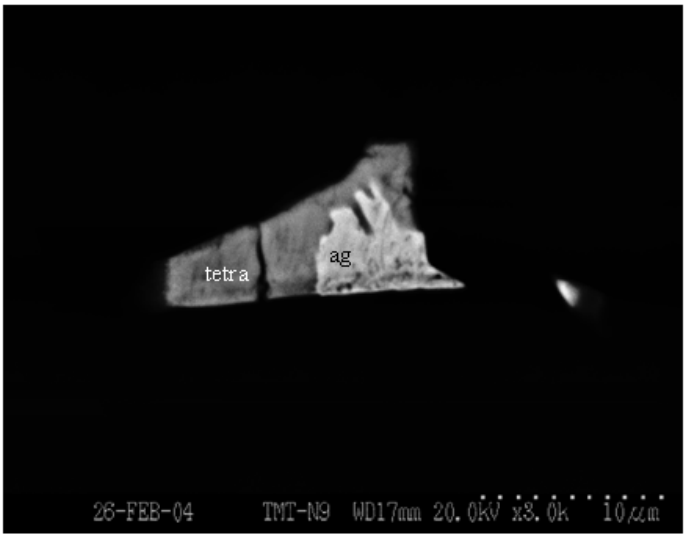


Figure A-9: Aguilarite ($Ag_2Se_{0.72}S_{0.28}$) and tetrahedrite group mineral (possibly giraudite) BM-14a, BSE

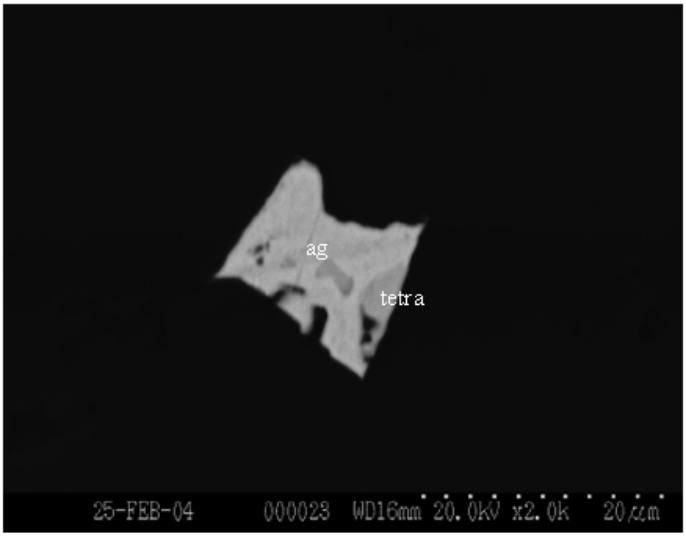


Figure A-10: Tetrahedrite group mineral inclusions in aguilarite, BM-14a, BSE.

sulfide and is found associated with Ag selenides and selenian galena, often with inclusions of selenides suggesting co-precipitation (Fig. A-5). Trace pyrargarite ($Ag_3SbS_3$) was also observed. No Hg was detected in any of the minerals observed in this sample. Textures and mineralogy are similar to stage 2b of Vikre (1985), the main stage of gold ore deposition in the Bell vein.

**BM-14b**

This sample from the Hatch-Halcyon level dump consists of banded quartz vein. Sulfides, selenides and sulfosalts occur as anhedral masses in wide bands. Minor sericite clots are found in the quartz bands. Rare chlorite in a thin veinlet cutting type 2b textures and minor clay alteration (after sericite?) suggests late stage supergene effects. Electrum ($Au_{40-50}Ag_{50-60}$) is common (Fig. A-11) and often has Au-rich rims ($Au_{70}Ag_{30}$) (Fig. A-13). Electrum can contain between 0-3 at.% Hg. Gold also occurs in a Ag-Au-Se-S phase intermediate to fischesserite ($Ag_3AuSe_2$) and uytenbogaardatite ($Ag_3AuS_2$) containing 0.2-1.5 at.% Hg (Fig. A-14). Silver minerals throughout the naumannite-aguilarite-acanthite series are also common. Tetrahedrite (Ag>>Cu, Fe, Zn) with several atomic % Se substituting for S (possibly giraudite) is present with Hg contents of 0.5-1.0 atomic %. Several grains with compositions close to pyrargarite ($Ag_3SbS_3$) with minor Se substitution were also analyzed (Fig. A-13). Textures and mineralogy correspond to stage 2b of Vikre (1985).

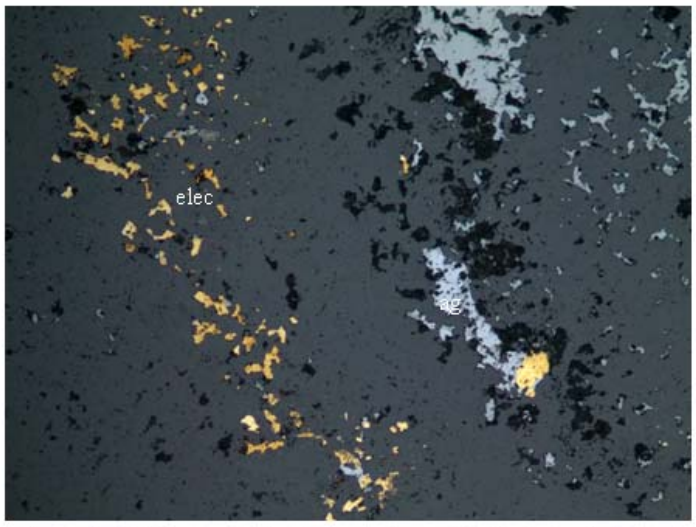


Figure A-11: Numerous electrum (and possible fischesserite) grains and aguilarite. BM-14b, reflected light, FOV = 2.6 mm.

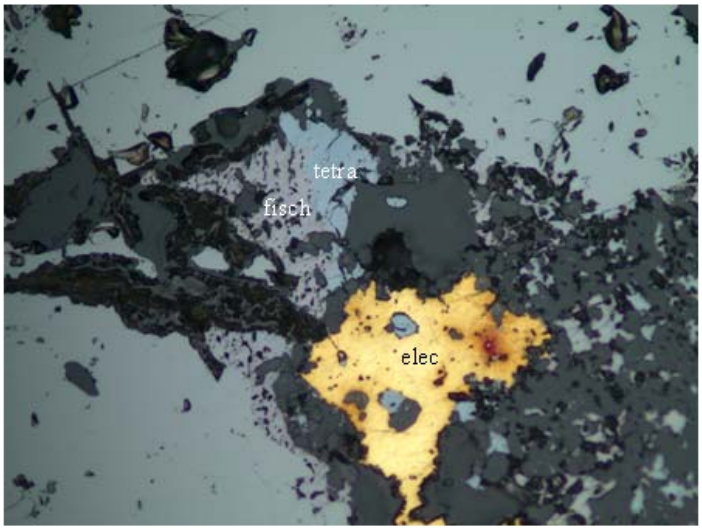


Figure A-12: Electrum, fischesserite?(AuSe) and a tetrahedrite group Mineral, BM-14b, reflected light, FOV = 0.26 mm.

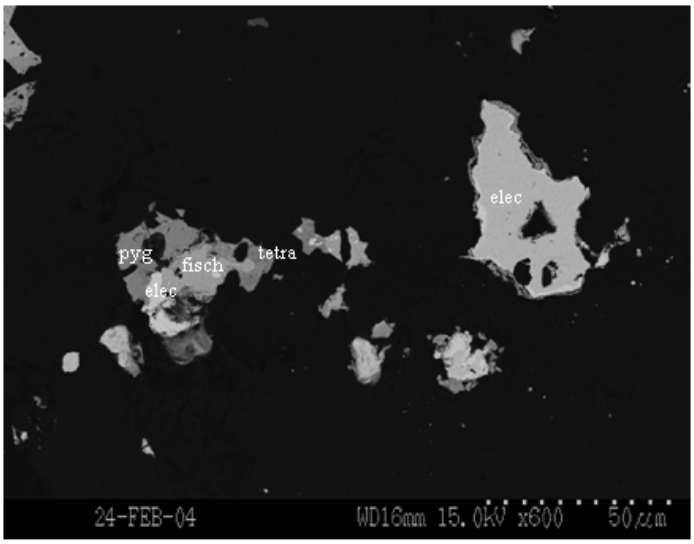


Figure A-13. Electrum, fischesserite (fisch), pyrargarite ($Ag_3SbS_3$)(pyg) and a tetrahedrite group mineral, BM-14b, BSE.

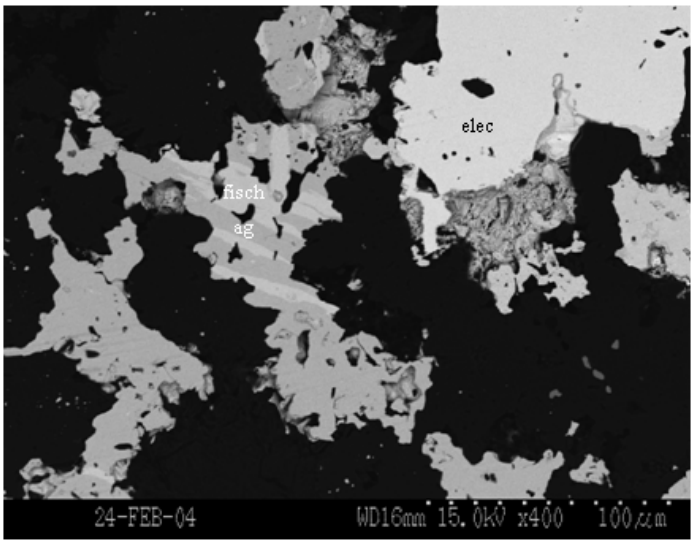


Figure A-14. Bands of aguilarite and fischesserite (exsolution?), BM-14b, BSE.

**BM-15**

This Bell vein sample taken from the Hatch-Halcyon level dump consists of bladed and banded quartz, silicates and banded sulfides and selenides. Silver minerals in aguilarite-acanthite series are common with compositions varying between the end members. A selenian silver-germanium mineral, selenian argyrodite ($Ag_8Ge(Se,S)_6$) was analyzed (Fig. A-16). This mineral was first reported by Botova et al. (1983) and occurred in near-surface quartz-adularia veins hosted in rhyolitic volcanic rock similar to the environment at Buckskin Mountain. Supergene (?) chlorargyrite (AgCl) after naumannite was analyzed (Fig. A-15). A few grains of pyrargarite(?) were observed. Electrum was absent from this thin section. The textures and mineralogy are similar to stage 2b of Vikre (1985).

**BM-16**

This vein sample from the Bell vein dumps has a vuggy, euhedral massive sulfide assemblage similar to stage 3 of Vikre (1985). More than 50% of the sample is euhedral marcasite and pyrite, some of which exhibit a bladed texture. Smaller, euhedral arsenopyrite grains coat the fringes of the larger Fe-sulfide grains (Fig. A-17). Late anhedral stibnite fills vugs in the quartz (Fig. A-18). Arsenopyrite and stibnite have low levels of Hg (0.1-0.3 at.%). Dark gray chalcedonic silica fills vugs and voids.

**Acknowledgments**

The author would like to thank Jim Hinchcliff for making the thin sections used in this study and Carl Henderson for assistance with the SEM. Eric Essene is thanked for the insights provided by numerous discussions of Ag-selenides. The scanning electron microscope used in this study was acquired under EAR 96-28196 from the NSF.

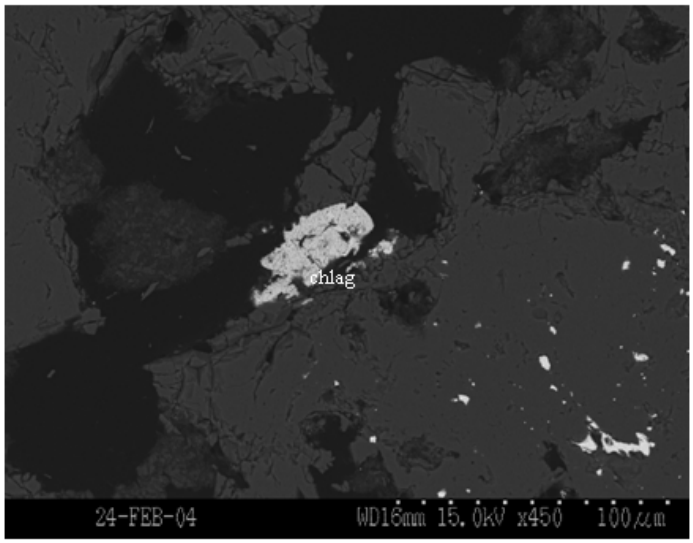


Figure A-15. Chlorargyrite (AgCl) possibly after aguilarite, BM-15, BSE.

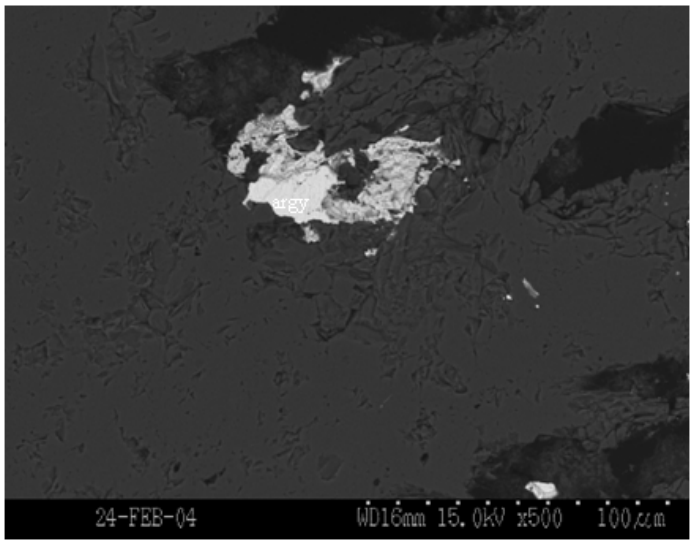


Figure A-16. Argyrodite ($Ag_8GeS_6$) (argy) indicating Ge-rich solutions during mineralization, BM-15, BSE.

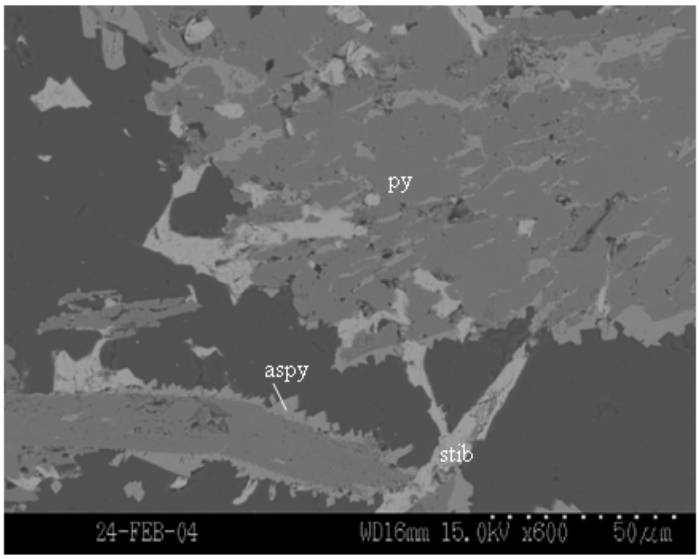


Figure A-17. Late stage arsenopyrite and stibnite coating early Pyrite, BM-16, BSE.

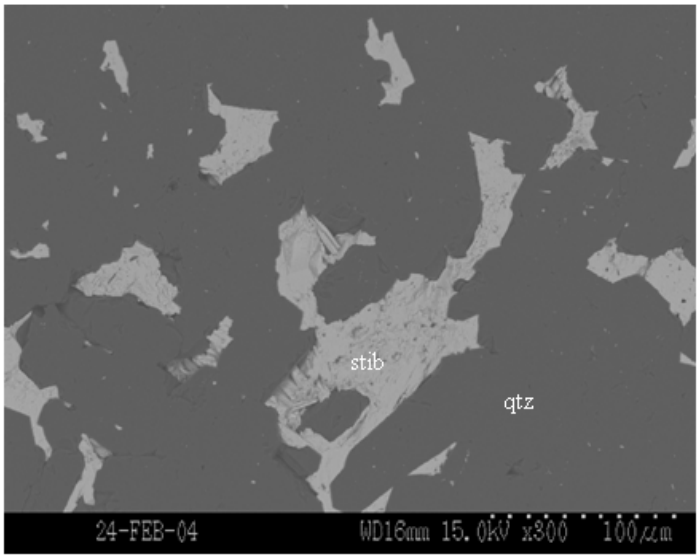


Figure A-18. Late stibnite filling voids in quartz, BM-16, BSE.

**References Cited**

Boctor, N.Z., Shieh, Y.N., and Kullerud, G., 1987, Mercury ores from the New Idria Mining District, California: geochemical and stable isotope studies. Geochimica et Cosmochimica Acta, v. 51, p. 1705-1715.

Botova, M.M., Sandomirskaya, S.M. and Chuvikina, N.G., 1983, First find of selenium argyrodite**.** Doklady, Academy of Sciences of the USSR, Earth Sciences Section, v.260, p 148–150.

Dickson, F.W., and Tunell, G., 1958, Equilibria of red HgS (cinnabar) and black HgS (metacinnabar) and their saturated solutions in the systems HgS-$Na_2S$-$H_2O$ And HgS-$Na_2S$-$Na_2O$-$H_2O$ from 25 ˚C to 75 ˚C at 1 atmosphere pressure. American Journal of Science, v. 256, p. 655-679.

Krupp, R.E., and Seward, T.M., 1990, Transport and deposition of metals in the Rotokawa geothermal system, New Zealand. Mineralium Deposita, v. 25, p. 73-81.

Rytuba, J.J., and Heropoulos, C., 1992, Mercury: an important byproduct in epithermal gold systems. U. S. Geological Survey Bulletin 1877, p. D1-D8.

Vikre, P.G., 1985, Precious metal vein systems in the National District, Humboldt County, Nevada. Economic Geology, v. 80, p. 360-393.

# APPENDIX B.

# Hg ISOTOPE SIGNATURES OF MISSISSIPPI VALLEY, CARLIN AND ALMADÉN-TYPE ORE DEPOSITS

## Introduction

Recent experimental studies of Hg isotope fractionation have confirmed field observations that volatilization causes measurable changes in Hg isotopic compositions by the preferential reduction and vaporization of lighter Hg isotopes (Zheng et al., 2007). This is significant in the study of ancient hydrothermal systems because it supports other lines of evidence (e.g. fluid inclusions and vein textures) for boiling and vapor separation in a near surface environment (Smith et al., 2005, 2008). Laboratory studies have also confirmed that biological reduction and abiotic photoreduction cause significant mass dependent fractionation of Hg isotopes in surficial environments (Bergquist and Blum, 2007; Kritee et al., 2007). In both biotic and abiotic reduction, lighter isotopes of Hg were preferentially reduced to the volatile $Hg^0$ species, leaving isotopically heavier Hg in the remaining residue. These studies indicate that Hg isotopes might be useful in studies of ore deposits by: 1) providing insight on the physical conditions of the hydrothermal system during ore formation; 2) assessing the role of biological interactions in ore deposition; and 3) quantifying the role of ore deposits and active hydrothermal systems in the global cycling of Hg.

In an effort to evaluate these possibilities, reconnaissance isotopic analyses were carried out on mercury from three different types of ore deposits. The following sections describe these ore deposits, explain the problem to which mercury isotope analyses might provide insight, and summarize the results.

## Ore Deposit Geology

### Mississippi Valley-type Zn-Pb deposits

Mississippi Valley-type (MVT) Zn-Pb deposits form in carbonate host rocks from metal-rich brines (10 to 30 wt% NaCl) circulating in sedimentary basins at temperatures between 75 and 200 ˚C (Leach and Sangster, 1993). Most Hg in these deposits is in solid solution in sphalerite ((Zn,Hg)S) (Schwartz, 1997). Fluids that formed MVT deposits interacted with large volumes of rock and deposited ore largely by mixing two fluids, one S-bearing brine and the other metal-rich (c.f. Kesler et al., 1997). Most MVT fluids are not considered to have undergone large-scale boiling or vapor separation.

Leaching and fluid transport of Hg was shown to cause only very small amounts of isotopic fractionation in the Hg deposits of the California Coast Ranges (Smith et al., 2008; Chapter IV) and the greatest amount of fractionation was associated with boiling and de-gassing of fluids in the near-surface (Smith et al., 2005, 2008). It is therefore expected that MVT deposits will not show the same range of isotope ratios as epithermal and hot-spring type Hg-Au deposits and may preserve the Hg isotopic signature of the source rocks from which the Hg was derived. Low-temperature MVT ore deposition might also involve sulfur that has been reduced by bacterial activity (Druschel et al.,

2002), and isotopic compositions characteristic of these processes might also be observed in Hg in the ores.

Carlin-type Au deposits

Carlin-type Au deposits located in northeastern Nevada are examples of basin-hosted ore deposits that formed from fluids in large, almost regional, scale hydrothermal systems. The fluids that formed these ore deposits are characterized by low salinity (~ 2-3 wt% NaCl), high Au/Ag and Au/base metals ratios, reduced, hydrocarbon-rich compositions at moderately low temperatures (180 – 240 ˚C) that replaced the silty carbonate host rocks with silica along structural zones and permeable strata (Hofstra and Cline, 2000; Cline et al., 2005). Hg is found in Au-rich arsenian pyrite rims and in late stage orpiment, realgar and cinnabar (Cline, 2001; Reich et al., 2005). The Carlin district is host to numerous Au deposits that range in size from <1 M to > 20 M oz Au.

Key questions remain unanswered as to the origin of the heat, fluids and metals that formed these deposits and their possible link to magmatic activity and/or regional heating events (recently summarized by Ressel and Henry, 2006). Comparisons have been drawn between Carlin-type deposits and other large Au-only deposits, such as orogenic lode Au deposits, and it is hypothesized that these deposits formed from a uniform ore fluid derived from a large, relatively homogenous source (Phillips & Powell, 1993; Muntean et al., 2007).

Hg isotopes may provide insight into these questions. The Hg isotopic signatures of ores formed from large-volume, homogeneous fluids derived from crustal-scale processes should have a limited range of $\delta^{202}$Hg values that reflect the Hg isotopic composition of the source region, similar to the expectations for Mississippi-Valley-type

deposits. This narrow range of $\delta^{202}$Hg values should be distinct from ores derived from near-surface hydrothermal activity, which typically display a much broader range of $\delta^{202}$Hg values currently known to range from $\delta^{202}$Hg values of –1 to –3.4 (Chapter IV, Smith et al., 2008).

Almadén-type Hg deposits

The mines at Almadén, Spain, access the largest Hg ore deposits on Earth. The ore consists of replacements of cinnabar and native Hg in quartzite or chlorite-carbonate altered volcanic rock and black shale (Saupe, 1990; Hernandez, 1999). Two types of mineralization have been described by Hernandez (1999): stratabound deposits, which includes the giant Almadén deposit, which is hosted mainly in the lower Silurian Criadero Quartzite; and fully discordant ore bodies, which includes several of the satellite deposits to the main ore body, such as the Las Cuevas, which is hosted by mafic volcanoclastic rocks. Both are deposit types have a close spatial association with Silurian-Devonian Frailesca volcanic breccias (Higueras et al., 1999).

The size of the ore deposits at Almadén, carbonate-dominant alteration assemblages and the links to regional heating are similar to the largest silica-carbonate-type Hg deposits of the California Coast Ranges, New Almaden and New Idria. Both the Almadén and California examples have abundant Hg-rich sedimentary source rocks adjacent to the districts and both are related in some way to volcanic activity. At Almadén, potential source rocks include thick quartzite sequences, inter-bedded black shales with TOC contents up to almost 8 wt%, basaltic lavas and Frailesca-type breccia pipes (Saupe, 1990; Higueras et al., 1999).

Initial measurement of Hg isotope ratios from the Almadén deposit indicated surprising homogeneity among the ores and refined mill product, although these early analyses have a poor level of external reproducibility (Klaue and Blum, 2000; Lauretta et al., 2001). New data were needed to determine if there were significant variations in Hg isotopic compositions and whether they could help determine whether the source of Hg for the Almadén-type deposits was sedimentary or volcanic.

**Materials and Methods**

North American MVT ore samples were obtained from the collection of S.E. Kesler of the Department of Geological Sciences at the University of Michigan. B. Ahlers of the Doe Run Mining Company provided samples from the Bushy Park MVT deposit. M. Reich of the Departamento de Geología, Facultad to Ciencias Físicas y Matemáticas, Universidad de Chile and Kesler collected the Carlin-type ore samples that were used in this study. Ores from the Almadén and Las Cuevas mines were collected from the mine site and core collections of the Minas de Almadén y Arrayanes SA by the author. Additional Almadén and Las Cuevas samples (Alm-8, LC-1b) were collected by Kesler.

Unless otherwise indicated in Table B-1, samples were mineral separates that were hand-picked from the ore specimens and crushed in a boron-carbide mortar. Bulk ore and jasperoid samples were hand crushed in an agate mortar. Small aliquots (10-20 mg) of powdered samples were leached in aqua regia. The leachates were then diluted and analyzed for Hg isotopic composition by the method described in Smith et al. (2005, 2008) and Chapter II.

**Results**

MVT Deposits

Samples of sphalerite were selected from a variety of MVT deposits in different mining districts to examine the isotopic compositions of Hg in ores formed from basin-scale diagenetic processes (Table B-1, Fig. B-1). The $\delta^{202}$Hg values for the sphalerite samples analyzed range from +0.2 to –1.0 ‰ $\delta^{202}$Hg. Samples from Bushy Park and Nanisivik have a relatively narrow range of $\delta^{202}$Hg values, close to the analytical resolution of the method, while samples from the Central Tennessee District range cover a larger span. It is noteworthy that 4 of the 5 samples from Bushy Park are > 0 ‰. Two samples from Nanisivik are clustered at the low end of the range of $\delta^{202}$Hg values. Samples from the Central Tennessee district show a much larger range than can be attributed to the precision of the analyses. In general, MVT ores have higher $\delta^{202}$Hg values than the Carlin-type deposits and fall in a similar range as Almadén-type deposits.

Carlin-type

The $\delta^{202}$Hg values for Carlin-type ore and mineral samples range from -1.6 to -0.3 ‰ (Table B-1). The isotopic compositions of a pyrite sample from the Meikle deposit and pyrite and pyrite-bearing ore from the adjacent Rodeo deposit are virtually identical within the external precision of the measurements (±0.1 ‰)(Fig. B-1). Late-stage ore minerals from Rodeo, galkhaite and cinnabar, have low $\delta^{202}$Hg values, with the galkhaite having the lowest $\delta^{202}$Hg value measured for this deposit type. Jasperoid material, which may have been deposited as paleosurface sinter, has a similar low $\delta^{202}$Hg value.

Table B-1 Summary of ore deposit analyses

| Sample[a] | Locality | Mineral | $\delta^{202}$Hg |
|---|---|---|---|
| ***MVT*** | | | |
| CT-1 | Central Tennessee District | Sphalerite | -0.2 |
| CT-3 | Central Tennessee District | Sphalerite | 0.0 |
| CT-4 | Central Tennessee District | Sphalerite | -0.1 |
| CT-7 | Central Tennessee District | Sphalerite | -0.7 |
| CT-8 | Central Tennessee District | Sphalerite | -0.4 |
| TS-WC-1 | Tri-State District | Sphalerite | -1.0 |
| Ark 9 | Northern Arkansas District | Sphalerite | -0.4 |
| Webb City | Viburnum Trend, SE Missouri | Sphalerite | -0.1 |
| SP4310 | Nanisivik, Canada | Sphalerite | -0.6 |
| SP4315 | Nanisivik, Canada | Sphalerite | -0.8 |
| BP-1 | Bushy Park, South Africa | Sphalerite | 0.1 |
| BP-2 | Bushy Park, South Africa | Sphalerite | -0.4 |
| BP-3 | Bushy Park, South Africa | Sphalerite | 0.2 |
| BP-4 | Bushy Park, South Africa | Sphalerite | 0.0 |
| BP-9 | Bushy Park, South Africa | Sphalerite | 0.2 |
| ***Carlin-type*** | | | |
| GS-03-03 | Goldstrike, Nevada | Pyrite | -0.5 |
| M-03-03 | Meikle, Nevada | Pyrite | -1.1 |
| R-03-03 | Rodeo, Nevada | Pyrite | -0.9 |
| R-03-05 | Rodeo, Nevada | Ore | -0.8 |
| R-11-151M-02 | Rodeo, Nevada | Galkhaite | -1.6 |
| Surface sinter | Rodeo, Nevada | Jasperoid | -1.3 |
| SEK UG cinnabar | Rodeo, Nevada | Cinnabar | -1.1 |
| S-03-03 | Screamer (Post-Betze), Nevada | Ore | -1.5 |
| DP-03-03 | Deep Post (Post-Betze), Nevada | Realgar | -0.3 |
| ***Almadèn-type*** | | | |
| Alm-8 | Almadèn deposit, Spain | Cinnabar | -0.5 |
| CS04AL56 | Almadèn deposit, Spain | Cinnabar | -0.1 |
| LC-1b | Las Cuevas deposit, Spain | Cinnabar | -0.5 |
| CS04AL28 | Las Cuevas deposit, Spain | Cinnabar | 0.0 |
| CS04AL28 | Las Cuevas deposit, Spain | Native Hg | -0.9 |

[a]All samples prepared by acid digestion.

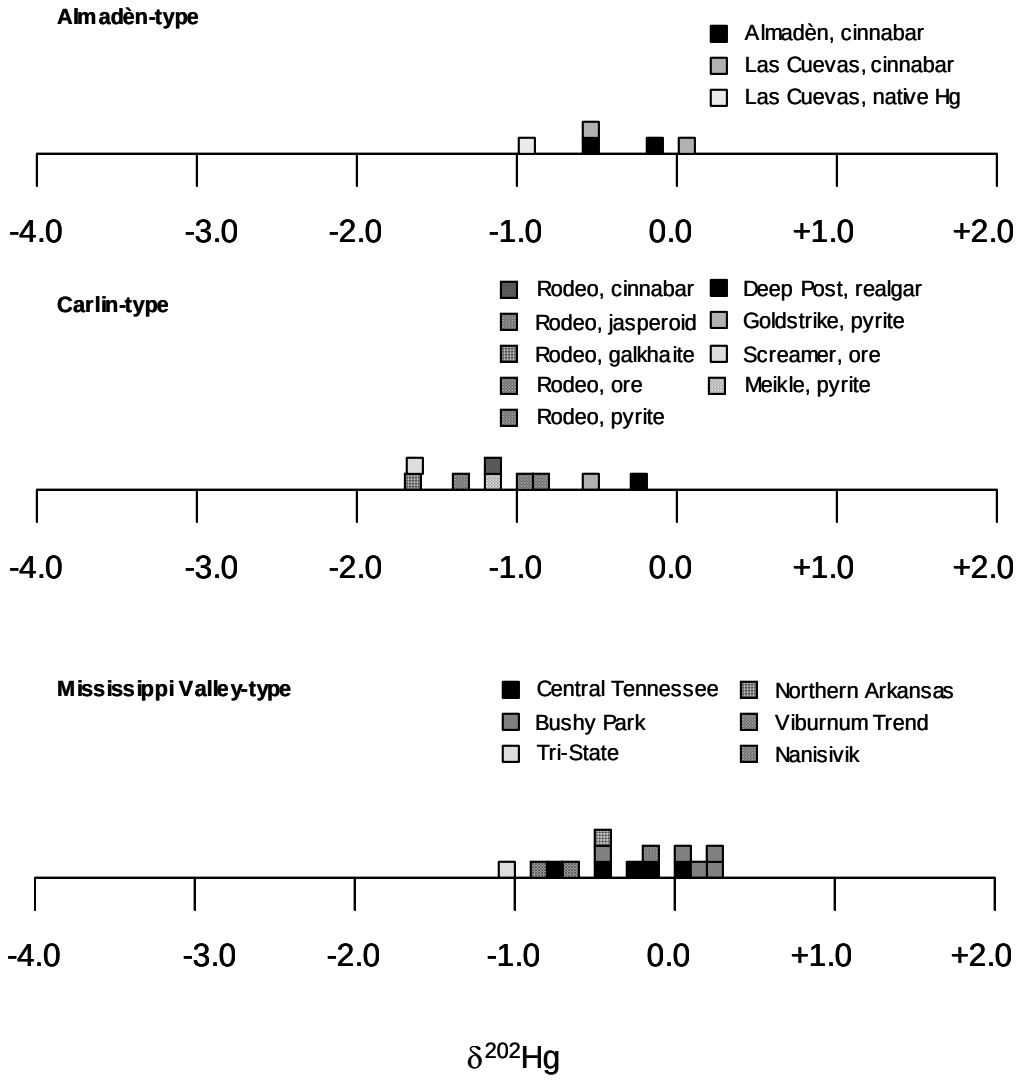


Figure B-1. Histograms of $\delta^{202}$Hg values by deposit type.

Late-stage realgar from Deep Post has the highest $\delta^{202}$Hg value at –0.3 ‰, while ore from the neighboring Screamer deposit is at the low end of $\delta^{202}$Hg values at –1.5 ‰. The range of $\delta^{202}$Hg values is greater than for the Almadén- and MVT deposits, and extends to much lower $\delta^{202}$Hg values than these deposit types.

Almadén

The $\delta^{202}$Hg values of the cinnabar from the Almadén and Las Cuevas ore bodies range from -0.9 to 0.0‰ (Table B-1). The different $\delta^{202}$Hg values of co-existing cinnabar (0.0 ‰) and native Hg (-0.9 ‰) from the same sample (CS04AL28) may be the result of mineral-specific isotope fractionation effects that occurred during the reduction of $Hg^{2+}$ in cinnabar to liquid $Hg^0$. Abiotic and bacterially-mediated Hg reduction were found to produce reduced $Hg^0$ with a lower $\delta^{202}$Hg value than the precursor in laboratory experiments (Kritee et al., 2007; Bergquist and Blum, 2007). The $\delta^{202}$Hg values of cinnabar from the sedimentary-rock hosted Almadén and Frailesca breccia-hosted Las Cuevas deposits span a narrow range of 0.5 ‰ (Fig. B-1).

**Discussion**

MVT

The isotopic compositions of the two MVT deposits from which multiple samples were analyzed, Bushy Park and Nanisivik, appear to be largely uniform. This is in contrast to, for example, the Maycamas Hg deposit district, where the range of isotopic compositions in individual deposits is the same as that in the entire district. This suggests a common source of Hg for the ore forming fluid in these MVT deposits, with little or no subsequent fractionation caused by processes such as boiling or vapor separation. The

various MVT deposits that comprise the Central Tennessee District show a greater range of $\delta^{202}$Hg values than the individual deposits, possibly suggesting larger-scale heterogeneities in Hg sources district-wide. Little fractionation (< ±0.5 ‰) is expected during leaching and transport of Hg from source to ore deposit based on similarities in $\delta^{202}$Hg values among deep ore deposits and source rocks in the California Coast Ranges (Smith et al., 2008; Chapter IV). The average $\delta^{202}$Hg value of the small population of Bushy Park sphalerites, 0.0 ± 0.4 ‰ (2 SD, n = 5), suggests that this might also be true for at least some MVT deposits as well (Fig. B-1).

Bushy Park is located in the world's oldest MVT district, which is hosted in the late Archean-early Proterozoic Transvaal Basin. Ar-Ar analyses of illite interpreted to accompany ore deposition at Bushy Park yield an age of 2.145 ± 0.007 Ga (Schaefer, 2002). It is notable that 4 of the 5 Bushy Park $\delta^{202}$Hg values are > 0 ‰. These values are at the high end of the range of $\delta^{202}$Hg values for all the MVT samples analyzed (Fig. B-1) as well as most other ore deposits (Chapter III; Chapter IV). The other MVT samples are from deposits that formed in the Mesoproterozoic (Nanisivik) and the Phanerozoic (Central Tennessee, Viburnum Trend, Northern Arkansas, and Tri-State), after the Great Oxidation Event, and during a time when seawater sulfate concentrations were much closer to present values (see review by Kesler and Reich, 2006). It is possible that the high $\delta^{202}$Hg values of the Bushy Park deposit reflect different processes of sulfate concentration and ore formation during a time when seawater sulfate levels are thought to be <1%, possibly up to ~25%, of modern values (Kah et al., 2004; Ohmoto, 2004).

Few processes are currently known to produce high $\delta^{202}$Hg values. Reduction of Hg by bacteria produces gaseous $Hg^0$ that is lighter than the Hg that remains in the

sediment, enriching it in heavier Hg isotopes (Bergquist and Blum, 2007; Kritee et al., 2007). Trace metal utilization by cyanobacteria has been an important process in the global cycling of metals as far back as 3.2 Ga, and it is possible that bacterial Hg reduction also occurred during the Proterozoic (cf. Saito et al., 2003). Burial and subsequent diagenesis of sediments enriched in heavy Hg isotopes could have formed a source rock with a high $\delta^{202}$Hg value.

Bacterially mediated methylation of Hg may be another process that could concentrate heavier Hg isotopes in the sediment. Analyses of the dogfish muscle certified reference material DORM-2, in which 96% of the contained Hg is in the methylated form, are isotopically heavy at +0.18 ‰ (Chapter II; Bergquist and Blum, 2007). Bacterially-mediated sulfate reduction was recently linked to ZnS precipitation in biofilms and might be involved in some MVT and SEDEX deposits (Druschel et al., 2002). Processes such as these may form a reservoir of heavy Hg isotopic compositions (>0 ‰ $\delta^{202}$Hg) in organic-rich sedimentary rocks and MVT ore deposits that form from fluids that contain Hg derived from this reservoir may record that heavier Hg isotopic signature.

Carlin-type

Carlin-type deposits have a range of $\delta^{202}$Hg values that is larger and distinctly lower than MVT and Almadén-type deposits. Within the Rodeo deposit $\delta^{202}$Hg values range from –0.8 to –1.6 ‰ (Fig. B-1). While mineral-specific fraction effects might be the cause of this variation, these effects are probably much less than for the effect observed between cinnabar and $Hg^0$ at Almadén, because Hg is in the same redox state in all the Rodeo mineral samples analyzed ($Hg^{2+}$). The $\delta^{202}$Hg values of ores from Rodeo

and Screamer differ by 0.7 ‰ and these deposits are < 1.5 km apart. Pyrite from Meikle, Rodeo and Goldstrike range from –0.5 to –1.1 ‰ $\delta^{202}$Hg and these locations are separated by < 5km. These variations are not consistent with the interpretation that these ore deposits formed from a uniform fluid composition derived from a large homogenous source region.

The range of $\delta^{202}$Hg values and low $\delta^{202}$Hg values, averaging -1.0 ± 0.8 ‰(2SD, n = 9), of the Carlin-type deposits suggests several possibilities: 1) the Hg in the deposits was derived from a source rock(s) with a $\delta^{202}$Hg value lower than values measured in the source rocks of the California Coast Ranges; 2) rather than a uniform ore fluid, mineralizing fluids were heterogeneous mixtures (metamorphic, magmatic, exchanged meteoric) with different Hg isotopic compositions; 3) Hg isotopes were fractionated by boiling and the generation of isotopically light Hg vapor during formation of these deposits in a process similar to that observed in the epithermal ore deposits and hot springs systems described in Chapter III and IV., or 4) Hg isotopes were fractionated by an as yet unrecognized process.

It is certainly possible that there are source rocks with $\delta^{202}$Hg values less than those measured for the bulk of the rocks in the California Coast ranges. Two samples of metamorphic rocks of the Franciscan Complex had similarly low values (Chapter IV). Deep crustal melting and involvement of basement structures have been proposed as metal sources for Carlin-type deposits and these materials have not been analyzed for Hg isotopic compositions (Cline et al., 2005).

Most studies of the stable isotopic composition of Carlin-type deposits conclude that meteoric water was the dominant component, although Cline and Hofstra (2000)

present evidence for the involvement of metamorphic or magmatic fluids in the formation of the Getchell and Deep Post deposits. In the California Coast Ranges, connate fluids derived from the Great Valley Sequence formed the mineralizing fluid and dilution with meteoric water produced fluids with much lower Hg concentrations, but similar $\delta^{202}$Hg values (Smith et al., 2008, Chapter IV). To form significant variations in ore minerals, the mixing fluids would be required to be Hg rich and have distinctive $\delta^{202}$Hg values.

In the Carlin-type sample suite, some of the late-stage minerals (cinnabar and galkhaite) and jasperoid deposited at or near the paleosurface are isotopically lighter than the bulk of the ore mineral samples (Table B-1). It is possible that these minerals were deposited by an epithermal-like hydrothermal system either during the main stage of Carlin-type ore deposition or at some later time.

Given the limited amount of data currently available on the Hg isotope systematics of ore deposits, as yet unrecognized fractionation might be associated with a well known ore depositing mechanism. For instance, sulfidation of reactive Fe in the host rock and precipitation of As-pyrite are known to be important mechanisms for ore formation, but the isotopic effects of incorporating Hg into pyrite rims and onto pyrite surfaces in unknown (Kesler et al., 2003; Reich et al., 2005).

Almadén-type

Samples from the Almadén district show much less variation in $\delta^{202}$Hg values than the Carlin-type deposits, and are similar in range to MVTs and silica-carbonate type Hg deposits from the California Coast Ranges (Fig. B-1; Chapter IV). The largest variation in the Almadén deposits might be attributed to mineral-specific isotopic fractionation between cinnabar and co-existing native Hg. The reduced form (native Hg)

has a $\delta^{202}$Hg value that is 0.9 ‰ lower than that of the co-existing cinnabar, a fractionation that is similar in magnitude and favoring lighter isotopes as determined in laboratory experiments (Bergquist and Blum, 2007; Kritee et al., 2007).

Evidence from ore deposits in the California Coast Ranges suggests that only small fractionations (< ±0.5 ‰) occur during transport and deep deposition (> 1000 m) of Hg (Smith et al., 2008; Chapter IV). The $\delta^{202}$Hg values of the Almadén cinnabar samples analyzed range from 0 to –0.5 ‰, with an average –0.3 ± 0.5 ‰ (2SD, n = 4). It is conceivable that with the uncertain external precision of the P54 instrument used in the earlier analyses and analytical methods used by Lauretta et al. (2001), all the samples from Almadén previously analyzed could appear to have homogeneous Hg isotopic compositions.

Small differences between the two deposits analyzed in the Almadén district suggest that the isotopic signature of the source may be preserved in the deposits. Pb isotope data from cinnabar suggests a mixed sedimentary source for the Hg in the Almaden district (Higueras et al., 2005). These authors propose that hydrothermal leaching of organic matter in sedimentary rocks and Hg transport as organic complexes was the main processes that concentrated Hg and formed the ore deposits of the district. The Hg isotope data presented here are in agreement with this model of formation.

**Future Work**

More extensive studies of individual MVT deposits are needed to confirm if the limited range of $\delta^{202}$Hg values measured in Bushy Park is a characteristic of MVTs in general. Further comparisons of the Hg isotopic compositions of Paleoproterzoic MVTs

with deposits that formed after the Great Oxidation Event may also be useful in unraveling the history of the evolution of the Earth's oceans and atmosphere. Detailed studies of potential Hg source rocks in MVT basins might fingerprint metal sources if limited fractionation is shown to occur during leaching, transport and MVT ore deposition. The role of organic matter in the formation of MVT deposits needs further exploration. Hg will no doubt be involved because of the effects of bioaccumulation. An examination of Hg isotope ratios in both organic-rich and organic-poor MVT deposits may be of use in this respect.

A comprehensive study of source and host rock types available from the Carlin District would provide insight on the Hg isotopic composition of the rocks of the region. The presence of an epithermal system overprinting or operating during main stage ore deposition in Carlin-type deposits is a controversial idea. Detailed studies that focused on early and late mineralization, different modes of occurrence (stratabound, fault/fold controlled and breccia hosted) and paragenetic mineral sequences from individual mines might be useful for determining the evolution of Hg isotopic compositions in Carlin-type deposits.

The source of the Hg for the supergiant Almadén deposit, while made somewhat clearer by recent Pb isotope studies (Jébrak et al., 2002; Higueras, 2005) and this Hg isotope study, is still a question open for future research. Hg isotopes combined with other studies of provenance (e.g. Pb) may shed new evidence on the metalogensis of the district. A study of the Hg isotopic composition of the volcanic and sedimentary source rocks of the district may be able to distinguish a Hg source, although there is evidence for significant Hg re-mobilization in the district since the Paleozoic.

**Acknowledgments**

The author would like to thank Prof. Pablo Higueras of the University of Castilla-La Mancha for his assistance with sample collection at the Almadén mine and his excellent tour of the Almadén district. Also to be thanked are the many helpful geologists at the Minas De Almadén y Arrayanes SA. Field work in Spain was supported by a Scott Turner award to the author.

**References Cited**


Bergquist, B.A. and Blum, J.D., 2007, Mass-dependent and -independent fractionation of Hg isotopes by photoreduction in aquatic systems. Science, v. 318, p. 417-420.

Cline, J. S. & Hofstra, A. H. 2000. Ore fluid evolution at the Getchell Carlin-type gold deposit, Nevada, USA. European Journal of Mineralogy, 12, 195–212.

Cline, J.S., 2001, Timing of gold and arsenic sulfide mineral deposition at the Getchell carlin-type gold deposit, north-central Nevada. Economic Geology, v. 96, p. 75-89.

Cline, J. S., Hofstra, A. H., Muntean, J. L., Tosdal, R. M. & Hickey, K. A. 2005. Carlin-type gold deposits in Nevada: critical geologic characteristics and viable models. *In*: Hedenquist, J. W., Thompson, J. F. H., Goldfarb, R. J. & Richards, J. P. (eds) Economic Geology 100th Anniversary Volume. Society of Economic Geologists inc., Littleton, Colorado, p. 451–484.

Druschel, G.K., Labrenz, M., Thomsen-Ebert, T., Fowle, D.A., and Banfield, J.F., 2002. Geochemical Modeling of ZnS in Biofilms: An Example of Ore Depositional Processes. Economic Geology, v. 97, p.1319-1329.

Hernandez, A. et al., 1999. The Almaden mercury mining district, Spain. Mineralium Deposita, pp. 539-548.

Higueras P., Oyarzun R., Lunar R., Sierra J., & Parras J. 1999. The Las Cuevas deposit, Almadén district (Spain): Unusual case of deep-seated advanced argilitic alteration related to mercury mineralization. Mineralium Deposita, v. 34, p. 211–214.

Higueras, P., Munha, J., Oyarzum, R., Tassinari, C.C.G., and Ruiz, I.R., 2005. First lead isotopic data for cinnabar in the Almaden district (Spain): implications for the genesis of the mercury deposits. Mineralium Deposita, v. 40, p. 115-122.

Hofstra, A.H., and Cline, J.S., 2000, Characteristics and models for carlin-type gold deposits. Reviews in Economic Geology, v. 13, p. 163-220.

Jébrak, M., Higueras, P., Marcoux, E., and Lorenzo, S., 2002. Geology and geochemistry of high-grade, volcanic rock-hosted, mercury mineralization in the Nuevo Entredicho deposit, Almadén, Spain. Mineralium Deposita, v. 37, p. 421-432.

Kah, L.C., Lyons, T.W., and Frank, T.D., 2004, Low marine sulphate and protracted oxygenation of the Proterozoic biosphere. Nature, v. 431, p. 834–838.

Kesler, S.E., Friedman, G.M., and Krstic, D., 1997. Mississippi valley-type mineralization in the Silurian paleoaquifer, central Appalachians. Chemical Geology, v. 138, p.127-134.

Kesler, S.E., Fortuna, J., Zaojun Ye, Alt, J.C., Core, D.P., Zohar, P., Borhauer, J., and Chryssoulis, S.L., 2003. Evaluation of the Role of Sulfidation in Deposition of Gold, Screamer Section of the Betze-Post Carlin-Type Deposit, Nevada. Economic Geology, v. 98, p. 1137 - 1157.

Klaue, B. and Blum, J.D., 2000. Mercury isotopic analyses by single and multi-collector magnetic sector inductively coupled mass spectrometry. Journal of Conference Abstracts: Goldschmidt 2000, 5, 591 pp.

Kritee, K., Blum, J.D., Johnson, M.W., Bergquist, B., Barkay, T., 2007. Mercury stable isotope fractionation during reduction of Hg(II) to Hg(0) by mercury resistant bacteria. Environmental Science & Technology, v. 41, p.1889-1995.

Leach, D.L., and Sangster, D.F., 1993, Mississippi valley-type lead-zinc deposits. Special Paper - Geological Association of Canada, v. 40, p. 289-314.

Muntean, J.L., Coward, M.P., and Tarnocai, C.A., 2007. Reactivated Palaeozoic normal faults: controls on the formation of Carlin-type gold deposits in north-central Nevada. Geological Society, London, Special Publications, v. 272; p. 571-587.

Ohmoto, H., 2004, The Archean atmosphere, hydrosphere and biosphere, *in* Eriksson, P.G., Altermann, W., Nelson, D.R., Mueller, W.U., and Catuneanu, O., eds., The Precambrian Earth: Tempos and events. Developments in Precambrian Geology, v. 12, p. 361–388.

Phillips, G. N. & Powell, R. 1993. Link between gold provinces. Economic Geology, v. 88, p. 1084–1098.

Reich, M., Kesler, S.E., Utsunomiya, S., Palenik, C.S., Chryssoulis, S.L., and Ewing, R.C., 2005, Solubility of gold in arsenian pyrite. Geochimica et Cosmochimica Acta, v. 69, p. 2781-2796.

Ressel, Michael W., Henry, Christopher D., 2006. Igneous Geology of the Carlin Trend, Nevada: Development of the Eocene Plutonic Complex and Significance for Carlin-Type Gold Deposits. Economic Geology, v. 101, p. 347-383.

Saito, M.A., Sigman, D.M., Morel, F.M.M., 2003. The bioinorganic chemistry of the ancient ocean: the co-evolution of cyanobacterial metal requirements and biogeochemical cycles at the Archean/Proterozoic boundary. Inorganic Chimimica Acta 356, 308–318.

Saupé, F. 1990. Geology of the Almaden Mercury Deposit, Province de Ciudad Real, Spain. Economic Geology, v. 85, p. 482–510.

Schaefer, M., 2002, Paleoproterozoic Mississippi Valley-Type Pb-Zn Deposits of the Ghaap Group, Transvaal Supergroup in Griqualand West, South Africa [Ph.D. dissertation]: Johannesburg, Rand Afrikaans University, 367 p.

Schwartz, M.O., 1997, Mercury in zinc deposits; economic geology of a polluting element. International Geology Review, v. 39, p. 905-923.

Smith, C.N., Kesler, S.E., Klaue, B. and Blum, J.D., 2005. Mercury isotope fractionation in fossil hydrothermal systems. Geology, v. 33, p. 825-828.

Smith, C.N., Kesler, S.E., Blum, J.D., and Rytuba, J.J., 2008. Isotope Geochemistry of Mercury in Source Rocks, Mineral Deposits and Spring Deposits of the California Coast Ranges, USA. Earth and Planetary Science Letters, v. 269, p. 399-407.

Zheng, W., Foucher, D. and Hintelman, H., 2007. Mercury isotope fractionation during volatilization of Hg(0) from solution into the gas phase. Journal of Analytical Atomic Spectrometry, 22, 1097-1104.